Denudation rates derived from spatially-averaged cosmogenic nuclide analysis in Nelson/Tasman catchments, South Island, New Zealand

Abby Jade Burdis

A thesis submitted to

Victoria University of Wellington

in partial fulfilment of requirements for the degree of

Master of Science

in

Physical Geography

School of Geography, Environment and Earth Sciences

Victoria University of Wellington

2014

Abstract

New Zealand's tectonically and climatically dynamic environment generates erosion rates that outstrip global averages by up to ten times in some locations. In order to assess recent changes in erosion rate, and also to predict future erosion dynamics, it is important to quantify long-term, background erosion. Current research on erosion in New Zealand predominantly covers short-term (100 yrs) erosion dynamics and Myr dynamics from thermochronological proxy data. Without competent medium-term denudation data for New Zealand, it is uncertain which variables (climate, anthropogenic disturbance of the landscape, tectonic uplift, lithological, or geomorphic characteristics) exert the dominant control on denudation in New Zealand. Spatially-averaged cosmogenic nuclide analysis can effectively offer this information by providing averaged rates of denudation on millennial timescales without the biases and limitations of short-term erosion methods.

Basin-averaged denudation rates were obtained in the Nelson/Tasman region, New Zealand, from analysis of concentrations of meteoric ^{10}Be in silt and in-situ produced ^{10}Be in quartz. The measured denudation rates integrate over ~2750 yrs (in-situ) and ~1200 yrs (meteoric). Not only do the ^{10}Be records produce erosion rates that are remarkably consistent with each other, but they are also independent of topographic metrics. Denudation rates range from ~112 – 298 t km^{-2} yr^{-1}, with the exception of one basin which is eroding at 600 - 800 t km^{-2} yr^{-1}. The homogeneity of rates and absence of a significant correlation with geomorphic or lithological characteristics could indicate that the Nelson/Tasman landscape is in (or approaching) a topographic steady state.

Millennial term (^{10}Be-derived) denudation rates are more rapid than those inferred from other conventional methods in the same region (~50 – 200 t km^{-2} yr^{-1}). This is likely the result of the significant contribution of low frequency, high magnitude erosive events to overall erosion of the region. Both in-situ and meteoric ^{10}Be analyses have the potential to provide competent millennial term estimates of natural background rates of erosion. This will allow for the assessment of geomorphic-scale impacts such as topography, tectonics, climate, and lithology on rates of denudation for the country where many conventional methods do not. Cosmogenic nuclides offer the ability to understand the response of the landscape to these factors in order to make confident erosion predictions for the future.

Acknowledgements

Firstly the biggest thanks to my supervisor Kevin Norton. I'm so thankful for the opportunity to embark on this project, the experience has been amazing. Thank you for your patience in reading my thesis (so very many times) and for your enthusiasm for science, which has always been infectious. And thanks to Kevin and also Bethanna Jackson for the opportunity to go the AGU conference. That was certainly an experience I won't forget and I'm so grateful for it. Thanks also to Steve Tims for all the help with sample collection and for sharing your expertise in meteoric method. Thanks to Richard for helping with field and lab work, your fabulous photography, and general support when I was experiencing cosmo-related explosions (both physical and mental). Thanks to Bob Ditchburn and Albert Zondervan for completing the preparation of my samples out at GNS and processing them in the AMS, I appreciate it hugely.

Thanks so much to my office mates for the welcomed distractions as we ploughed (sometimes crawled and fumbled) our way through the Masters journey. Kirsten and Melody you guys have been a great support and heaps of fun. And finally thanks to my friends and family, without you I wouldn't be where I am today. Sam, thanks for being my rock, it has meant the world to me. Mum thanks for your constant support, and Dad for your belief in me and your guidance - thank you both for making me who I am today.

Contents

Table of Contents

List of figures

List of Tables

Chapter one: Introduction and Background

1.1 Introduction

New Zealand is a rapidly eroding country; rivers draining the western Southern Alps and the East Cape of the North Island have sediment yield estimates of 1.7 – 60000 t km $^{-2}$ yr^{-1} which are up to ten times higher than the global average (Griffiths, 1979; 1982). This dynamic environment is largely the result of the tectonic activity of New Zealand, high relief terrain, and oceanic climate. When removal of material from the surface of a landscape outstrips the rate of soil production beneath the surface, the landscape becomes degraded. Erosion can have detrimental effects on the landscape and the ecosystems within (Dymond et al., 2010a), and has the potential to generate significant hazard where mass movement of material is involved (Hovius et al., 1997) (*figure 1.1*). It is therefore important to understand the rate at which the landscape has eroded recently and in the past, and to understand factors that control the denudation of the landscape.

Figure 1.1: Landsliding in the Manawatu Gorge, New Zealand. Photo courtesy of NZTA (left) and Warwick Smith (right).

As the climate warms, many areas of New Zealand are likely to experience increases in annual rainfall (most of the West Coast of New Zealand) while areas already subject to occasional drought are likely to experience a decrease (Otago, Canterbury, Marlborough, Hawkes Bay). While there is variation in the effects of climate change on annual rainfall, it is expected that the entire country will be subject to an increase in the intensity and frequency of storm events (MfE, 2008). This could in turn increase the erosive power of rainfall events (Mullan et al., 2012) and the impact of increased

sediment movement across New Zealand. Anthropogenic clearing of indigenous forests in New Zealand has also accelerated soil erosion, particularly in hill country where vegetation is essential for the stabilisation of the landscape (Dymond et al., 2010a). Accelerated erosion from the landscape increases the amount of sediment that is delivered to the stream network. Fine sediments in the stream network are considered a major pollutant and the main stressor on ecology habitats and freshwater environments (Morrison et al, 2009). Ecosystems have evolved in order to cope with the episodic nature of sediment disturbance; however, they have not evolved to respond to the persistent disturbance induced by anthropogenic clearing (Yount & Niemi, 1990). The combined effects of increased storm activity and anthropogenic clearing could drive major increases in the detrimental effects of sediment movement in the environment.

Monitoring erosion from the landscape is important for assessing human-induced changes that could impact the habitats of ecological systems (Basher et al., 2011). In order to assess recent erosion changes, and also to the predict future erosion dynamics, it is important to have a competent record of long term erosion as a basis for natural or background rates of erosion. It is important to understand what is driving erosion in the landscape and understand the extent to which factors such as climate, tectonics, lithology, and anthropogenic clearing may have impacted the landscape. With knowledge of the way the landscape responds to variation in these factors it is then possible to better understand how the landscape may respond to changes in these factors; how the landscape may respond to climate change in the future.

1.2 Erosion in New Zealand

A number of methods have been used in New Zealand to quantify erosion including direct erosion measurements such as sediment yield estimates, micro-erosion meters, thermochronology, proxy methods such as sedimentation rate estimations, longitudinal profiling of fluvial terraces, and landslide inventories, and erosion modelling from lithological and climatic variables. These methods will be discussed in regards to their application, results, and limitations for erosion quantification in New Zealand.

1.2.1 Sediment yields

Sediment yield gauging of rivers is the most common method used for inferring erosion rates in New Zealand, a country that shows major variation in quantities of river transported sediments from region to region. Yield calculations have produced results ranging from 1.7 – 30000 t km^{-2} yr^{-1} across New Zealand. Sediment yields are considered a basin-averaged representation of the total short term yield assuming the stream network remains connected to the hillslope.

Traditionally, sediment yields are calculated by integrating suspended sediment rating relationships with flow records (Griffiths, 1979). Sediment loads are plotted against flow and the sediment rating is calculated by least-squares regression. The rating is then applied to the flow data to obtain a sediment load over the period of time covered by the flow record (Adams, 1979). Griffiths (1979) calculated suspended sediment yields for 16 gauged rivers in the South Island. Estimations suggested that the Hokitika River's sediment yield was about 2.4 times higher than the highest measured yield of the Ching River in China. Adams (1979) applied the suspended sediment yield method to obtain flow and sediment data for 40 catchments of varying sizes in the North Island. Sediment yield estimates ranged from 35 t km^{-2} yr^{-1} to 28 000 t km^{-2} yr^{-1} the highest of which were derived from the East Cape region. These results were supported by Griffiths (1982) who obtained similar results for North Island basins. Griffiths (1981) also applied this method to 33 basins of the South Island where sediment yields similarly varied over 3-4 orders of magnitude.

The Waipaoa catchment in the North Island of New Zealand, for example, has one of the highest sediment yields in the world (eg. Summerfield and Hulton, 1994). However, estimations vary considerably between studies from 7650 t km^{-2} yr^{-1} for the period 1960-1996 (Hicks et al., 2000), and 7770 t km^{-2} yr^{-1} for the period 1960-1965 (Jones & Howie, 1970), to 15100 t km^{-2} yr^{-1} for the period 1972-1977 (Adams, 1979) and 60000 t km^{-2} yr^{-1} for the period 1972-1980 (Griffiths, 1982). This highlights the short term variations in sediment yields and the uncertainties involved in calculation and measurements for sediment yield calculations.

Closer to the study area for this research, O Loughlin et al., (1978), estimated average yields of 55 m^3 km^2 yr (173 t km^{-2} yr^{-1}) and 5 m^3 km^2 yr (13 t km^{-2} yr^{-1}) over 2-3 year

periods for forested catchments in North Westland and Nelson, respectively. At the time these results could only be compared to temperate climate sediment yields measured in the USA (Megahan, 1976; Ursic & Dendy 1963). The comparison showed higher sediment estimations for the New Zealand catchments which were attributed to a storm event in 1975. To compare these to other studies in the northern South Island, Griffiths & Glasby's (1985) sediment yield estimates ranged from 152 – 2240 t km^{-2} yr^{-1} which were also in the range of Hicks et al.'s (1996) estimations of ~100 - 1000 t km^{-2} yr^{-1}.

1.2.2 Limitations

There has been discrepancy within sediment yield calculations highlighting the uncertainties involved in the application of sediment rating curves and the assumptions made for yield estimations (Walling, 1983). Fiordland has been an area of interest due to its high rainfall but low sediment yields. Adams (1980) obtained a yield estimation of 275 t km^{-2} yr^{-1}, Griffiths (1979 and 1981) an estimation of 13 000 t km^{-2} yr^{-1}, and Hicks et al., (1996) an estimation of 350 t km^{-2} yr^{-1}, however, all of these studies used the sediment rating approach and much of the same dataset (Hicks et al., 1996). Griffiths (1979) also acknowledged this issue suggesting errors for yield calculations could be as high as +60% for annual yields.

Some erosional landscapes can be disconnected from streams withholding erosional sediment from stream sediment measurements (Dymond et al., 2010a). The proportion of sediment that actually reaches the stream network must be considered in sediment yield calculations as the total contribution to the stream will vary between locations (Walling, 1983). Sediment yields ignore any storage processes that may intervene sediment transport between the catchment and the sample location (Walling, 1983; Burbank, 2002), and do not account for the addition or reworking of sediment from areas such as flood plains (Griffiths, 1979). Adams (1979) acknowledges that the calculations of river loads are only approximations; in his study, data were sparse and seasonal variability was not accounted for. Hicks et al. (1996) also acknowledge the errors and uncertainties involved in yield calculations including, again, the limited amount of data, and also sediment supply factors such as the variation in mean rainfall for each of the catchments.

Further constraints for sediment yield calculations in New Zealand are that many calculations are based on global basin characteristics which do not always fit the nature of New Zealand rivers. Gregory & Walling (1973) suggest a simple relationship between dissolved and suspended loads where it is likely that the loads are virtually the same for a runoff of 1/yr. Adams (1979), however, recognise this as false for North Island catchments where suspended load far exceeds dissolved load except where erosion is very low.

Perhaps the most poignant of limitations with sediment yield calculations is that long term erosion cannot be easily represented as they require long periods of gauging. New Zealand does not have the data for long term calculations, and the short periods of data collection may not account for low frequency, high magnitude events that contribute significantly to overall erosion. The periodicity of sediment yield gauging and the episodic nature of sediment delivery to the stream network can result in significant under- or over-estimations of erosion rates (Kirchner et al., 2001). Alternatively, sediment yields can be greatly affected by acceleration of erosion due to anthropogenic landuse changes (Milliman et al., 1987), producing very high erosion estimates (Vanacker et al., 2007). Sediment yields are effective in assessing short term erosion trends and the current contribution of sediment to rivers and ecosystems; however, the biases associated with sediment yield estimates (due to the short gauging periods and the episodic nature of erosion) make it difficult to infer relationships between processes that occur over geomorphic timescales and spatial trends in erosion. Sediment yield estimates are useful for assessing how the landscape responds to storm events in the short term; however, it is difficult to assess how the landscape's background erosion rates have responded to glacial-interglacial climate shifts, and geomorphic/geologic-scale tectonic and topographic changes.

1.2.3 Micro-erosion meter

The micro-erosion meter was developed by High & Hanna (1970) as a method for directly measuring surface lowering or erosion of bedrock at a point. This method uses a triangular device that measures the lowering of three points at chosen locations. Trudghill et al. (1981) modified the micro-erosion meter so that the dial gauge is separate from the base and the centre of the base is cut so that the dial gauge is able to move within the area of the bolts; this was called a traversing micro-erosion meter.

Stephenson (1997) then modified this further by fitting a digital dial gauge as opposed to analogue. This method has also been used to calculate terrestrial erosion rates (Stephenson & Finlayson, 2009) and modified to allow measurements to be taken underwater by divers (Askin & Davidson-Arnott (1981). A number of published New Zealand studies have used this method to measure rates of lowering on shore platforms in Kaikoura including Kirk (1977), Stephenson & Kirk (1996), Stephenson & Kirk (1998), Inkpen (2007) and Inkpen et al. (2010).

Kirk (1977) used a micro-erosion meter to examine surface lowering on shore platforms in Kaikoura. Each site was measured at two monthly intervals for a two year period between 1973-1975. Their results showed a mean lowering rate for the two years was 1.53 mm yr^{-1} and rates were generally higher on mudstone than on limestone. Stephenson & Kirk (1996) continued use of this method to further investigate lowering on platforms on the Kaikoura Peninsula. Their results showed that the long term results produce higher erosion rates than the short term, and that the short term results under-predict total surface lowering. This method was also used by Inkpen et al. (2010) who compared height change results after a two year and a ten year period to compare short and long term results. Contrary to Stephenson & Kirk (1996) they found that there was no significant variation between the long and short term data.

1.2.4 Limitations

This method is greatly restricted to point source, short term estimations as the lowering of a surface can be highly irregular. Similar to sediment yields, major lowering can occur in low frequency, high magnitude events that may or may not occur during the period where data is collected (Selby, 1974). Studies have shown that results can be affected by the length of data collection – erosion data over twenty year periods can be significantly more than two year periods due to the infrequency of high magnitude events (Stephenson & Kirk, 1996). While this method has the ability to provide competent point source short term physical erosion, it does not offer insight into geomorphic-scale erosion dynamics. It is difficult to infer relationships between erosion and topography, climate, and tectonics with point source erosion data that is likely biased due to the short gauging timescales. This method is also representative of erosion

at a single point, as opposed to a representation of erosion for a large area (such as basin-averaged) erosion.

1.2.5 Thermochronology

Thermochronology is a long term (geological timescale) method and has also been used to estimate erosion rates in New Zealand. This measures the time since a rock has cooled below a certain temperature (closure temperature). Damage from radioactive decay (fission tracks) or decay products (alpha-particles) become trapped in the crystal lattice. Closure temperature varies significantly for different minerals and systems and where these are well-constrained it is possible to estimate rates of exhumation. To calculate erosion, a geothermal gradient and closure temperature are assumed and then the erosion rate is calculated as equal to the cooling age divided by the depth of eroded crust (Rahl et al., 2007). Thermochronology has been widely applied to New Zealand and elsewhere (eg. Seward & Kohn, 1997; Kamp, 2000; Hermann et al., 2009) but not as a way of determining erosion rates. Herman et al., (2010) is to date the only study that uses thermochronology to explore erosion in the Southern Alps.

Hermann et al. (2010) developed a thermochronometer of very low closure temperature OSL-thermochronology to measure relief evolution and rates of exhumation in the last glacial cycle in the Southern Alps. They inverted thermochonological data to obtain exhumation rates and found that extreme exhumation rates of about 800m in 100 ka have remained steady over million year time scales for a small area of the Southern Alps. Although this is considered point source erosion not catchment-wide and as such is not strictly speaking representative, this broadly converts to 20800 t km^{-2} yr^{-1}. Thermochronology has not been further applied in New Zealand locations as a method for calculating erosion rates but clearly has promise for future research.

1.2.6 Limitations

Thermochronology is useful in that it measures long term erosion and smooths out anomalies because of crustal flexure that might misrepresent rates of erosion in short term and small area measurements. It also has a relatively simple, although lengthy, measurement procedure. A number of studies, however, have suggested that assuming an effective closure temperature depth may result in significant errors (Rahl et al., 2007;

Mancktelow & Grasemann, 1997; Ehlers et al., 2003). Herman et al., (2010) acknowledged that the main limitation with their OSL technique occurred with saturation of the traps – exposure to radiation could no longer trap radiation because the electron traps become full. Sometimes saturation could be reached very quickly rendering the method inapplicable. From the geologic timescales which thermochronlogical studies represent it is also difficult to understand trends in faster geomorphic processes.

1.2.7 Sedimentation rates

Sedimentation rates have been used globally as a proxy for calculating long term erosion rates (eg. van der Post et al., 1997; Loso et al., 2004). Sedimentation rate studies involve the extraction of cores in such places as basins, lakes, or offshore canyons or sea-beds. Stratigraphic analysis of the core is then undertaken with reference to known dates of events, such as volcanic eruptions that leave layers of tephra within the core. Various dating methods can be used including palynology, radiocarbon dating, tephra chronology, and foraminifera analysis to establish ages of sediments and the rates at which they accumulated. This method has been applied to a few locations in New Zealand including the Kaikoura Canyon (Lewis & Barnes, 1999), Lake Tutira (Page et al., 2004; Orpin et al., 2010), East Cape (Carter et al., 2002), Fiordland (Pickrill, 1993), Hawke Bay (Barnes et al., 1991) and the Poverty Bay shelf (Wilmhurst et al., 1999).

With the use of sedimentary chronological techniques (eg. pollen analysis, radiocarbon and tephra dating, stratigraphy), Page et al. (1994) and Orpin et al. (2010) produced estimations of sedimentation rates for Lake Tutira in the North Island. Page et al. (1994) estimate that Cyclone Bola (1988) delivered 1184000 m^3 via landsliding, 28000 m^3 via channel erosion, 25000 m^3 from tunnel gully erosion, 96000 m^3 from sheet erosion, with a total of 1349000 m^3 from a single event. Orpin et al.'s (2010) results suggest a sedimentation rate of 3.3 mm yr^{-1} (3960 t km^{-2} yr^{-1}) for the pre-European period of 7.1 ky and then a rapid increase to 10 mm yr^{-1} (10200 t km^{-2} yr^{-1}) since ca 1880 AD or following post-European settlement. They were able to establish the source of sediment through pollen, spore, carbon, and nitrogen analyses, and produce a storm event record from diatom sampling and analysis. These sedimentation data show not only long term erosion for the area but also the frequency of major storm occurrences that dramatically increase sedimentation (therefore erosion) (Page et al., 1994; Orpin et al., 2010).

Lewis & Barnes (1999) used the Kaikoura Canyon to obtain an indirect measurement of sedimentation and therefore accumulation of river-transported sediment from the eastern South Island rivers. The study's intention was of analysing the transport of sediment to the deep ocean. They estimated that 1.5 x 10^6 m^3yr^{-1} of sediment from the 40 million tonnes supplied by the eastern South Island rivers (Griffiths & Glasby, 1985) falls into the canyon. Pickrill (1993) used seismic reflection profiling, coring, and radiometric dating to estimate sedimentation rates and volumes in three Fiordland basins over the Holocene. This study estimated sediment yields ranging from 28 – 209 t km^{-2} yr^{-1}.

Carter et al. (2002) established long term estimates of terrigenous sediment flux to the deep ocean off the East Cape of the North Island. They used palynology to assess anthropogenic influence on sediment flux, and also used calcium carbonate and planktonic foraminifera tests, radiocarbon dating, and tephra chronology to assist their study. Their results estimated a long term maximum flux of 6 g cm^2 ka (300 t km^{-2} yr^{-1}) between 11 and 8.5 ka and the modern flux of ~3 g cm^2 ka (300 t km^{-2} yr^{-1}) to the deep ocean.

1.2.8 Limitations

While this method provides useful proxy information on long term (millennial) erosion trends, there are a number of deficiencies in spatial and temporal accuracy of its application. Sediment accumulation can be biased due to erosion and deposition processes such as reworking of sediment from flood plains, or by removal of sediments during storm events (Allen et al., 2013). Sedimentation rates are also sensitive to tectonic changes such as subsidence or uplift which may alter the input of erosive material (Armitage et al., 2013). They are also limited spatially due to the requirement of a suitable reservoir in which sediment can be stored.

1.2.9 Longitudinal profiling of fluvial terraces

Longitudinal profiling of fluvial terraces and estimations of the timing of fluvial incision has been used in New Zealand as a proxy for long term (millennial) erosion rates (Grant, 1981; Litchfield, 2008). Grant (1981) used fluvial profiling of the Tukituki River in the East Coast of the North Island to better understand past erosion in New Zealand. Tree ages were used to determine the ages of depositional terraces and produce

a record for erosional periods in New Zealand since the 17th century. Erosion rates however were defined only qualitatively with 'moderate', 'slow', 'very fast' etc. Litchfield (2008) used a similar though more advanced approach by profiling onshore fluvial terraces in north-western Hawke Bay and using these to project terraces offshore, reconstructing the paleo-coastline. This method assumed that fluvial terraces at river mouths recorded uplift since the Late Pleistocene from which erosion rates can then be inferred. This study inferred a Holocene erosion rate of 0.5 ± 0.1 mm yr (520-1200 t km^{-2} yr^{-1}) and a rate of 0.02 - 0.5 mm yr (22-500 t km^{-2} yr^{-1}) from ~1880-1980.

1.2.10 Limitations

Similar to sedimentation rate research, this proxy method is limited by its spatial and temporal accuracy. Determining the age a terrace was when fluvial incision began (Burbank, 2002), or the location of a paleo-coastline (Litchfield, 2008; Burbank, 2002) is commonly difficult due to the erodibility of terrace formations (Litchfield, 2008), particularly for un-vegetated terraces. Using fluvial terraces for estimations of long term erosion is again restricted by the limited suitable locations for the application of the method.

1.2.11 Landslide inventories

A common method for measuring erosion in New Zealand is use of landslide inventories to estimate the contribution of landslides to denudation rates. This is achieved by using Digital Elevation Models to estimate landslide volumes with confirmation from aerial photography and ground surveying. Further ground truthing may include sampling river sediments to calculate particle size and trapping efficiency (Griffiths & McSaveney, 1986)

In British Columbia this method was used to calculate landslide-derived sediment yields of ~ 180 t km^{-2} yr^{-1} (Martin et al., 2002) - rates which are some of the highest derived for Pacific Northwest and coastal British Columbia. For comparison, Hovius et al. (1997) applied this method to the Southern Alps and obtained yields that exceeds Martin et al.'s (2002) rates by two orders of magnitude (~10000t km^{-2} yr^{-1}). These estimations were obtained using a number of calculations to derive volume of eroded

material and then distributed over each catchment's surface area to estimate annual sediment discharges material. These findings were in agreement with Griffiths (1979) and Hicks et al.'s (1996) suspended sediment yield calculations for the region (Korup et al. 2004). Korup et al. (2004) produced estimations of short term landslide-derived sediment pulses for the western Southern Alps. They estimated the immediate short term contributions of three large landslide events to erosion of the western Southern Alps to be greater than 70000 t $km^{-2}yr^{-1}$ This highlights the significant contribution of low frequency high magnitude events to erosion.

1.2.12 Limitations

A common problem in using landslide inventories to estimate denudation is that evidence for landsliding may no longer be visible. Underestimations are inevitable as magnitudes are unclear and some landslides may go unnoticed all together. This is particularly a problem for the Western Southern Alps where vegetation is thick and regrowth is rapid which can remove much of the evidence for landslides, often within a few years of their occurrence (Whitehouse, 1983). Another issue with landslide-derived erosion rates is that the estimations are usually obtained from Digital Elevations Models which is an effective method but must be applied with care due to the high chance of error (Korup et al., 2004). The error is due to it being difficult to obtain accurate scaling of depth and widths of landslides from Digital Elevation Models.

1.2.13 Modelling in New Zealand

The Suspended Sediment Yield Estimator (SSYE) was developed by The National Institute of Water and Atmospheric Research (NIWA) and Landcare Research as an interactive tool for estimating sediment yields across New Zealand. It incorporates river-gauging data from 200 river stations across New Zealand and an empirical model. The model is based on knowledge of slope, lithology, soils, and rainfall and their predicted influences on erosion rates (*figure 1.2*).

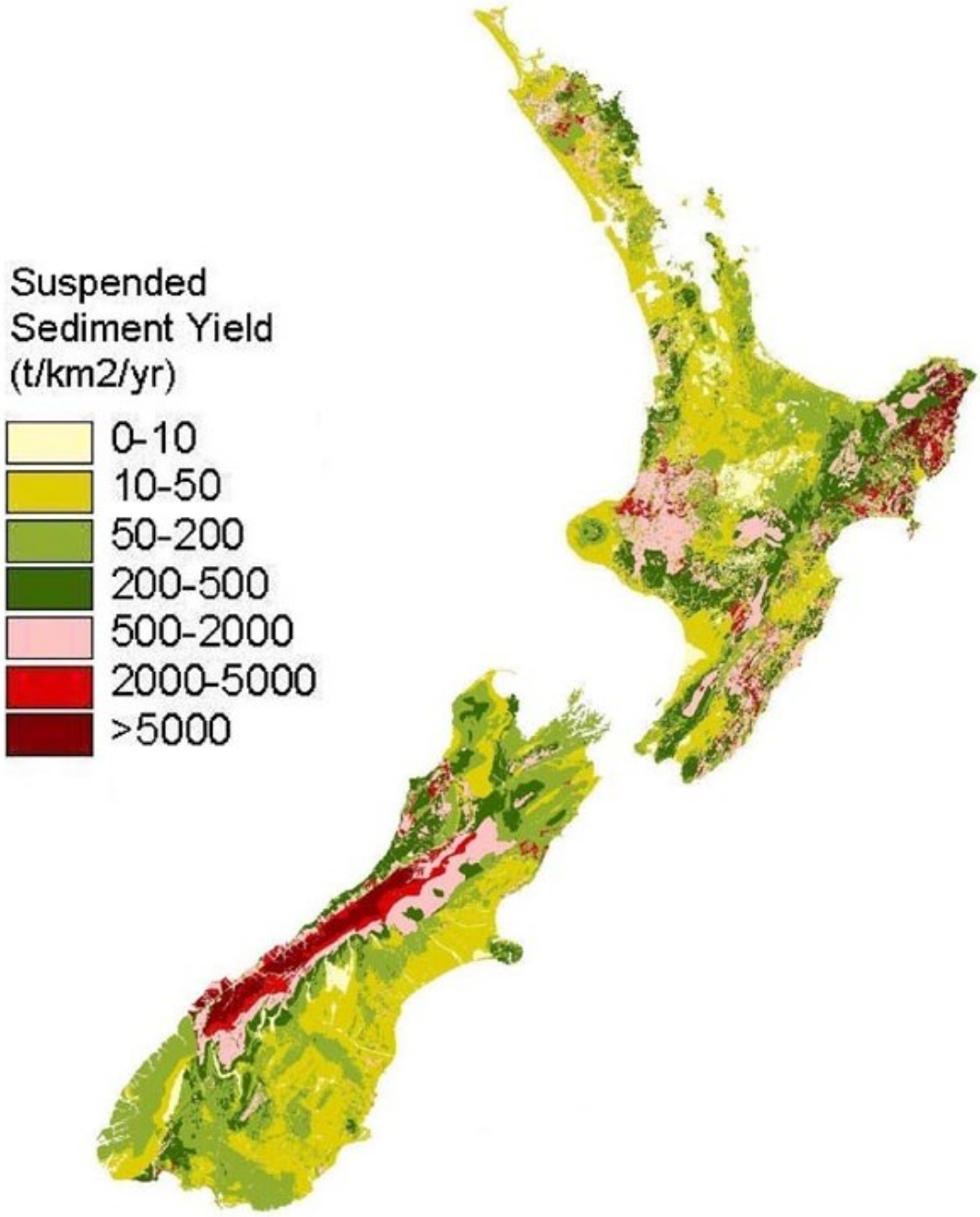

Figure 1.2: SSYE-derived estimations of suspended sediment yield (t km^{-2} yr^{-1}) across New Zealand. Note the extreme yields of the Western Southern Alps and the East Cape of New Zealand which are in excess of 5000 t km^{-2} yr^{-1}. (Source: NIWA, 2013)

Hicks et al. (1996) estimated sediment yields across New Zealand with use of an empirical model component for which they applied two GIS-based databases. They used multiple regressions to assess the influence of mean annual rainfall, the

coefficient-of-variation of annual rainfall, the ratio of the average rainfall in the wettest month to the annual average rainfall, and the 5-year return period 24 hr intensity on sediment yields. Dymond et al. (2010a) expanded on Hicks et al.'s (1996) model to incorporate the influence of land cover to sediment yield estimations. Their model calibrated a vegetation cover factor, sediment delivery ratio, and a rainfall factor. It also used a long term mean sediment yield for each erosion terrain produced by NIWA to calibrate coefficients for each erosion terrain for some groupings. They used a sediment delivery ratio of 1 which assumes that over very long periods all parts of the landscape must erode to keep in balance with uplift. They acknowledged a number of reasons why the sediment delivery ratio may or may not be 1, including frequency and magnitude of storm events, sediment deposited in flood plains. They assign a ratio of 1 to erosion processes that are connected to a stream network, and 0 to processes that are disconnected.

Dymond (2010b) alternatively used erosion models to estimate spatial distribution of erosion and analysed a map of soil organic carbon content to obtain a spatial distribution of carbon erosion. They apply two models: the first was the NZ empirical erosion model (NZeem) which was used to estimate total erosion from all processes, and the second was the New Zealand Universal Soil Loss Equation (NZUSLE) which was used to estimate surficial erosion processes. The intention was to understand the amount of carbon being transferred between the atmosphere and soils due to erosion. Herzig et al., (2011) used the erosion model approach to assess the effectiveness of afforestation in gullies of the East Coast region. Their model incorporates factors such as vertical incision or degradation, spatial extension or growth, stabilisation or closure, and the influences of forest cover and underlying geologic terrain. They use this to estimate sediment yield derived from gullies for catchments including the Waipaoa, Waiapu, and Uawa for a number of forestation scenarios.

Dymond et al. (1999) used an erosion model to estimate the effects two affforestation scenarios could have on the soil loss and sediment delivery due to landsliding for a simulated large storm event in the Waipaoa catchment. A limitation of this model is that it does not consider sediment delivered to the streams by gully erosion which contributes a significant proportion of the total sediment to the stream network. Marden

et al. (2012) recently used Digital Elevation Models to assess sediment generation from earth flows and shallow landslides also in the East Coast region. He applied Herzig et al.'s (2011) model to estimate the reduction in landslide-derived sediment that could be made in the next 20 years with reforestation. Their models suggested landslide-derived sediment could be reduced by 20% by 2030 as a result of reforestation. This major impact was also predicted by Herzig et al. (2011) who suggest that reforestation could reduce sediment yields from 22 million to 11 million t yr^{-1} by 2050.

1.2.14 Limitations

Erosion modelling is an effective and potentially invaluable tool for future erosion predictions in New Zealand (Hicks et al., 1996; Dymond et al., 1999; 2010a; Herzig et al., 2011); however, it is limited by understanding of long term erosion trends in New Zealand. Competent long term erosion test data is not available for validation of model effectiveness – models are largely based on short term data from potentially biased data sets. It is also limited by understanding of the long term processes and feedbacks involved in erosion, sediment transport, and deposition (de Vente & Poesen, 2005). This and the previous sections highlight the need for a long-term technique that can be applied over wide areas to confidently measure erosion in New Zealand. A better understanding of long term erosion dynamics and erosion-driving variables would allow for more reliable predictions for future erosion trends.

1.3 Controls on erosion

The geomorphology of a landscape is a function of complex interactions between tectonics, climate, lithology, and erosion. It is important to assess the controlling influences of erosion rates across differing landscapes to better understand what is driving rates of erosion and the way in which the landscape responds to variation in factors such as tectonics, climate, geomorphology, and lithology. The dominant controlling factor on the landscapes' geomorphology varies considerably between landscapes and all factors interact with one another in different ways. Controlling influences on erosion dynamics such as geomorphology, tectonics, climate, and lithology will be discussed in the following sections.

1.3.1 Geomorphic controls on erosion

Studies have recognised a number of relationships between hillslope morphology characteristics and rates of denudation (eg. Bellin et al., 2014). A common finding is a positive correlation between terrain steepness and erosion rate (eg. Ahnert, 1970; Summerfield & Hulton, 1994; Granger et al., 1996; Schaller et al., 2001; Montgomery and Brandon, 2002; Vance et al., 2003; Kober et al., 2007). An increase in relief commonly coincides with an increase in denudation rates; high relief terrain enhances fluvial incision and therefore channel steepness and the erosive power of rivers, with hillslopes keeping pace (Willett et al., 2001). Coincidently, channel steepness and erosion rate have also been found to correlate (Safran et al., 2005); however, channel steepness has often been found to be directly related to precipitation rate (Roe et al., 2003) and/or tectonic perturbation (Safran et al., 2005); its controlling influence on erosion is therefore disputable. Here the complex relationships between erosion-influencing variables (such as precipitation and relief) are apparent.

Slope angle is also a commonly acknowledged erosion driving mechanism; increase in slope angle is thought to increase erosion (eg. Riebe et al., 2000; Matmon et al., 2003a; Palumbo et al., 2010). Threshold slope angles are considered the angle at which erosion occurs predominantly as a result of mass wasting as opposed to diffusive hillslope processes (Montgomery, 2001)(commonly acknowledged as slope angle > ~30º). Erosion is commonly found to increase ~linearly with increasing slope angle up to threshold where it then increases non-linearly (Roering et al., 1999; 2001; Montgomery & Brandon, 2002). It has been considered that exceeding threshold slope angle may destroy any relationship between relief and denudation (Binnie et al., 2007; Ouimet et al., 2009).

1.3.2 Tectonic controls on erosion

Erosion rates can be used to discern landscapes that have recently been affected by tectonics or landscapes that are in ‘disequilibrium’. The proximity of basins to fault scarps has been found to affect rates of erosion in some locations (Riebe et al., 2000; Quigley et al., 2007). Quigley et al. (2007) recognised three large surface rupturing earthquakes in the Flinders ranges, Australia in the past ~67ka that had greatly affected

rates of erosion in the vicinity of the ruptures. Malusa & Vezolli (2006) noted a lack of influence from relief, climate and lithology on erosion variation in the Western Alps of Italy but a distinct relationship between exhumation rate of rock and faultlines. Molnar et al. (2007) further suggest that tectonics do not solely raise topography and therefore increase erosion rates - tectonics also fracture bedrock which can contribute to the susceptibility of the landscape to erosion processes.

1.3.3 Climatic controls on erosion

Much of the literature is in agreement that trends in erosion are greatly affected by glacial-interglacial climate shifts (eg. Riebe et al., 2001b; Hinderer, 2001; Wittmann et al., 2007; Norton et al., 2010). Glacier retreats contribute to increased sediment fluxes due to the exposure of loose material and the expansion/increased discharge of rivers which contribute to erosion via incision. Erosion rates have been found to experience 4× to 10× increases while undergoing adjustments from glacial perturbations (Norton et al., 2008; 2010; Valla et al., 2010). Hallet et al. (1996) also suggest that both mechanical and chemical denudation tend to be more elevated in areas that are currently glaciated. The influence of spatial variation in precipitation, however, is variable across the literature. Some studies show a direct correlation between precipitation gradients and erosion rates (eg. Grujic et al., 2006), while others find a distinct independence of denudation from precipitation (eg. Burbank et al., 2003). A number of studies recognise a coupling between relief and precipitation. Some indicate that precipitation determines the relief of landscape (Roe et al., 2003; Zaprowski et al., 2005; Schlunegger et al., 2011; Trauerstein et al., 2013) by unloading causing an isostatic response. Alternatively, others suggest relief determines the precipitation rate by orographic rainfall (Roe et al., 2003**;** Elhers & Poulsen, 2009). There is no consensus as to which factor is the main driver of erosion, again highlighting the complex interactions between erosion-driving variables. It is also very apparent that erosion dynamics vary considerably in space and time.

1.3.4 Lithological controls on erosion

Various studies have identified lithology as an important factor in the variation of denudation rates (Schaller et al., 2001; Palumbo et al., 2010; Korup & Schlunegger,

2009; Norton et al., 2011a). The rate of erosion in the landscape can be directly related to the physical properties and therefore erodibility of rocktypes. Lithology is often found to be a contributing factor in erosion variation as opposed the dominant factor which is more often related to topography and climate. Korup & Schlunegger (2009) recognised that the lithological control was only apparent where channels had adjusted to uplift; it diminished in oversteepened channels undergoing adjustment to tectonics. Lithology, however, can exert an important control on the geomorphology of the landscape. The erodibility of rocks can determine the steepness of slopes and therefore relief and elevation of an orogen; this in turn can affect rates of erosion, highlighting the complex interactions associated with landscape evolution.

1.3.5 Steady state

Topographic steady state occurs when all morphological components of landscape evolution, including vertical movement, horizontal movement, and erosion, have obtained a balance; when removal of material via erosion and weathering equals the movement of the entire tectonic velocity field (Willett et al., 2001). Flux/tectonic steady state is obtained when horizontal uplift of the landscape equals the removal of material from the surface. It differs from topographic steady state in that it is not necessary that the elevation of an orogen remains constant (*figure 1.3*). The uplift component during flux steady state may not include the entire horizontal flux as some of it may go toward building a crustal root. It therefore accounts only for the rate of vertical uplift versus the rate of erosion at the surface (Willett & Brandon, 2002).

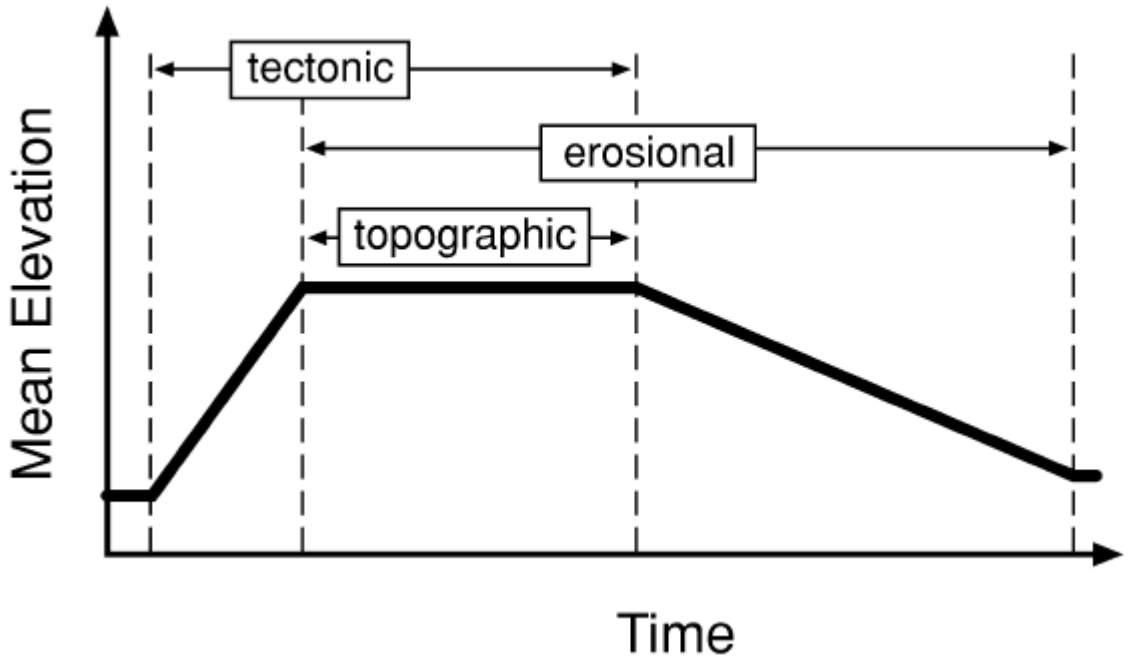

Figure 1.3: Illustration of the steady state evolution of a mountain range through uplift and erosion. Tectonic (or flux) steady state occurs when vertical uplift rates balance erosion but other horizontal forces may drive the landscape to change geomorphically. Topographic steady state occurs when all components of the tectonic velocity field balance rates of denudation resulting in the maintenance of elevation of the mountain range until uplift slows. Once uplift rates have decreased, erosion dominates and the mountain will decline in elevation (Montgomery, 2001).

Spatially and temporally homogenous erosion rates can be an indication that the landscape is in flux and/or topographic steady state (Matmon et al., 2003b). Studies such as Matmon et al. (2003b) in the Appalachians and Burbank et al. (2003) in the Himalaya, have obtained erosion rates do not vary spatially or temporally despite significant geomorphic and climatic variation. They have concluded that it is likely due to topographic steady state. A number of other studies found temporal homogeneity of erosion rates including the Fort Sage mountains, western USA (Granger et al., 1996), Arnhem Land, northern Australia (Nott & Roberts, 1996), the Olympic mountains, northwestern USA (Montgomery & Brandon, 2002;Pazzaglia& Brandon, 2001), a Namibian escarpment, southern Africa (Bierman & Caffee, 2001), the Himalaya (Vance et al., 2003), the Western Alps, Italy (Malusa & Vezolli, 2006), the European Alps (Wittman et al., 2007), the Appenines (Cyr & Granger, 2008), and the San Gabriel Mountains of California (DiBiase et al., 2010). Each study compared two or more of the

following erosion quantification methods that represent differing timescales: thermochronological exhumation analysis, ^{10}Be analysis, and sediment accumulation volume. Their conclusions also support the idea of topographic steady state in these landscapes.

Alternative theories were found where there was spatial homogeneity but not temporal (Ferrier et al., 2005; Abbuhl et al., 2011). Ferrier et al. (2005) suggested that although Casper Creek in California produced spatially uniform erosion rates it did not necessarily indicate topographic steady state. Uplift rates in the region derived from marine terraces were significantly more rapid than rates of denudation indicating disequilibrium. In the Peruvian Andes, Abbuhl et al. (2011) found that denudation correlated with channel and hillslope steepness downstream of a knickpoint. However, upstream of the knickpoint, denudation was completely independent of channel and hillslope steepness, suggesting spatial homogeneity. Here it is again apparent that spatial homogeneity of denudation rates does not necessarily mean the landscape is in topographic steady state.

1.3.6 Current theories on the controlling influences of erosion in New Zealand

Griffiths (1982) attributed most of the sediment yield variation to rainfall in the South Island and lithology and tectonics in the North Island. From his results he suggested that a simple power law relationship between yield and rainfall is useful for estimating suspended sediment yields for mountainous regions of temperate maritime climate, except where catchments had been largely modified by man. Hicks et al. (1996) further explored the influence of rainfall and also geology on sediment yield variation around New Zealand. They examined 203 catchments in a wide range of basin characteristics and found that rainfall, lithology, and tectonics had the dominant controls on sediment yields (*figure 1.4*) which again ranged over 3-4 orders of magnitude in both North and South Islands. Basher et al. (2008) also suggest that lithology controls erosion in the North Island while rainfall variation controls erosion in the South Island.

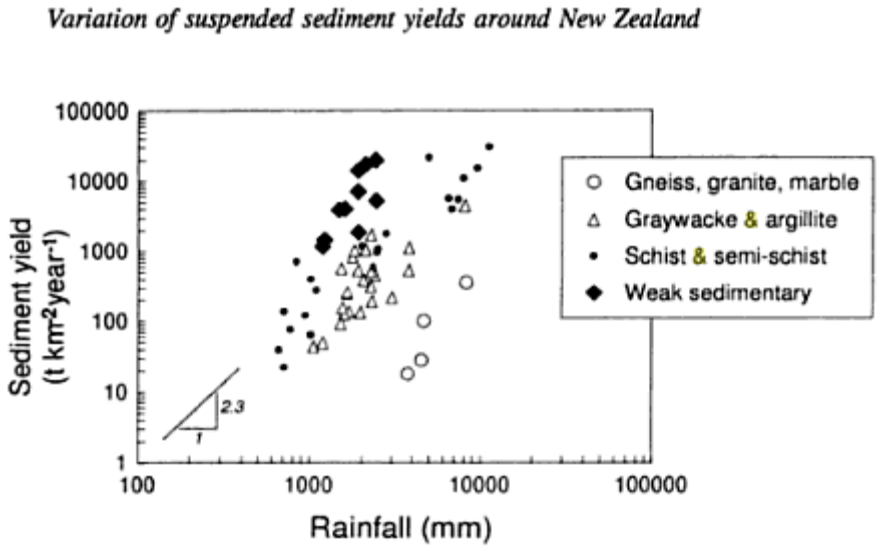

Figure 1.4: Increase in sediment yield with increasing rainfall in New Zealand. Note also that lithology also shows a relationship with sediment yields; gneiss, granite, and marble landscapes appear to contribute less sediment than landscapes underlain by weak sedimentary rocks (Source: Hicks et al., 1996).

Carter et al.'s (2002) sedimentation rate study recognised anthropogenic clearing as an important factor in the increase in sedimentation in the late 19th century, a finding that corresponds well with other sedimentation studies on the Poverty Bay shelf (Wilmhurst et al., 1999) and Hawke Bay (Barnes et al., 1991). Their results suggested that there have been fluctuations over the Holocene as a result of expanding vegetation cover with climate warming and then declining vegetation cover with anthropogenic clearing. They also acknowledged the short term impacts of earthquake and volcanic events which they suggest contributed to the long term maximum flux. Page et al. (1994) and Fahey et al. (2003) recognise the effects of deforestation on erosion concluding that extreme increases in sediment yields have occurred as a result.

Extreme climatic events have been widely acknowledged as a major contributor to erosion in New Zealand due to the initiation of landsliding (Griffiths, 1981; 1982; Hicks et al., 1996; Glade, 2003). Crozier (2005) recognised large storm events and rainfall intensity and duration as the main influences in landsliding which greatly contributes to erosion. Page et al. (2000) and Marden et al. (2008) alternatively recognise that anthropogenic clearing has increased gully erosion that is initiated by low magnitude,

high frequency events. They suggest that constant elevated gully erosion as a result of deforestation contributes more significantly than infrequent landsliding to erosion.

1.4 Discussion

The unique interactions between climatic, tectonic, geomorphic and lithological characteristics and denudation rates of different landscapes limit the precision of erosion modelling to landscapes where extensive research has been undertaken. While conventional erosion quantification methods such as sediment yields, micro-erosion meters, and landslide inventories provide a basis for short term trends, it is difficult to understand how the landscape responds to the variables above and changes in these variables over time. The erosion trends from periods that these conventional methods cover (~100 years) is exceptionally short on a geomorphic timescale meaning biases are likely, and natural background rates of erosion are unlikely to be obtained. While sedimentation rates and fluvial terrace profiling provide proxy data for long term erosion rates, their function as competent erosion records remains limited by their spatial selectiveness, and the complexity of erosion and deposition dynamics. Exhumation rates provide an indication of long term erosion (Myr) with the assumption that denudation equals exhumation; however, this indirect measurement is representative of a geologic timescale, larger than of that of geomorphic processes. There remains a lack of direct measurement that provides spatially-averaged millennial term erosion rates for New Zealand. Long term erosion trends, and the ways in which erosion has responded to external and internal changes in the past, are not yet understood sufficiently to provide suitable constraints for future erosion predictions, or to fully understand the dynamics of erosion in New Zealand. Here cosmogenic nuclides offer a valuable tool for understanding geomorphic processes and the impacts of climate, topography, tectonics, and lithology on erosion at millennial scale. With this understanding, erosion modelling and predictions for future erosion dynamics in New Zealand could be greatly improved.

1.5 Cosmogenic nuclides

Cosmogenic nuclides have commonly been used to date surfaces but can also be used to estimate the average denudation rate of a landscape (Granger et al., 1996). The eroded material from a landscape is delivered to rivers; therefore, it can be assumed that sediments from a river provide an average of the sediment and therefore nuclide

concentration of an entire catchment upstream of where the sample is taken (Brown et al., 1995). With these assumptions it is possible to estimate an average denudation rate for an entire catchment. An eroding surface's nuclide concentration is inversely proportional to the rate of denudation (Lal, 1991) of the landscape upstream of the sample location. In-situ cosmogenic nuclides have deep production profiles and are therefore relatively unaffected by any anthropogenic changes that have affected erosion dynamics, or by any previous large scale, short term increases in erosion (von Blanckenburg, 2006). As such, they are suitable for quantification of long term background denudation rates on the order of 10^2 – 10^5 yrs (eg. Brown et al., 1995; Granger et al., 1996; Schaller et al., 2001; Vanacker et al., 2007; von Blanckenburg, 2006). Meteoric nuclides can be used to estimate denudation rates of variable timescales, depending on the depth at which the nuclide adsorbs and therefore the timescales which it represents (Willenbring & von Blanckenburg, 2010; von Blanckenburg et al., 2012).

The use of cosmogenic nuclides to estimate long term denudation provides a useful benchmark for comparison with short term erosion (Vanacker et al., 2007). This method can provide indication of the impact of anthropogenic clearing on sediment yields, allow estimations of denudation rates over millennial time scales to assess changes in erosion rates during past climate cycles, and allow the examination of the impact of topography, tectonics, and lithology on erosion rates among differing sites (Granger et al., 1996). Particularly for New Zealand, this could be a valuable tool to understand the complex interactions between erosion-driving variables and the erosion rates they produce, in order to better predict how the landscape may respond in the future.

Currently, there are two studies in New Zealand that have applied ^{10}Be to address sediment production, transport, and denudation. Larsen et al. (2014) examined soil production, chemical weathering, and catchment-wide denudation rates in the Southern Alps with the use of in-situ ^{10}Be. While their study was mainly concerned with soil production, their results also indicate rapid catchment-wide denudation rates of 1-9 mm/yr (1200 - 9200 t km^{-2} yr^{-1}) in West Coast basins. Reusser & Bierman (2010) used meteoric ^{10}Be to identify major sediment sources and understand the transport and mixing of sediment downstream in the Waipaoa. Their study showed the utility of meteoric ^{10}Be in determining sediment movement and mixing dynamics in New Zealand settings, but did not directly quantify rates of erosion. The application of

cosmogenic nuclides to quantify rates of denudation in New Zealand is limited to these two studies, hence there is ample room for further application to better understand the temporal and spatial trends of erosion in New Zealand. To date, no one has combined the use of both in-situ and meteoric ^{10}Be analysis for quantification of denudation rates.

1.6 Objectives

The purpose of this research is first to validate the effectiveness of the use of spatially–averaged cosmogenic nuclide analysis in New Zealand by comparing cosmogenic nuclide-derived denudation rates to current erosion data from the same sample region, and by comparison of both the in-situ and meteoric methods. Second, this research will examine the temporal and spatial trends of erosion in a catchment in New Zealand. Third, this research will quantify the anthropogenic impact on the landscape by comparing benchmark in-situ cosmogenic nuclide denudation rates to existing short term erosion data for the same sample region. These objectives will be addressed with the following questions:

- Can the application of spatially-averaged cosmogenic nuclide analysis be used in New Zealand to determine denudation rates to an acceptable accuracy?
- What are the spatial and temporal trends of long term and short term denudation in the Nelson/Tasman region, New Zealand?
- How did anthropogenic landuse changes impact rates of denudation in the Nelson/Tasman region, New Zealand?

1.7 Thesis structure

Chapter two of this thesis will address the theory and methodology for the application of in-situ and meteoric ^{10}Be analysis and discuss how it is used for quantifying rates of denudation. Chapter three will provide an overview of the Nelson/Tasman region including the geomorphology, geology, soils, tectonics, climate, and erosion of the region. Chapter four will cover the sampling techniques used and laboratory procedures involved in ^{10}Be analysis. Chapter five will provide a review of the results obtained from both ^{10}Be methods. Finally chapter six will address the applicability of the methods in New Zealand and discuss the spatial and temporal trends of denudation in the Nelson/Tasman region.

Chapter two: Cosmogenic Nuclides

2.1 Cosmic Rays

2.1.1 Cosmic ray origins and cascades

The atmosphere is bombarded by cosmic rays from all directions predominantly in the form of protons (90%), but also helium nuclei (~9%), and electrons (~1%) (Dunai, 2010). Cosmic rays can originate from outside the solar system (galactic) or within the solar system from the sun (solar). Interactions of galactic cosmic rays with the earth's atmosphere and surface will be considered because their energies are much higher (MeV up to ~10^{20} eV) than solar cosmic rays (<1GeV; 1-100 MeV) meaning they account for most cosmogenic nuclide production (Masarik & Reedy, 1995). Most solar cosmic rays are blocked or their energies are too low to cause reactions. The majority of cosmic rays that reach the earth's atmosphere originate from the Milky Way galaxy; however, it is believed that some are able to penetrate from major supernova events outside the Milky Way. Supernova explosions generate the conditions to accelerate cosmic rays to the high energies needed to enter the earth's atmosphere. The galactic cosmic ray flux for the past 10 Myrs is considered constant – originating from supernova explosions that have occurred in our galaxy ~once every 50 years (Diehl et al., 2006).

Cosmic rays enter the earth's atmosphere as primary rays and reactions can occur with atoms in the atmosphere resulting in a secondary cascade (Dunai, 2010; von Blanckenburg, 2006). Secondary cascades of cosmic rays (predominantly neutrons and muons) account for most of the production of cosmogenic nuclides in the atmosphere and at the earth's surface. 98% of nuclide production at the earth's surface occurs as a result of secondary cosmic ray cascades–the other 2% may reach the earth's surface as very high energy primary cosmic rays (Dunai, 2010).

2.1.2 Cosmic ray intensity and interactions with the magnetic field

Primary cosmic ray intensity is directly related to the strength of the geomagnetic field (Lal, 1991). The geomagnetic field protects the earth from primary cosmic radiation and relents only to high-energy charged galactic particles. Low energy particles (including solar cosmic radiation) have negligible contribution to cosmogenic nuclide

concentrations. Latitudinal variation in the magnetic field results in the poles receiving considerably more radiation than the equator (*figure 2.1)* due to the magnetic field's decrease in intensity and increase in inclination with increase of latitude. The equatorial magnetic field's rigidity prevents many primary particles from penetrating the atmosphere meaning energies of cosmic rays must be in excess of 10GV while only >0.6GV at the poles (Michel et al., 1996). Secondary cosmic ray cascades then also become dependent on the pressure of the air (and therefore altitude) because of attenuation (Lal & Peters, 1967) – altitudinal pressure variation determines the intensity of cosmic rays and therefore the production of nuclides. Higher air pressures (lower altitudes) have lower production rates while lower air pressures (higher altitudes) have higher production (Stone, 2000). However, where the total thickness of the atmosphere is greater, there are more target nuclei for reactions to occur and vice versa, adding to the complexity of production and delivery of atmospheric nuclides (Willenbring & von Blanckenburg. 2010) which will be further discussed. Despite a constant galactic cosmic ray flux, there has been significant variation in the intensity of cosmic rays on earth over geological timescales, for example, 20ky ago cosmic ray intensity was only 60% of today's intensity (von Blanckenburg, 2006).

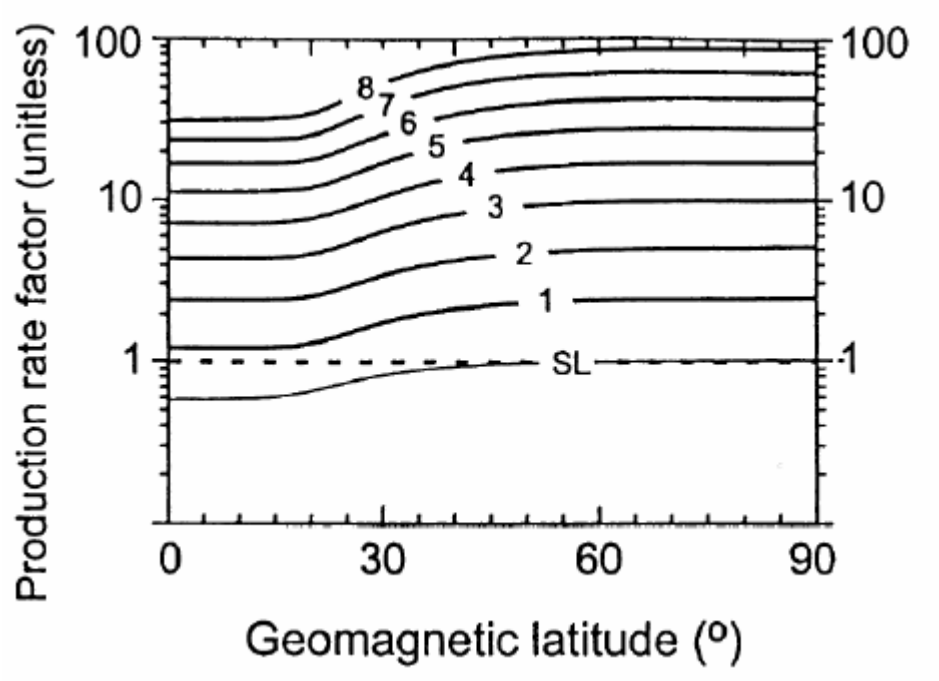

Figure 2.1: Variation of nuclide production rates with latitude and altitude from sea level to 8km above sea level. Note the increase in production between ~30° - 60°, and little variation between ~0° - 30° and ~60° - 90°. (Source: Lal, 1991; Gosse & Phillips, 2001; Norton, 2008)

2.2 Cosmogenic nuclide production

2.2.1 Production of meteoric nuclides

As cosmic rays collide with atmospheric gases such as nitrogen and oxygen they cause nuclear reactions with the gases' nuclei and ultimately result in the production of meteoric cosmogenic nuclides. Reactions most commonly occur as spallation where high energy nucleons collide with atomic nuclei which results in fragmentation and the release of several lighter protons and neutrons (Gosse & Phillips, 2001). Meteoric nuclides are produced at a rate of ~10^6 atoms cm^{-2} yr^{-1} (McHargue & Damon, 1991; Gosse & Phillips, 2001), 99% of which occurs at altitudes greater than 3km (Willlenbring & von Blanckenburg, 2010).

At high latitudes the production of nuclides is greater because the over-lying atmospheric column of air is shallower, making it easier for primary and secondary cosmic rays to penetrate. However, at lower latitudes the atmospheric column contains a greater mass of air in which reactions can occur and nuclides can accumulate (Willenbring & von Blanckenburg, 2010). For these reasons, atmospheric nuclide flux to the earth's surface is greatest at mid-latitudes. Meteoric ^{10}Be is distributed to the earth's surface via wet (precipitation) or dry (dust fall) deposition where it readily adsorbs to sediment particles – typically on to fine grain sizes in the top 1.5m of the soil profile. The highest concentration of nuclides most commonly resides in the uppermost surface which then decreases exponentially with depth; however, adsorption can vary according to the mineralogy and grainsize distribution of the soil profile (Willenbring & von Blanckenburg, 2010).

2.2.2 Production of in-situ nuclides

In-situ nuclide production is essentially the same as meteoric production however the production occurs in the earth's surface in the mineral lattices of soil particles or bedrock. More than 98% of in-situ cosmogenic nuclides are produced from secondary cosmic ray particles (nucleons and muons) with varying nuclear reactions related to the energy of the particle (Dunai, 2010). Production rates of in-situ nuclides is much poorer than meteoric at only ~2-20 atoms $g_{mineral}^{-1}$ yr^{-1} (McHargue & Damon, 1991; Gosse & Phillips, 2001), depending on the nuclide and the mineral in which it is produced. This is due to the loss of energy in the secondary cascade. Nuclei produced by the in-situ and meteoric processes are easily separatedfrom one another because in-situ nuclides are

locked in the mineral where the reaction has occurred requiring dissolution of the crystal lattice for analysis, whereas meteoric nuclides are sourced from the atmosphere which then bind to sediment particles and can be analysed through chemical stripping of the grain (Willenbring & von Blanckenburg, 2010).

Production of nuclides decreases exponentially with depth according to the cosmic ray mean free path (Λ) and the density of the minerals in which the cosmic rays are interacting with; this is referred to as an absorption depth (Lal, 1991). Nucleonic absorption decreases substantially with depth in rock – at 2 metres depth, production rate is only ~3% of the rate of surface production. For muonic absorption, however, the decrease in production with depth is much slower, meaning muonic reactions contribute to deeper rocks and sediment (~7-10 m) than nucleonic reactions (Dunai, 2010). There are a variety of nuclide types produced in the atmosphere and in the earth's surface with large variability in their rates of production. The type of nuclide that is produced is dependent on the energy of the cosmic ray and the chemical conditions of the target mineral (Gosse & Phillips, 2001). These include stable nuclides such as ^{3}He, ^{21}Ne, ^{36}Ar, and radio-nuclides such as ^{10}Be, ^{14}C, ^{26}Al, ^{36}Cl (eg. Lal, 1991; Cerling & Craig, 1994; Gosse & Phillips, 2001; Porcelli et al., 2002; Balco & Shuster, 2009). Of particular interest here is the production of the radionuclide ^{10}Be which has proven useful for a number of cosmogenic nuclide analyses in earth science.

2.2.3. Production of ^{10}Be

Appreciable ^{10}Be is found only in material that has been exposed to cosmic radiation where it decays with a half-life of 1.39 Myr (Nishiizumi et al., 2007; Chmeleff et al., 2009; Korschinek et al., 2009) (*figure 2.2*).

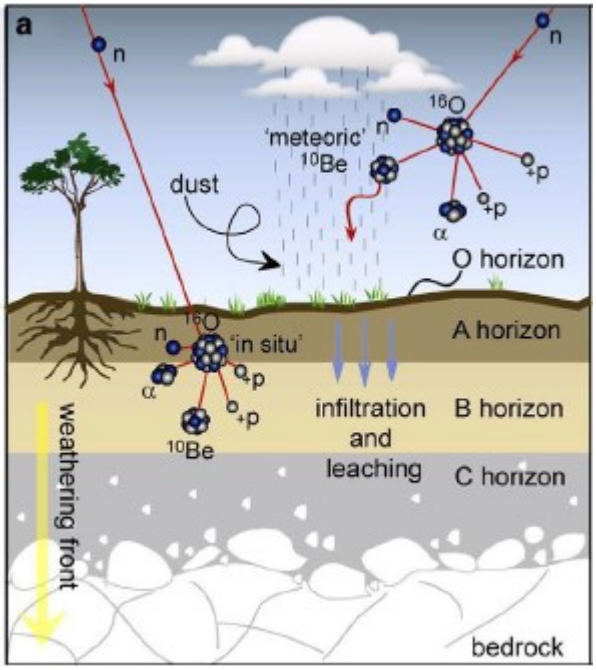

Figure 2.2: Production of meteoric ^{10}Be in the atmosphere, delivery to the earth's surface via dust and precipitation, and infiltration and leaching into the soil column, and production of in-situ ^{10}Be in the earth's surface. (Source: Willenbring & von Blanckenburg, 2010)

The production rate of in-situ ^{10}Be in quartz has been constrained with analysis of in-situ ^{10}Be concentrations of surfaces of known ages such as landslide scarps and glacially-polished areas to 4.99 ± 0.3 atoms g^{-1} yr^{-1} when scaled to sea level at high latitudes (SLHL) (Stone, 2000) (*figure 2.3*). This production rate is relatively slow in comparison to the likes of ^{3}He in olivine which produces ~119 atoms g^{-1} $year^{-1}$ at SLHL (Licciardi et al., 1999).

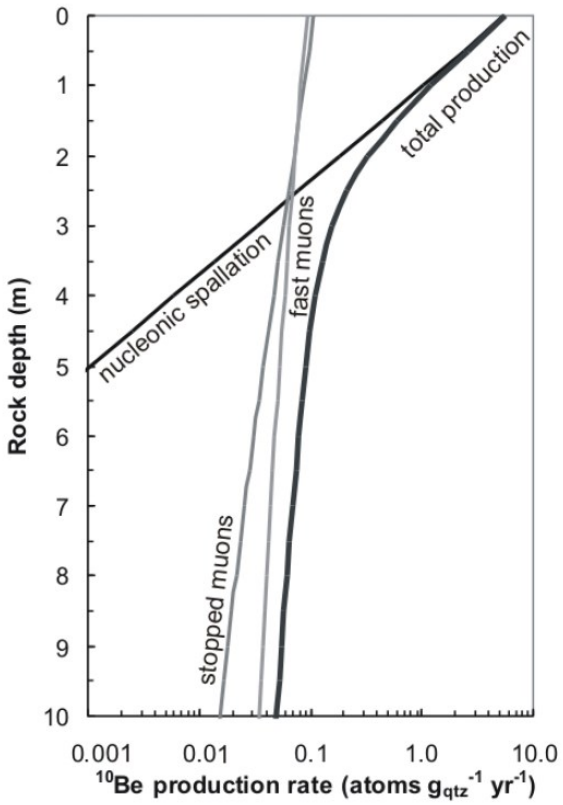

Figure 2.3: Production of in-situ ^{10}Be (atoms g $_{quartz}^{-1}$ yr^{-1}) with rock depth below the surface (m) assuming a rock density of 2.7 g cm^{-3}. Note the production of nucleonic ^{10}Be decreases exponentially below the surface while muonic ^{10}Be is produced as deep as ~10m. Muonic production contributes ~30.6% of surface production in a rapidly eroding setting, and ~<5% in a slow eroding setting rendering its importance for inclusion in nuclide production calculations (Granger and Smith, 2000; Schaller et al., 2002) (Source: Norton, 2008)

Global production rate of meteoric ^{10}Be varies with latitude and altitude (*figure 2.4*) but has been constrained to ~1 x 10^{6} atoms cm^{-2} yr^{-1} (McHague & Damon, 1991; Gosse & Phillips, 2001).

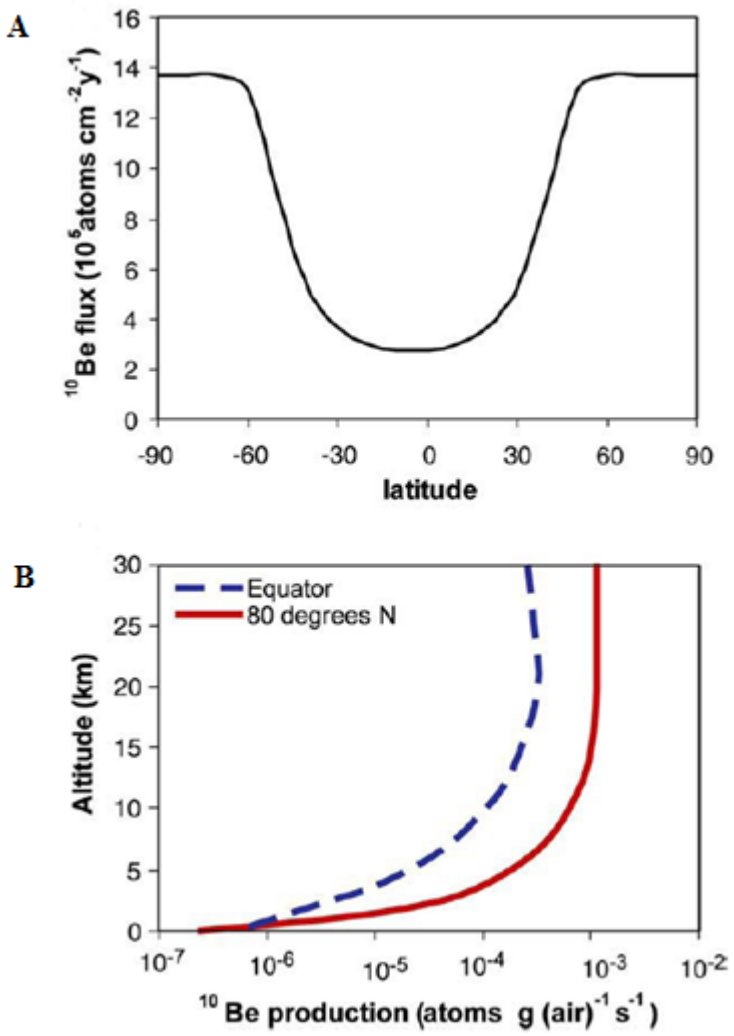

Figure 2.4: A) Latitudinal variation of meteoric ^{10}Be production (10^5 atoms cm^{-2} yr^{-1}) derived for long term solar modulation (ϕ=550 MeV) and present geomagnetic field intensity at sea level (Masarik & Beer, 1999; Willenbring & von Blanckenburg, 2010). B) Altitudinal variation (km) in meteoric ^{10}Be production (atoms g (air)$^{-1}$ s^{-1}) at the equator and at 80° N (Masarik & Beer, 1999) derived for long term solar modulation (ϕ=550 MeV) and present geomagnetic intensity (with the use of Staiger et al., 2007's data translated to altitude) (Source: Willenbring & von Blanckenburg, 2010).

Calibration of in-situ production rates in the central Southern Alps was completed by Putnam et al., (2010) suggesting a sea level high latitude (SLHL) production rate of 3.4 - 4.15 atoms g^{-1} yr^{-1}. Meteoric ^{10}Be production has been constrained for three locations in New Zealand including Leigh (near Auckland), Gracefield (near Wellington), and Dunedin. The Gracefield production rates are in the order of ˜27 × 10^9 atoms m^{-2} y^{-1}, while in Dunedin, production is 9 × 10^9 atoms m^{-2} y $^{-1}$ (Graham et al., 2003).

2.3 Application of ^{10}Be for rates of denudation

2.3.1 Applications

^{10}Be and a number of other radionuclides have been used commonly for dating exposed surfaces (eg. Ivy-Ochs, 1995; Kelly et al., 2004; Wilson et al., 2013) as the concentration of nuclides in an exposed surface increases with time. The production of ^{10}Be at different latitudes, altitudes, and in different minerals (particularly quartz), has been well enough constrained that it can provide a confident age of the exposure time of the mineral at the surface (an age).It has been possible to date such things as lava flows (Shephard et al., (1995), de-glaciation (eg. Badding et al., 2013), terraces (eg. Cording et al., 2014), and fault scarps (eg. Hippolyte et al., 2006). They have further been used to estimate time since a mineral was buried through knowledge of the rate of decay and therefore the time since the mineral was blocked from cosmic ray exposure (Granger, 2006; Denhert & Schluchter, 2008; Balco & Rovey, 2008a). It is also possible then to infer the rate of denudation at the surface giving indication as to how much material has been removed in denudation relative to surrounding sample sites. This will be considered in the following sections.

2.3.2 Denudation rates derived from in-situ ^{10}Be analysis

Particles move toward the surface in proportion to the rate of denudation as nuclides accumulate over time. With a constant rate of nuclide production, Lal (1991) introduced an equation for the calculation of denudation rates from nuclide concentration at depth:

$$N(z,t) = N(z,0)e^{-\lambda t} + \frac{P(0)}{\lambda+\frac{\rho\varepsilon}{\Lambda}} e^{\frac{-z\times\rho}{\Lambda}} \times \left(1 - e^{1\left(\lambda+\frac{\rho\varepsilon}{\Lambda}\right)t}\right) \qquad \text{(eq. 1)}$$

where P is the production rate at depth, N is the nuclide concentration, $N(z,0)e^{-\lambda t}$ is the term for inheritance, P(0) is the surface production rate in relation to latitude and altitude, λ is the half-life of the measured nuclide, t is the time of exposure, ρ is the rock density, ε is the denuation rate, and Λ is the cosmic ray mean free path.

Erosion occurs at the surface of the landscape therefore we are interested in a z value of 0. Additionally, in an eroding landscape it can be assumed that there is no inheritance (ie. $N(z,0)e^{-\lambda t} = 0$) therefore this can be excluded in the equation:

$$N(t) = \frac{P(0)}{\lambda + \frac{\rho\varepsilon}{\Lambda}} \times \left(1 - e^{-\left(\lambda + \frac{\rho\varepsilon}{\Lambda}\right)t}\right) \quad \text{(eq. 2)}$$

For the landscape to attain isotopic steady state (this will be further discussed), it is required that the time over which steady erosion has occurred is be much greater than the erosional timescale (ie. $t >> \rho\varepsilon/\Lambda$). Here, denudation rates from surface in-situ nuclide concentrations (N) can be measured using the following equation:

$$N(t) = \frac{P(0)}{\lambda + \frac{\varepsilon}{z^*}} \quad \text{(eq. 3)}$$

where P(0) = cosmogenic production rate in relation to latitude and altitude, z* is the attenuation depth (Λ divided by ρ),and (λ) is the decay constant of the known nuclide.

2.3.3 Erosion rates derived from meteoric ^{10}Be analysis

The apparent age of soil can also be calculated with an inventory of meteoric nuclide concentrations through a soil column with the assumption that change in inventory through time = loss through radioactive decay and erosion and gains through meteoric ^{10}Be flux:

$$\frac{d}{dt}I(t) = -\lambda I(t) - N_{\text{surf}}(t)\rho\varepsilon(t) + Q(t) \quad \text{(eq. 4)}$$

where λ is the half-life of ^{10}Be, $\varepsilon(t)$ is the erosion rate of the surface (cm y^{-1}), and N_{surf} is the concentration of ^{10}Be at the surface (atoms g^{-1}). With the assumption that isotopic steady state exists and the radioactive decay time is sufficiently longer than the apparent

age, the landscape's erosion rate can then be calculated from meteoric ^{10}Be concentrations using the following equation:

$$E = \frac{\mathrm{Q}}{\rho N_{surf}} \qquad \text{(eq. 5)}$$

where Q is the local flux of atmospheric nuclides, ρ is the soil density, and N_{surf} is the nuclide concentration of a sample taken from the surface.

2.3.4 Apparent ages and denudational timescales

The concentration of nuclides in basin-averaged samples can be referred to as an apparent age because it represents the mineral's exposure time at the surface. The apparent age is used in calculating the denudational timescale which represents the time it takes to erode one attenuation depth scale (or the residence time in soil and rock) (von Blanckenburg, 2006). In-situ averaging timescales are calculated by dividing the denudation rate by an attenuation depth scale. The attenuation depth is a function of the density of materials that rays are passing into (2.6 g cm^{-3} for bedrock) and the cosmic ray mean free path (150 g cm^{-2}) (Lal, 1991). The attenuation depth commonly used for in-situ ^{10}Be analysis is 0.6m for bedrock and 1.0m for soil and timescales will vary depending on rate of denudation (*figure 2.5*).

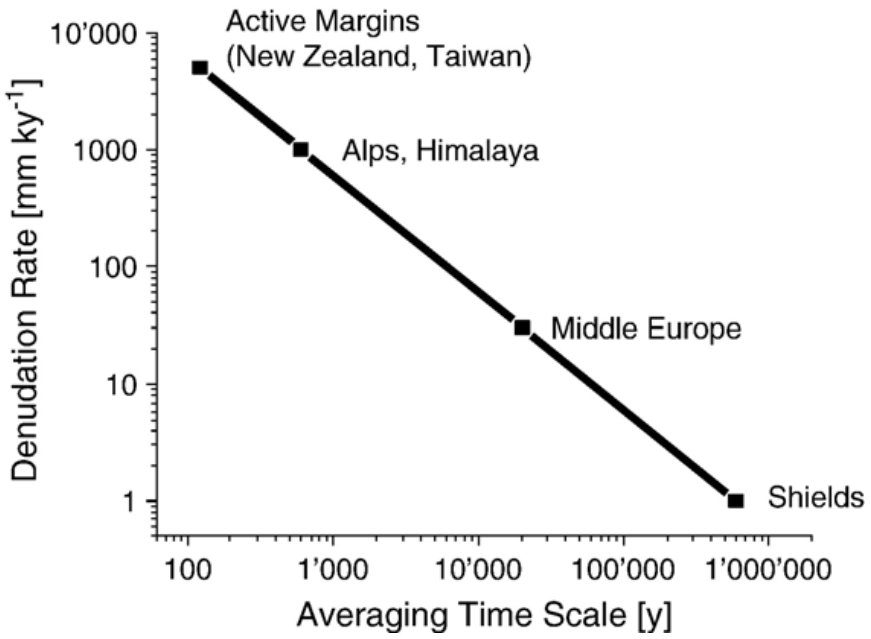

Figure 2.5: Averaging timescales for in-situ-derived denudation rates. Timescales are directly related to the denudation rate – rapid denudation will result in a shorter averaging timescale as the time it takes to erode one adsorption depth length will be shorter (von Blanckenburg, 2006). Note the short timescales represented in studies in active margins such as New Zealand (e.g. the West Coast rates from Larsen et al., 2013). (Source: von Blanckenburg, 2006)

Similar to in-situ, meteoric averaging timescales represent the time it takes to erode the soil column or the time it takes to reach equilibrium. The surface concentration is divided by the adsorption length (derived by obtaining a depth inventory of nuclide concentrations) to obtain the timescale in which the concentrations are representative of (Willenbring & von Blanckenburg, 2010). Timescales for meteoric ^{10}Be analysis can be variable due to the unique behaviour of different types of regolith and the efficiency of adsorption through the regolith profile (*figure 2.6*).

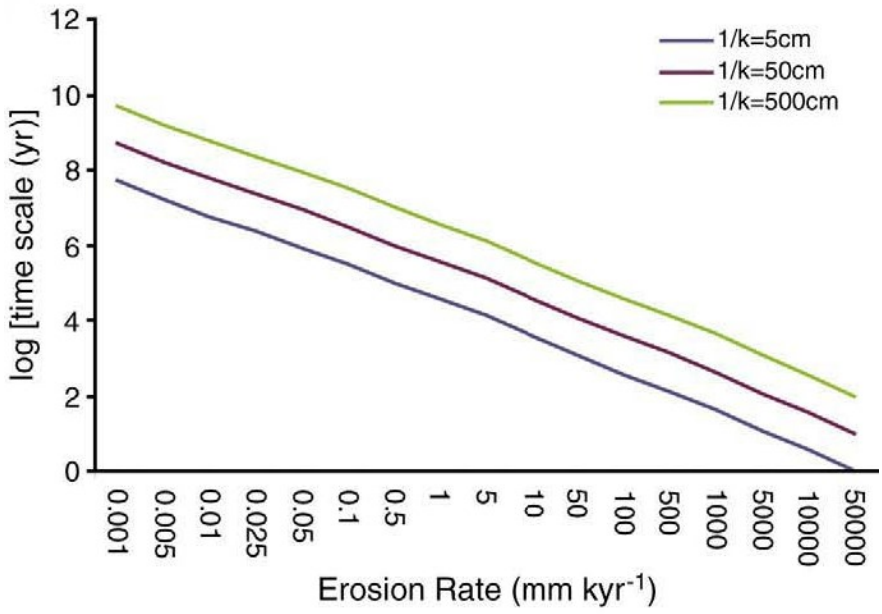

Figure 2.6: Similar to in-situ, meteoric averaging timescales decrease with increasing denudation rate. (Source: Willenbring & von Blanckenburg, 2010).

2.4 Basin-averaged denudation

2.4.1 Basin-averaged theory

As the landscape erodes, new material is brought to the surface to be exposed to cosmic rays and atmospheric inputs. The surface of the earth will accumulate cosmogenic nuclides via atmospheric delivery or direct surface production, and nuclides will be removed by denudation. A high nuclide concentration would suggest that significant exposure time has allowed for the accumulation of nuclides and therefore is indicative of slow erosion of the landscape (Granger et al., 1996; Binnie et al., 2006; Savi et al., 2014). A low nuclide concentration would suggest that exposure time has been shorter and minerals have not had time accumulate nuclides before material has been removed from the landscape, and therefore, is indicative of rapid erosion (Granger et al., 1996).

The eroded material from a landscape is delivered to rivers where it is mixed; therefore, it can be assumed that sediments from a river provide an average nuclide concentration of an entire catchment upstream of where the sample is taken (Brown et al., 1995) (*figure 2.7*). Samples should be obtained from location where material is most likely truly mixed - i.e. sufficiently downstream of confluences to ensure thorough mixing of material. With these assumptions it is possible to estimate a basin-averaged denudation rate. In-situ ^{10}Be concentrations are suitable for quantification of long term background

erosion rates with averaging timescales on the order of 10^2 - 10^5 years (eg. Brown et al., 1995; Granger et al., 1996; Schaller et al., 2001; Vanacker et al., 2007; von Blanckenburg, 2006). Meteoric ^{10}Be can be used to estimate erosion rates of variable timescales, depending on the depth at which the ^{10}Be adsorbs and therefore the timescales which it represents (Willenbring & von Blanckenburg, 2010; von Blanckenburg et al., 2012). The term 'erosion' is used for meteoric analysis (as opposed to denudation) as meteoric ^{10}Be resides in the soil column where sediment is already weathered meaning chemical weathering (which is included in denudation) is not considered.

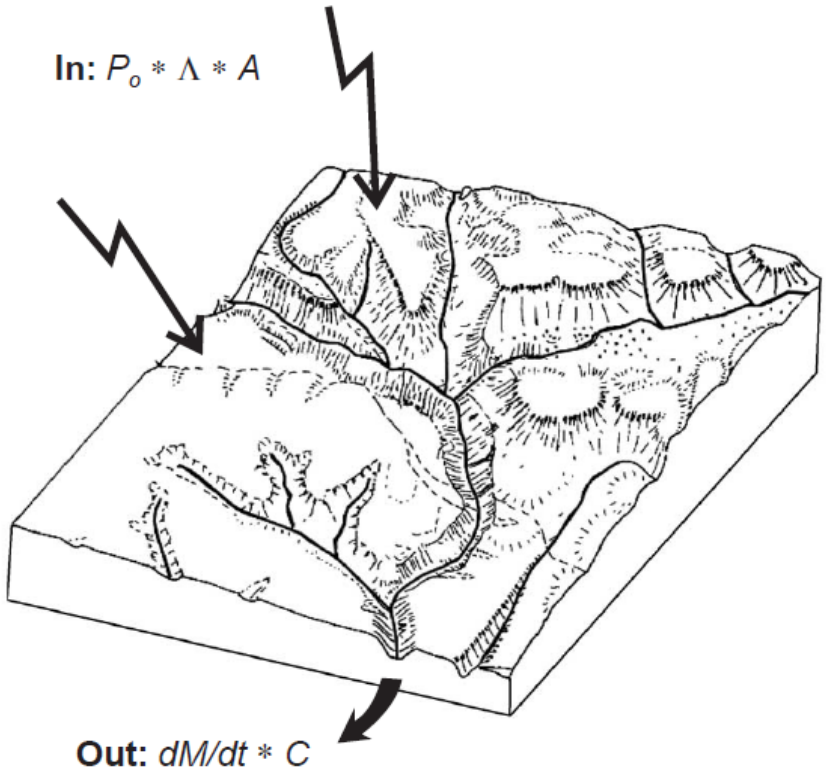

Figure 2.7: Illustration of basin-averaged theory. Nuclides are produced throughout the catchment and are delivered to rivers. Rivers mix the sediment meaning river sediment samples can provide a representation of all erosion sources of the catchment upstream of the sample. With the assumption that the influx of nuclides (production rate * half-life * basin area) equals the outflux via denudation, and that steady state exists, basin-averaged denudation rates are inversely proportional to nuclide concentrations in river sediments (Source: von Blanckenburg, 2006).

2.4.2 Basin-averaged denudation from analysis of in-situ ^{10}Be

In-situ cosmogenic nuclide concentrations are relatively unaffected by any recent anthropogenic changes that have affected erosion dynamics, or by any previous large scale, short term increases in erosion (von Blanckenburg, 2006). This presents their

suitability for quantification of long term background rates of denudation, representative of timescales on the order of $10^2 – 10^5$ yrs (Granger et al., 1996; von Blanckenburg, 2006). To account for lithological differences and for the contributing catchment area, the mass flux is divided by the catchment area and the rock density – this provides a catchment-wide denudation rate ε (mm ky^{-1}) (von Blanckenburg, 2006).

The most commonly used in-situ nuclide for basin-averaged denudation rates has been ^{10}Be, largely due to its abundance in quartz (a common mineral in the earth's surface), its long half-life, and its absence in rock before it has been exposed to cosmic rays. ^{26}Al is also relatively common although it has not been as well constrained as ^{10}Be and validation of its accuracy is poorer. ^{10}Be is commonly extracted from quartz due to its common abundance in rocks and sediments (von Blanckenburg, 2006). Quartz is also highly resistant weathering due to its physical hardness and minimal-reactivity to acids, meaning loss of nuclide through chemical erosion does not become a major factor affecting nuclide concentrations. It also provides a simple target chemistry for which the production rate of cosmogenic nuclides used will be uniform (von Blanckenburg, 2006)

2.4.3 Assumptions, considerations, and requisites

2.4.3.1 Isotopic steady state/uniform erosion

Isotopic steady state, where the amount of ^{10}Be that leaves the catchment in denudation via the river is equal to the amount of ^{10}Be that enters the system through production, is a requirement for both meteoric and in-situ ^{10}Be analysis (von Blanckenburg, 2006). This requires careful selection of a study location – the assumption becomes more tenuous in areas where mass wasting is prevalent (common in steep landscapes subject to high rainfall), where there is significant tectonic activity, or where the landscape is particularly slow at eroding (eg. shield landscapes). This also limits the applicability of the method to catchments that are reasonably sized so that it is plausible to assume that all erosion sources are represented in the samples taken (von Blanckenburg, 2006).

Deep seated landslides can expose material that was previously isolated from cosmic rays and contribute this material to basin-averaged samples, over-representing its erosion source. Yanites et al. (2009) used numerical models to understand the effect of landsliding on nuclide mixing and found that in a basin where shallow landsliding had occurred (soil only), ^{10}Be analysis could still produce reliable denudation rates even in small basins. Deep-seated landslides were found not to affect rates from large basins (≥

100 km^2) where mixing was sufficient. However, in small basins, factors such as mean landslide depth of the entire basin, percent sediment representative of background erosion, and proportion of landslide in the basin` may result in significant differences (Yanites et al., 2009). Furthermore, where intervals between landslides are short, larger catchments were needed to obtain accurate basin-averaged denudation rates. Sediment sampling has been found to produce accurate results where time intervals between landslides are sufficient (Niemi et al., 2005).

2.4.3.2 Lithology

The distribution of the desired mineral (commonly quartz) within the basin is important to consider in order to accurately represent the contribution of each lithology to the overall erosion rate of the landscape. If a significant portion of material in the catchment is delivered from a differing geology unit and contributes extensively to total denudation, results can be biased toward this. This potential problem is avoided by preferential selection of geologically homogenous catchments or lithologies with a similar quartz content (von Blanckenburg, 2006).

2.4.3.3 Storage and transport

Storage and transport of sediment must also be considered in the application of both the meteoric and in-situ ^{10}Be methods. Where sediments are stored for periods longer than the erosional timescale, nuclide concentrations can be affected by excess exposure near the surface from extended residence times, or by decay from shielding during prolonged deposition (Brown et al., 1992; Granger et al., 1996; von Blanckenburg, 2006). This is a more tenuous issue to address. Hippe et al. (2012) found excess storage of ^{10}Be in systems with very low gradients because they were transport-limited; however, Wittmann & von Blanckenburg (2009) showed that in most natural settings, ^{10}Be concentrations would not change appreciably.

2.4.3.4 Grainsize

It must be considered that denudation rates may be affected by variability of grainsize. Some studies have found that there has been no grainsize dependence for rates of denudation (Granger et al., 1996; Clapp et al., 2001). Other studies (Brown et al., 1995; Brown et al., 1998; Matmon et al., 2003b) however have found that concentrations are higher in smaller grainsizes than larger due to the contribution of variable sediment

sizes from differing erosion mechanisms. Brown et al. (1995) suggested particles < 1 mm were representative of diffusive erosion processes, while particles > 1 mm were representative of erosion via mass wasting. Matmon et al. (2003) proposed a sediment provenance mechanism where larger grainsizes were subject to more shielding. Alternatively, Belmont et al. (2007) found that gravel produced higher concentrations in downstream samples but lower concentrations in upstream samples. This suggests that variable erosion mechanisms produce variable grainsize dependencies and no global trends in which universal corrections can be determined.

2.4.3.5 Shielding

Shielding as a result of topographical variability has an influence on the production rate of nuclides – objects that obstruct cosmic ray exposure such as steep terrain shielding can have an influence on rates of nuclide production in minerals (Dunne et al., 1999; Codilean, 2006; Norton & Vanacker, 2009). Snow and vegetation cover can also greatly affect the penetration of cosmic rays and therefore must be accounted for in corrections for nuclide concentrations (von Blanckenburg, 2006).

2.4.3.6 Quartz enrichment

Quartz, a mineral resistant to erosion and weathering, can be preferentially retained in regolith where other minerals can experience dissolution (Riebe et al., 2001a). Intense chemical weathering is predominantly associated with tropical settings. Riebe et al., (2001a) found that areas of intense weathering could affect ^{10}Be-derived rates by up to 50%; however temperate climate environments such as New Zealand are likely to be affected by quartz enrichment by an average of only ~6%. This affect is minimal and is considered too small to address the effects at the basin-averaged scale; therefore it is plausible to make the assumption that quartz enrichment is not an issue that could significantly affect the validity of ^{10}Be-derived rates in New Zealand.

2.4.4 Basin-averaged denudation from analysis of meteoric ^{10}Be

When delivered to the earth's surface, meteoric ^{10}Be resides for the life-span of the soil/sediment particles until it decays or erodes with the landscape, providing a geochemical tracer from which erosion rates and soil residence times can be recorded. Of particular interest is the potential for basin-averaged erosion rates to be recorded from meteoric nuclide concentration in fine river sediments (eg. Willenbring & von

Blanckenburg, 2010). Meteoric ^{10}Be analysis can be undertaken in silt or clay regardless of the presence of quartz meaning its spatial applicability is relatively extensive. Currently the only meteoric nuclide to be used for erosion studies is ^{10}Be. Its suitability is largely due to its well-constrained production rates and the highly reactive nature of $Be(OH)_2$, ensuring the atoms bind tightly to sediment particles at most natural pH levels where a lot of nuclides do not (Willenbring & von Blanckenburg, 2010).

2.4.5 Assumptions, considerations, and requisites

Meteoric ^{10}Be analysis, similar to in-situ analysis, also functions under the assumptions that the landscape is in isotopic steady state, erosion is uniform, and radioactive decay time is considerably greater than the denudational timescale. Meteoric ^{10}Be analysis also requires that the delivery of ^{10}Be to the surface is known, all Be is within the soil column (ensuring a closed system for inventory), the concentration of ^{10}Be decreases exponentially with depth, and the production of soil on the bedrock equals the soil lost in erosion and decay (Willenbring & von Blanckenburg, 2010). In the following sections the steady state assumption will be discussed further for meteoric analysis. Adsorption of ^{10}Be through the soil profile and the retention behaviour of ^{10}Be to sediment particles and will also be discussed.

2.4.5.1 Isotopic steady state

Similar to in-situ, meteoric ^{10}Be analysis functions under the assumption that the landscape is in isotopic steady state. Alongside the considerations discussed in section 2.4.3.1, the effects of precipitation on delivery of atmospheric ^{10}Be must also be addressed. The atmospheric nuclide flux and the influence of precipitation on the delivery of nuclides to the earth's surface has been disputed amongst studies (*figure 2.8*); however, flux variation can be determined from fallout maps developed through analysis of the general circulation of the atmosphere and nuclide production rates (Field et al., 2006; Heikkila et al., 2008: von Blanckenburg et al., 2012). Flux values range from 0.4 to 1.5 x 10^6 atoms cm^{-2} yr^{-1} (von Blanckenburg et al., 2012), and are affected by orographic rainfall effects and by the potential for precipitation to have an additive or dilution effect (Willenbring & von Blanckenburg, 2010).

In zones where storm tracks dominate, such as the equatorial region, issues can develop where storms travel long distances scavenging ^{10}Be and delivering it far from its source,

producing an additive effect. The coastal/island environment of New Zealand, however, ensures precipitation is predominantly convective; moisture is uplifted close to where it is precipitated, travels only short distances meaning ^{10}Be fallout with precipitation is local. It is relatively unaffected by the addition of ^{10}Be from long distances as a result of advective clouds (Willenbring & von Blanckenburg, 2010). It seems that the rapid turnover of precipitation in New Zealand's island setting scavenges all ^{10}Be (although tested for ^{7}Be) where rainfall is greater than 6-10cm a month (Feely et al., 1989). Atmospheric ^{10}Be delivery, although it fluctuates in the in the short term, does not vary significantly over annual timescales because precipitation scavenges all atmospheric production (Willenbring & von Blanckenburg, 2010).

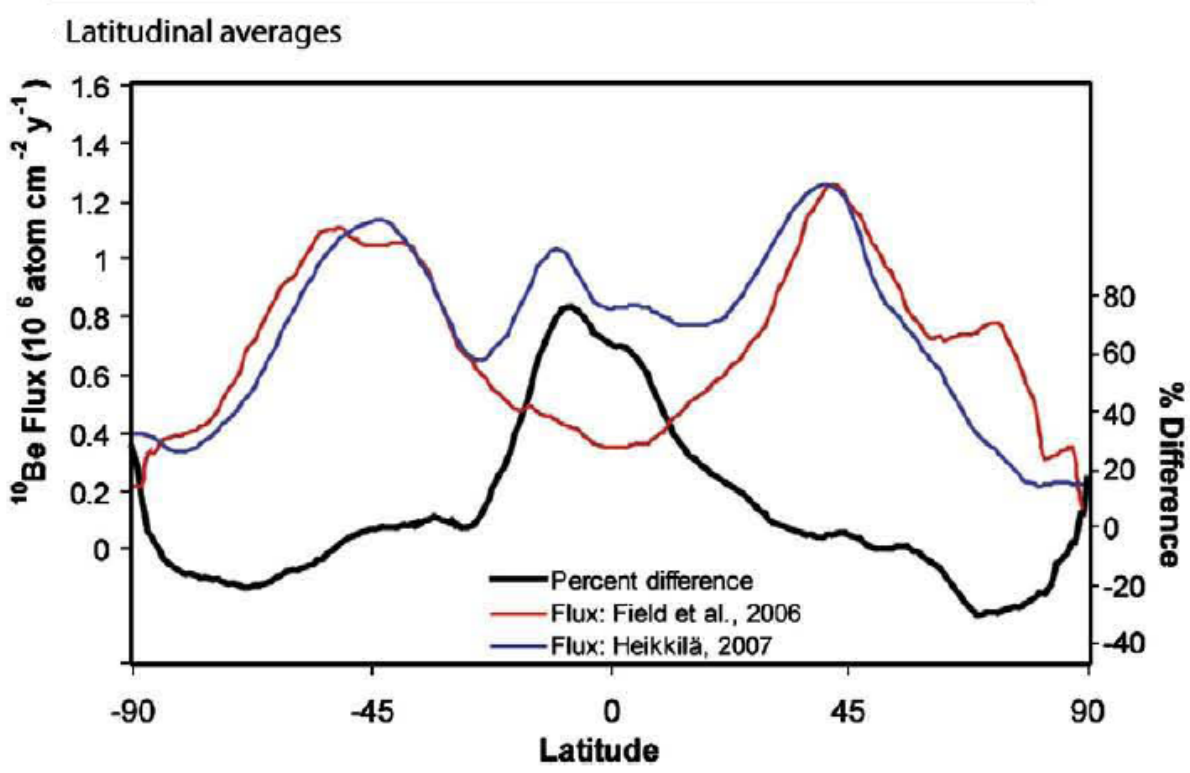

Figure 2.7: Comparison Field et al. (2006) and Heikkila (2007) modelled latitudinal variation in flux of meteoric ^{10}Be. Note the uncertainty regarding meteoric ^{10}Be flux at the equator. Both Field et al. (2006) and Heikkila (2007)'s models are relatively consistent for mid and high latitudes. (Source: Willenbring & von Blanckenburg, 2010)

2.4.5.2 Adsorption and retention

For basin-averaged applications, samples are taken from the surface; therefore it must be assumed that the concentration of nuclides is highest at the surface and that concentrations decrease exponentially with depth. As meteoric ^{10}Be falls to the surface and binds to sediment particles, it is attenuated though the soil column. This distribution occurs as a result of percolation of ^{10}Be-containing water droplets, diffusion and advection, and mobilisation of surface ^{10}Be containing particles via bioturbation. It must be assumed that reworking of sediment involves downward movement of ^{10}Be and the removal of the top soil layer via erosion (Willenbring & von Blanckenburg, 2010). It is typical that young or recently exposed sediments exhibit this exponential decrease in concentration with depth (Pavich et al., 1984; 1986) and this can be described by the following adsorption law:

$$N(z) = N_{\text{surf}} e^{-zk} \qquad \text{(eq. 6)}$$

where N is the concentration of ^{10}Be (atoms g^{-1}), z is the depth at which the concentration is taken, N_{surf} is the concentration at the surface, and k is an adsorption coefficient (Brown et al., 1992). This is plausible where the landscape is at steady state because here erosion rates from surface concentrations will not depend on the adsorption and retention behaviour at depth (Willenbring & von Blanckenburg, 2010).

Alternatively soil columns can display a mid-depth ^{10}Be spike. This has been attributed to the presence of a mid-depth clay rich subsurface horizon (Bt) where the efficiency of adsorption of ^{10}Be is heightened (Pavich et al., 1986; Monaghan et al., 1992). The greater surface area on smaller particles allows for more proficient ion exchange capabilities (Brown et al., 1992). This requires a normalising equation using a power-law function described by He and Walling, 1996; Wallbrink and Murray, 1996: Willenbring & von Blanckenburg (2010) when analysing bulk sediment samples; however, when analysis is undertaken with a single grainsize, normalisation should not be necessary.

When undertaking fluvially-transported ^{10}Be analyses, the retention behaviour of meteoric ^{10}Be is affected by the hydrological pH value (Willenbring & von Blanckenburg, 2010). The retention of beryllium to sediment particles occurs in most environments and most natural pH levels because $BeOH_2$ is very reactive. It is most tightly bound to particles when pH values exceed 6 (von Blanckenburg et al., 2012) which most natural waters tend to be. However, where soil pH is < 4.1, Al^{3+} is released from $Al(OH)_3$ (Berggren & Mulder, 1995) which is known to compete with Be for exchange sites. This is where ^{10}Be can be lost through release from lack of adsorption surface (Willenbring & von Blanckenburg, 2010).

Chapter three: Study Area

3.1 Introduction

New Zealand is situated on the obliquely converging Pacific and indo-Australian Plates which give rise to high relief and significant tectonic and volcanic activity. Climatically New Zealand is also very dynamic due to subjection to high intensity sub-tropical weather systems which contribute, alongside tectonics, to the high natural rates of erosion. The Nelson/Tasman Region was selected for the purposes of this study (*figure 3.1; 3.2*). This region is located in the northwest of the South Island of New Zealand at ~41.5° S 172.8° E, and is made up of two unitary authorities, including Nelson City and the Tasman District. The suitability of the Tasman region for the application spatially-averaged cosmogenic nuclide analysis is primarily due to the abundance in quartz (the mineral from which the in-situ cosmogenic nuclide concentrations were determined) while a lot of New Zealand is quartz poor. The region is predominantly underlain by Moutere gravel and Cretaceous granitic intrusions which are abundant in quartz. This provided a suitable test location for both meteoric and in-situ ^{10}Be analysis. Major features of the region include the western Tasman Mountains, the low-lying Moutere Depression, the Waimea-Flaxmore Fault System, and the Motueka and Waimea river catchments that drain northward into Tasman Bay (*figure 3.2*).The following sections will discuss geomorphology, geology, soil tectonics, climate, and erosion in the Tasman region.

A

B

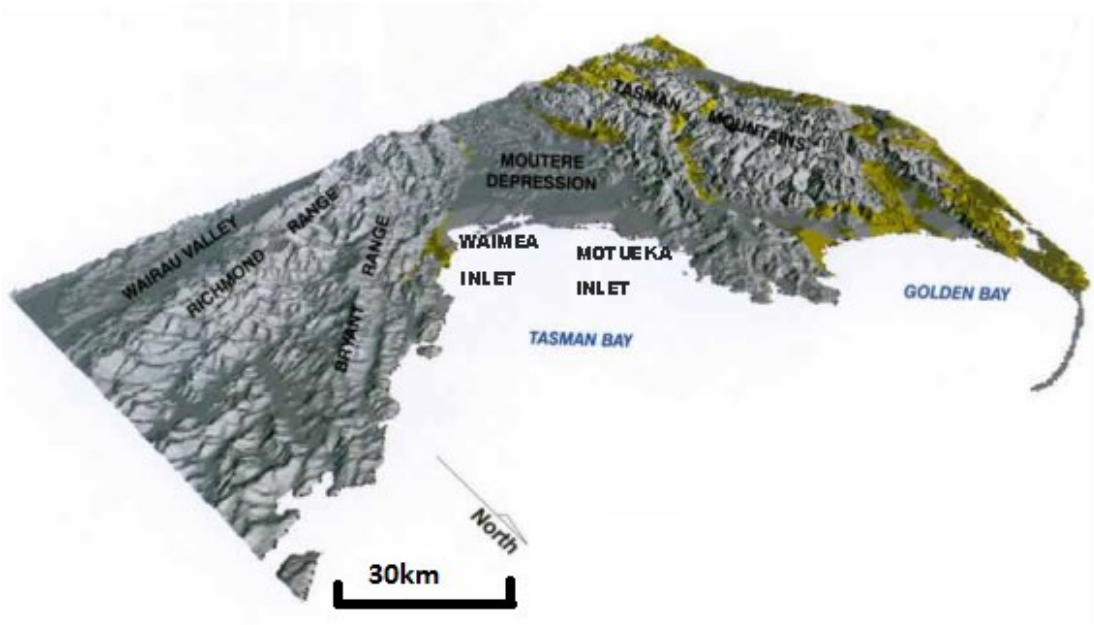

Figure 3.1: A) The Nelson/Tasman region located on the northern South Island of New Zealand (Modified from Google Maps, 2014). B) Geomorphology of the Nelson/Tasman Region. The Motueka and Waimea Rivers drain into Tasman Bay (Source: Rattenbury et al., 1998).

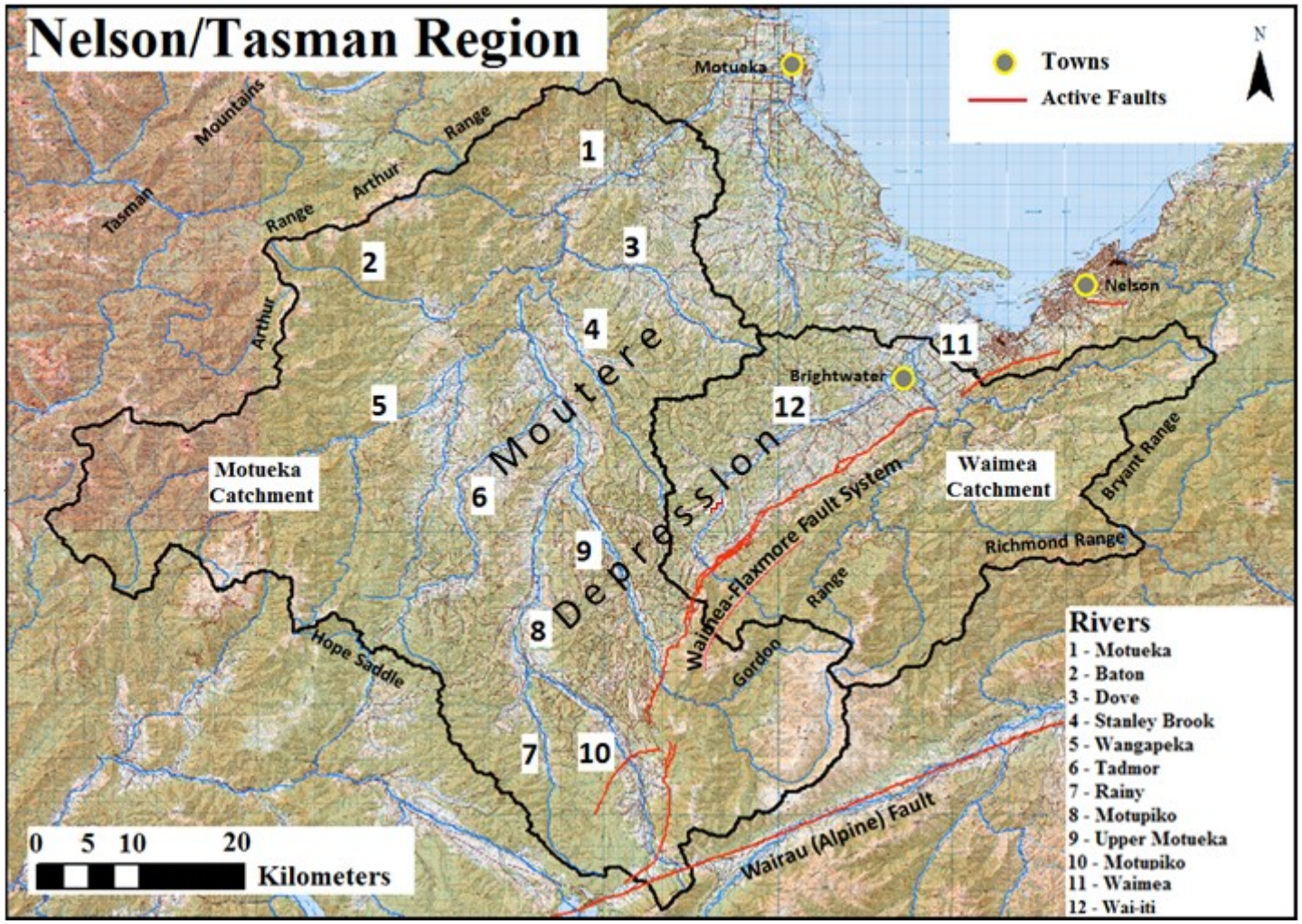

Figure 3.2: Topographic map showing the locations of major features of the Nelson/Tasman region, including the active faults, the Motueka and Waimea catchments and their major rivers, the ranges that surround the Moutere Depression, and some of the prominent settlements of the region.

3.2 Geomorphology

The Motueka, Moutere, and Waimea rivers incise the down-faulted Moutere Depression (*figure 3.*3) which lies between the Tasman Mountains (notably the Arthur Range) and the Richmond, Bryant, and Gordon Ranges (*figure 3.1B; 3.2*). It is a 30km wide depression that formed as a result of uplift of the surrounding mountains during the Pliocene-Pleistocene. The Buller River, which originally flowed north into Tasman Bay, transported gravels from the Spencer Mountains (south of the Moutere depression) to the Moutere Depression from 2.8 Ma – 500ka (Rattenbury et al., 1998). A number of valleys such as the Motupiko and Tadmor characterise the hilly terrain (up to 600m above sea level) of the Moutere Depression. The ranges that surround the Moutere Depression commonly exceed angles of 30°

Figure 3.3: The Moutere Depression looking northeast where much of the Motueka and Waimea catchments drain (Photo courtesy of Quentin Christie. Source: Walrond, 2012).

3.3 Geology

The Moutere Depression which is thought to reach depths of 2500m (Lihou, 1992), comprises predominantly Plio-Pleistocene greywacke-derived Moutere gravels. The Arthur Range, where many of the Motueka's western tributaries originate from, comprises a complex assortment of igneous and sedimentary rock types. These include Devonian to Cambrian basement rocks such as limestone, gabbros, greywacke, argillite,

and diorites, highly erodible Cretaceous granitic rocks, and younger Eocene to Miocene sediments such as limestone, sandstone, and mudstone (Rattenbury et al., 1998). The eastern ranges consist largely of the Dun Mountain-Maitai terrane comprising highly erodible Early Permian ultramafics and volcanic rocks of the Dun Mountain Ultramafics and Livingstone Volcanics groups, and more stable Late Permian to Middle Triassic metamorphosed sedimentary rocks of the Maitai Group (Rattenbury et a., 1998). The Early Permian ultramafics comprise harzburgite, minor dunite, minor wehrlite, gabbro, and plagiogranite (Walcott, 1969) and the Late Permian to Middle Triassic metamorphosed sedimentary rocks comprise breccia, sandstone, limestone, and siltstone (*figure 3.4*). Ultramafics in this area are sparsely vegetated due to high levels of nickel and magnesium (Robinson et al., 1996) which can lead to gullying (*figure 3.5*).

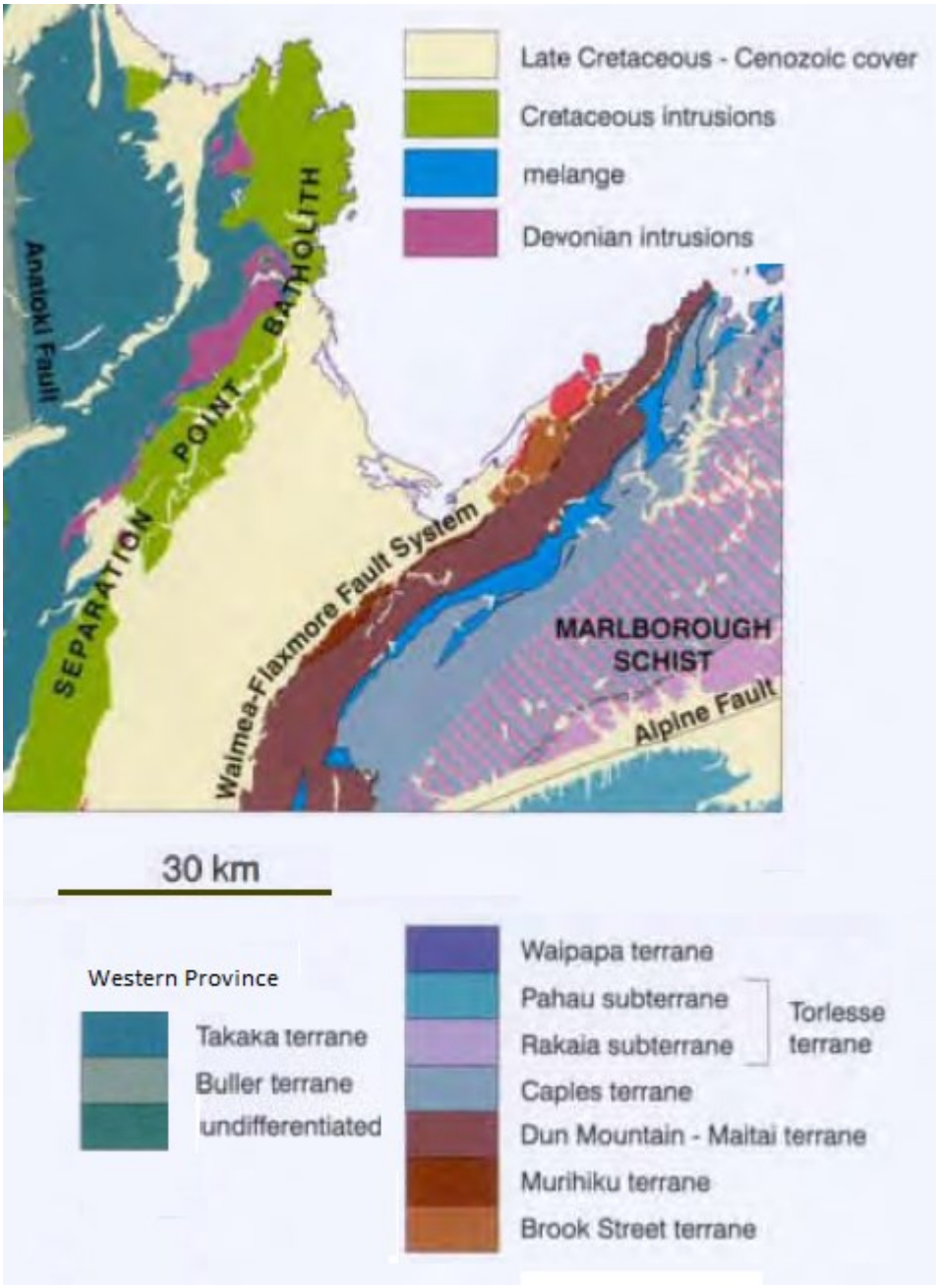

Figure 3.4: The geologic terrane of the northern South Island. (Source: Modified from Rattenbury et al., 1998)

Figure 3.5: Gullying of ultramafic rocks in the Upper Motueka which is located in the southern end of the Motueka catchment (*figure 3.2*) (Source: Basher et al., 2003a).

3.4 Soils and landuse

Soils of the Nelson/Tasman region comprise largely of brown and recent soils (*figure 3.6*). In the Moutere Depression soils are characteristically strongly weathered and leached commonly exhibiting a mid-depth clay (Bt) horizon (Basher & Jackson, 2002). Headwaters of some southern rivers, including the Tadmor and Rainy, comprise pan podzols (*Figure 3.6*) which are characteristically acidic (Landcare Research, 2014).

The Motueka catchment areas is used for commercial forestry (25%) and agriculture (19%), however most of the headwaters is covered by tussock (7%), scrub (12%), and protected indigenous forest (35%) (Kahurangi National Park and Mt. Richmond Forest Park) (Basher, 2003b) (*figure 3.7*). The eastern ranges of the Waimea catchment are largely covered by native forest (~40%), forest planted before 1989 (~15%), and low-producing grasslands (5%), while the grasslands (~20%) of Waimea Plains in the Moutere Depression are used for crops such as hops and grapes because their high productivity. The western side of the Waimea catchment is largely covered by forest that was planted before 1989 (~20%) (*figure 3.7*)

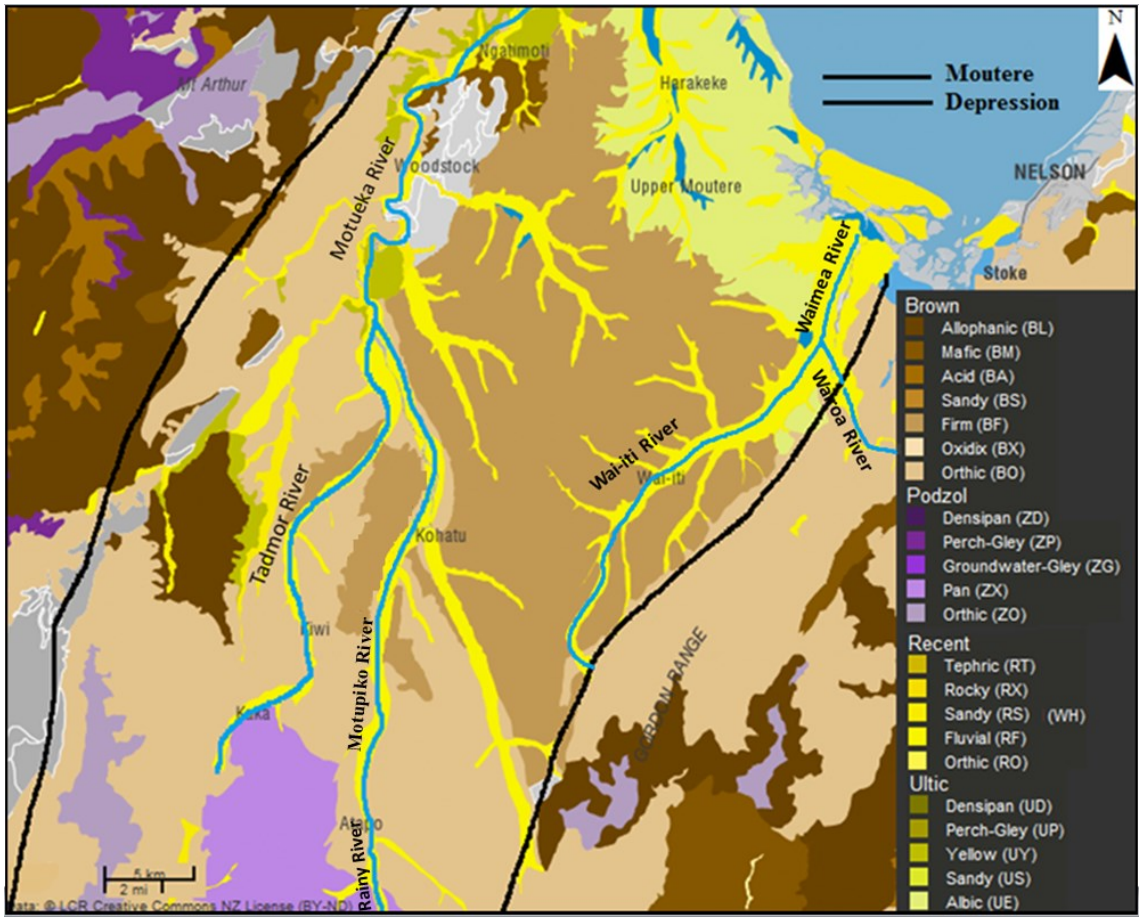

Figure 3.6: Soil cover of the Nelson/Tasman region. Note the location of pan podzols south of the Moutere Depression (Source: Modified from Landcare Research, 2014).

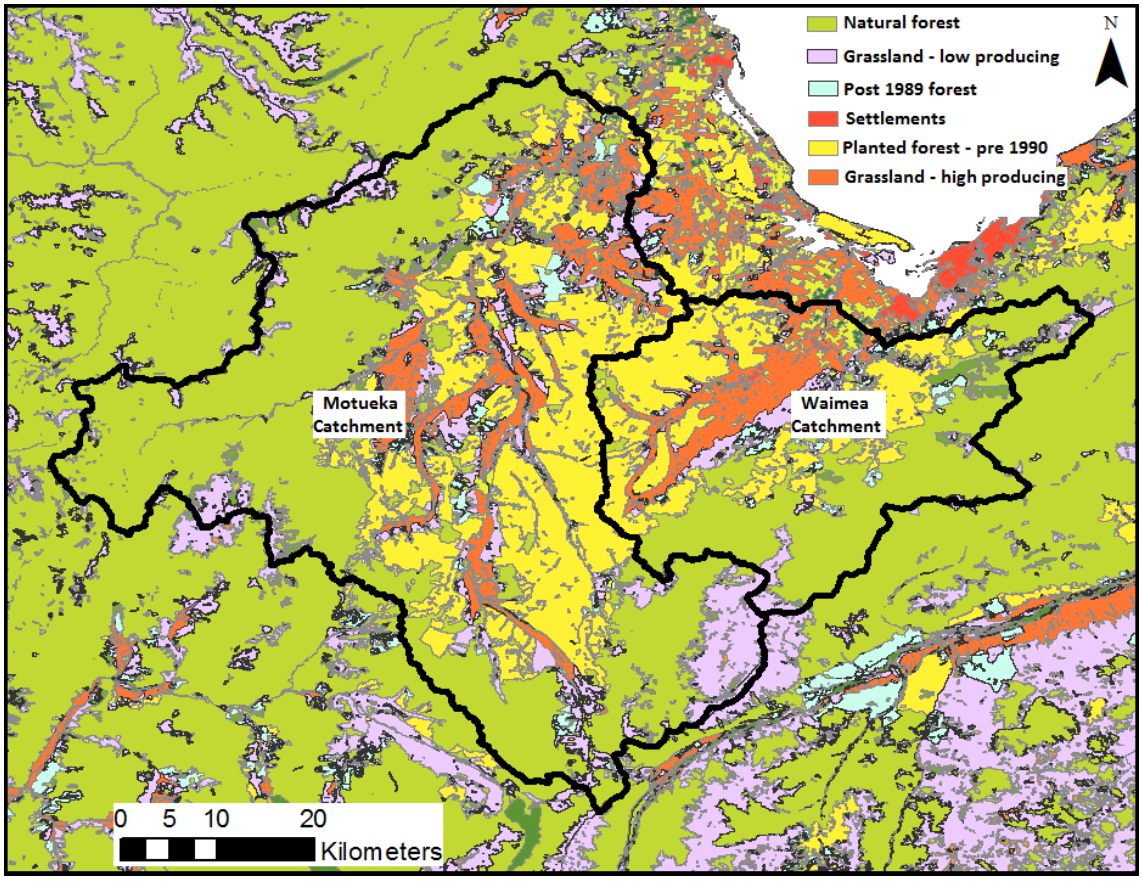

Figure 3.7 Landuse in the Nelson/Tasman region.

3.5 Tectonics

Nelson is a tectonically active region in close proximity to two of active fault systems and a large number of non-active faults (*figure 3.8*). Fault density across the region is relatively high, particularly across the ranges that surround the Moutere Depression. The lower fault density in the Moutere Depression could be the result of poor preservation potential of the Moutere gravel; this could mask minor structures hindering fault identification. The eastern Moutere Depression is fault-bounded by the Waimea-Flaxmore Fault System which includes the Waimea, Heslington, Eighty-eight, Whangamoa, Flaxmore, and Bishopdale faults. The last surface rupture of this fault system was on the Waimea Fault which radiocarbon and optically stimulated luminescence dating suggests was ~6ka (Fraser, 2005). However, a magnitude ~6.6 - 6.9 occurred on 11th February 1893 in the Waimea-Flaxmore Fault System that did not cause a surface rupture meaning its location is poorly constrained (Downes, 1995). The recurrence interval of surface ruptures within this fault system is approximately equal to

the time since the last rupture (6ka). Further notable tectonic influence for Nelson is the Wairau Fault which is considered a northern segment of the Alpine Fault, which lays some tens of kilometres from the region. The headwaters of the Motupiko River pass over the Wairau Fault which is thought to have last ruptured 1811-2301 yrs BP, with 23m displacement in the last 5610 years BP (Zachariasen et al., 2001). The eastern ranges of Nelson are bound by the Waimea-Flaxmore Fault System in the west and the Alpine fault in the south.

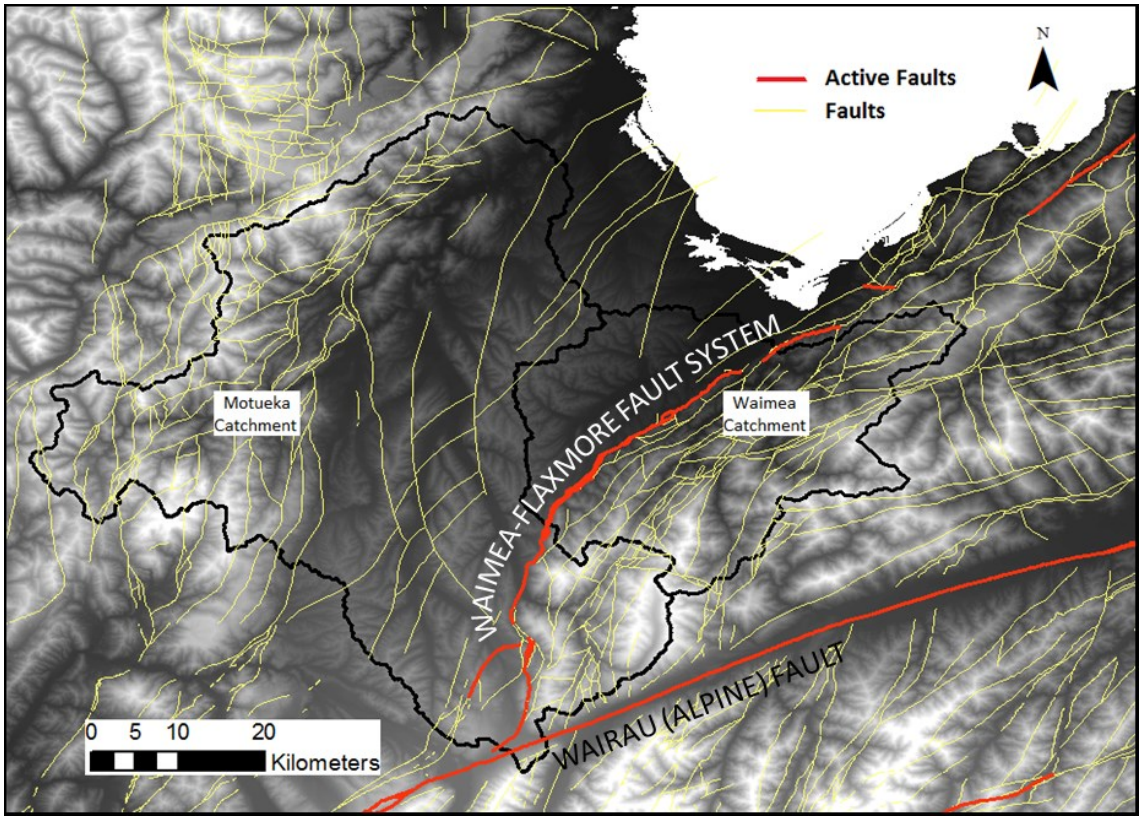

Figure 3.8: Faults (active and non-active) of the Nelson/Tasman region. Note the location of the Waimea-Flaxmore Fault System that largely underlies the Waimea catchment (East Moutere Depression), and the Wairau Fault (Alpine) in the headwaters of the Motueka catchment. Fault data were obtained from GNS Q-maps: Rattenbury et al., 1998).

3.6 Climate

The Tasman District is significantly sheltered from the prevailing westerly winds due to the Tasman Ranges and relatively sheltered from easterly winds due to the Bryant and Richmond Ranges. The area is therefore characterised by a sunny mild climate and is less influenced by wind than most other New Zealand centres (Wratt et al., 2008**)**. Median annual temperatures range from ~7 – 14°C (NIWA, 2012) across the Nelson

region, with coastal areas reaching a monthly average maximum of 29°. Annual rainfall averages range from < 1000 mm/yr at Tasman Bay and the Moutere Depression to >3000 mm/yr in the ranges that surround the Moutere Depression (NIWA, 2012). As one of the driest centres in New Zealand, it is not uncommon for the area to experience water insufficiencies in the summer and early autumn months (Wratt et al., 2008**).** Due to the area being significantly sheltered, it is also commonly exposed to frost during winter months. The region is also prone to extensive flooding events which can temporarily increase sediment delivery in rivers significantly.

3.7 Erosion in Nelson

The Suspended Sediment Yield Estimator (SSYE) suggests that suspended sediment yields across the Nelson/Tasman region range from ~50 - 200 t km^{-2} yr^{-1}, excluding the Upper Motueka and the Motupiko which are higher at 362 t km^{-2} yr^{-1} and 290 t km^{-2} yr^{-1}, respectively. The Motueka catchment is well monitored owing to the Integrated Catchment Management for the Motueka programme. Sediment gauging for this catchment has produced results that vary considerably from estimations from the SSYE (Basher et al., 2011) which is likely a result of the episodic nature of erosion in response to storm events. Sediment yield estimates of up to ~2800 t km^{-2} yr^{-1} were derived for some rivers of the Motueka following various storm-related episodic events (Coker & Fahey 1993; Basher et al., 2011). The Waimea catchment has received little publication on sediment yield estimates; however, Griffiths & Glasby (1985) estimate that the Waimea delivers ~ 152 t km^{-2} yr^{-1} and it is likely to be in the range of the SSYE for the Nelson/Tasman region (50 - 200 t km^{-2} yr^{-1}). Basher et al. (2003a) identified major sediment sources for the Motueka catchment which included the Upper Motueka and the Wangapeka Rivers (*figure 3.2*). There is relatively limited work in the region however the work available shows high variability in erosion rates across Nelson/Tasman, as well as its vulnerability to damage from climatic events.

Chapter four: Sample Collection and Laboratory Procedures

4.1 Sample locations and collection

4.1.1 Motueka Catchment

The Motueka catchment drains an area of 2075 km^2 approximately 116 km from the Red Hills in southeast Tasman to the western shore of Tasman Bay. Three major tributaries to the Motueka include the Wangapeka, Baton, Motupiko, and other smaller tributaries include the Tadmor, Stanley Brook, Pearce, Dove, and Rainy Rivers (*figure 4.1*). The small to medium sized eastern tributaries to the Motueka and the headwaters of the Motueka itself drain from relatively hilly alluvial terrain underlain by ultramafic and old sedimentary rocks (Rattenbury et al., 1998). The larger western tributaries drain from the Arthur Range (*figure 3.*2) which is geologically complex with an assortment of sedimentary and igneous rocks. The Upper Motueka catchment passes over the Waimea Fault and the Wairau Fault (Alpine) (*figure 3.8*). A minor interbasin transfer operates beneath the Hope Saddle in the summer months (October – April) from the Hope River (a tributary of the Buller River) to the Tadmor River (*figure 3.2*). The diversion transfers a maximum of 0.5 $m^3 s^{-1}$ along a 0.11 km connection.

4.1.2 Waimea Catchment

The Waimea catchment (*figure 4.1*) drains an area of 800 km^2 northward in to the southern end of Tasman Bay. Major tributaries to the Waimea include the Wai-iti and Wairoa Rivers**,** from which a confluence forms the Waimea River near Brightwater (*figure 3.2*). The Wai-iti flows northeast for 45km draining an area of 250 km^2. The hilly terrain of the Wai-iti drains from poorly consolidated alluvial sediments, predominantly the Moutere gravel (Rattenbury et al., 1998). The headwaters of the Wai-iti River and much of the Wairoa River are underlain by an assortment of sedimentary and meta-sediments including variably bedded sandstones, siltstones, and conglomerates. Both rivers drain areas that pass over various faults of the active Waimea-Flaxmore Fault System (*figure 3.8*).

4.1.3 Sand collection

Data collection for in-situ analysis was in the form of gathering 10 x 2-10 kg samples of sand depending on the quartz content of each. Surface sand material was collected from various active channel locations of the Motueka River and its tributaries (obtained from locations 1 – 8 in figure 4.1). Depending on availability of the required grainsize (sand), samples were taken from within the water or from the active channel banks (*figure 4.2*). Locations were chosen sufficiently downstream of confluences to ensure thorough mixing of material (e.g. Savi et al., 2014)

4.1.4 Silt collection

Data collection for meteoric analysis was in the form of gathering 20 x ~50g samples of silt. This was achieved by locating vegetation debris that had been transported fluvially by the Motueka and Waimea Rivers and tributaries, and obtaining the suspended sediment caught within the debris (obtained from locations 1 – 16 in figure 4.1). Each sample was located at the same level above the channel, likely representing one major flood event. By placing the vegetation in a bag and agitating, enough silt was collected for meteoric analysis. Locations 1 and 11 (*figure 4.1*) were obtained from the trunk rivers near the river mouths of the Motueka and Waimea, respectively. The samples taken from the Motueka catchment (locations 2-10) were taken from tributaries to the Motueka River. Samples taken from the Waimea catchment (location 12-16) were taken at intervals up the Wai-iti River, one of the two major tributaries to the Waimea River.

4.1.5 Depth profile collection

The depth profile samples were taken from a convex nose in the granitic terrain near the Wangapeka River (*figure 4.3*) selected for the ease of access at a recent road cutting. Granitic terrain was chosen because global studies that have taken undertaken meteoric ^{10}Be inventory studies have all done so in granitic terrain therefore maintaining consistency for the application of this method (*cf* Willenbring & von Blanckenburg, 2010 and references therein). Samples were collected by preparing a regolith section by cutting into the face by ~20cm. ~50g samples were scraped from the face at 10cm intervals down to 85cm depth.

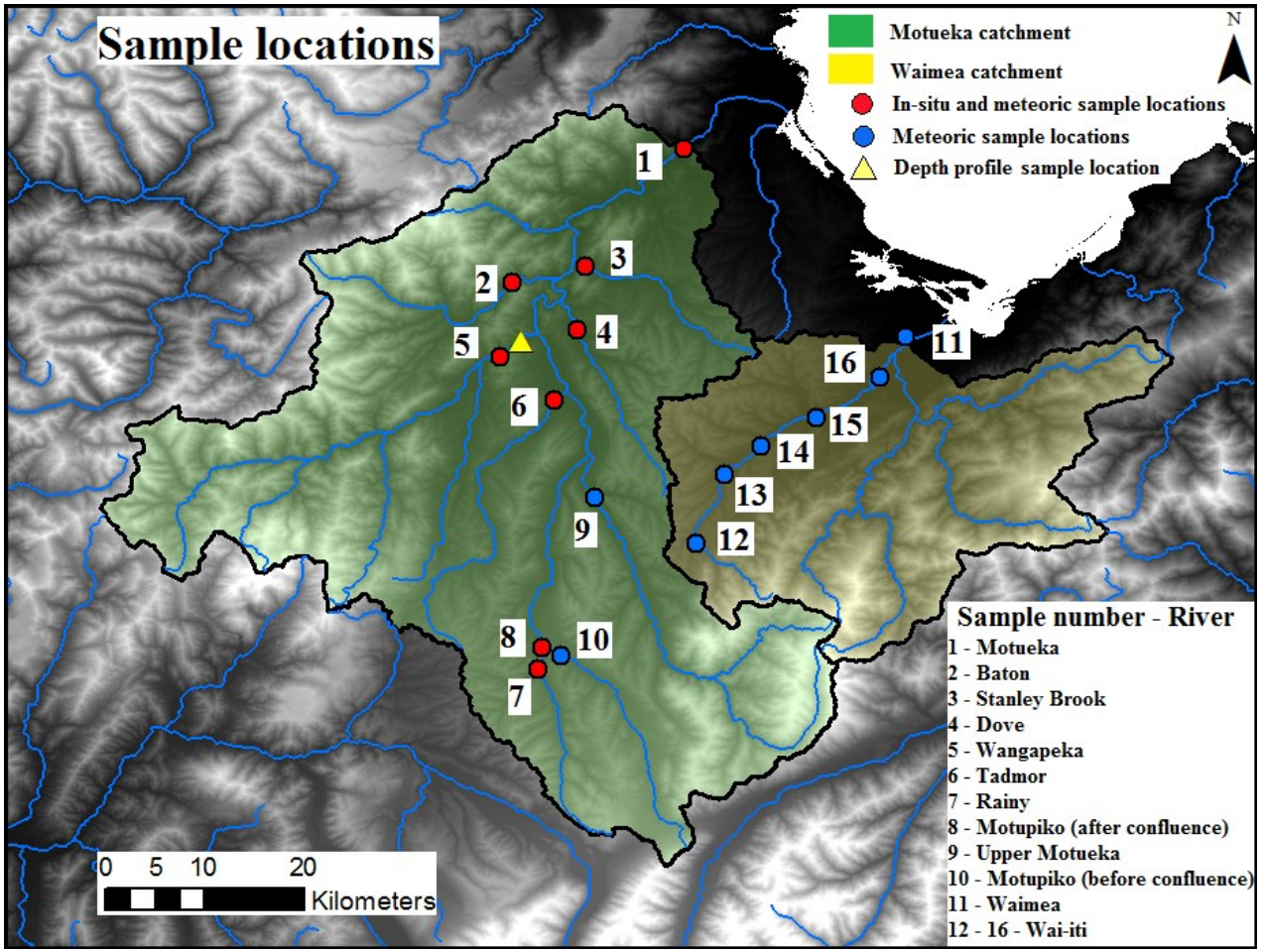

Figure 4.1: Sampling locations in the Motueka and Waimea catchments. Red points indicate locations where both meteoric and in-situ ^{10}Be results were obtained, blue points indicate where only meteoric results were obtained, and the yellow triangle indicates the sample location where the depth profile inventory was obtained.

Figure 4.2: Sand collection from the Wai-iti River, a tributary to the Waimea. Samples are roughly sieved at the site to avoid collection of large sediment and a hand lens is used to estimate the amount of quartz in the sand that is collection. (Photo courtesy of Richard Jones).

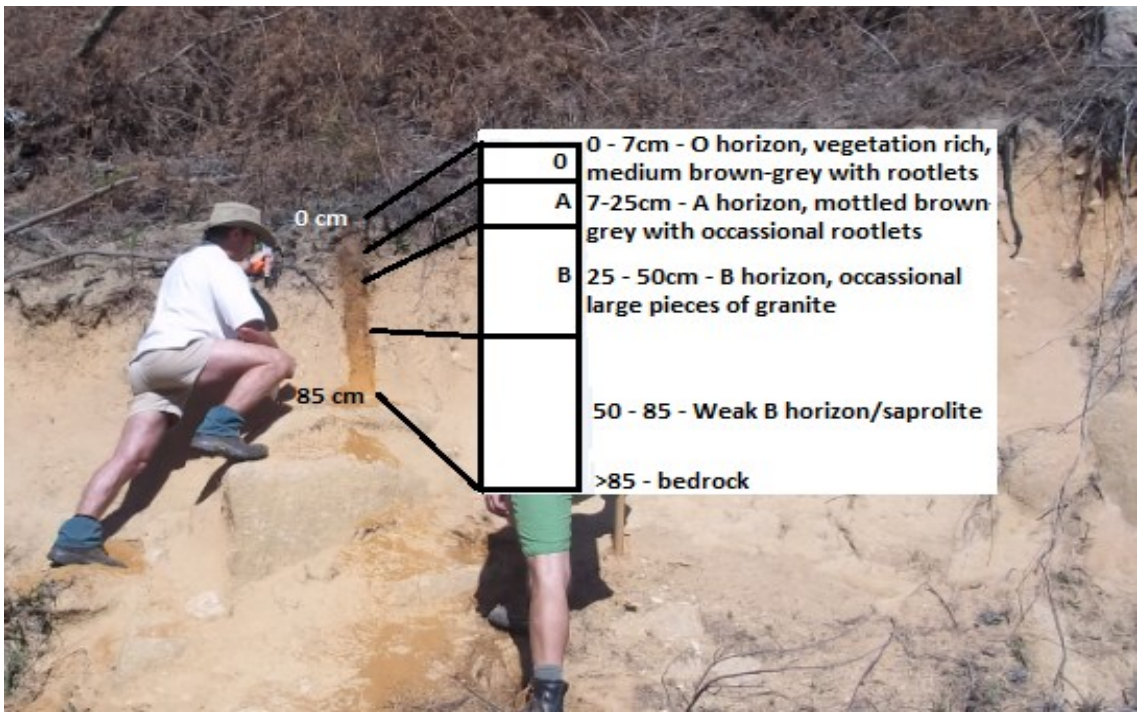

Figure 4.3: Location where depth profile of soil was taken for meteoric ^{10}Be analysis. Samples were taken at 10 cm intervals to the bedrock and the profile is briefly described.

4.2 Laboratory procedures

4.2.2 In-situ ^{10}Be laboratory preparation procedures

Samples were sieved to 0.25-0.5mm and this fraction was separated using a Franz isobaric magnetic separator, firstly at 0.6 amperes to remove highly magnetic sediments, then at 1 to separate remaining magnetic sediments. The residual non-magnetic fraction contains predominantly quartz and feldspars. ~200g of sample was divided into 2 x 1 litre bottles where ~800ml of 5% HF and ~ 8ml of HNO_3 was then added.~100ml was added initially and swirled through the sample to ensure no strong reaction before adding the remaining ~700ml. Lids were left loose for ~half an hour in order to allow for any significant reaction to occur. Lids were then tightened and placed on hotdog rollers at 40ºC, left for 60 minutes and then further tightened once the heat caused softening and loosening of lids. Samples were then rolled on hotdog rollers for 2 x 24 hours and 2 x 48 hours with 5 x rinsing with H_2O and refilling with new acid in between each session.

350 ml Teflon beakers were weighed without lids and then ~50g of pure quartz sample was added. Sample material was then covered with ~5ml excess of ~7M HF, swirled to ensure all sample material was immersed by the solution, and placed on a 120°C hotplate for ~60 minutes with the beaker lids firmly on. Beakers were removed from the hotplate and allowed to cool down before decanting the HF and rinsing with H_2O four times to remove HF and dissolved material. Each sample was then covered in aqua regia with ~5ml excess liquid in order to remove HF, placed on the hotplate for ~2 hours, and then decanted and rinsed four times in deionised H_2O. Samples were then dried and weighed in the beakers without lids, and ~1g of ^{9}Be carrier was added to each sample.

Δ (concentrated) HF (28M) was added gradually until sample was covered with ~5ml excess liquid and beakers sat for 20 minutes without lids on to allow for any significant reaction. Beakers were placed on hotplate to begin quartz dissolution. Samples were removed from hotplate and allowed to cool before adding further HF and placing on hotplate to continue dissolution. Further HF was then added and lids fastened to sit for ~2 days. Upon evaporation, samples were then dried down at which stage quartz dissolution was complete leaving a white fluoride cake at the bottom of each sample. If the fluoride cake was not clear further dissolution and dry down of HF was necessary until the desired result was obtained (von Blanckenburg et al., 2004).

4.2.1 Meteoric ^{10}Be laboratory preparation procedures

Silt samples were sieved to 45-60 μm and ~0.77g of sample was weighed into 11ml centrifuge tubes. Amorphous oxide-bound beryllium was extracted using 10ml of 0.5M HCl which was agitated at room temperature for 24 hours using a roller. Samples were centrifuged at 4000rpm for 15 minutes and supernate was decanted into 22ml Teflon beakers. Samples were rinsed with deionised H_2O, centrifuged and decanted again to extract all remaining amorphous oxide-bound beryllium. Crystalline oxide-bound beryllium was then extracted using 10ml of 1M hydroxylamine-hydrochloride solution which was agitated in an ultrasonic bath at 80°C for 4 hours. Samples were centrifuged at 4000rpm for 15 minutes before combining the crystalline oxide-bound fraction to the amorphous oxide-bound fraction. The remaining sediment was rinsed with deionised H_2O to ensure complete extraction of crystalline oxide-bound beryllium, centrifuged, and decanted into the combined fractions.

Hydroxalymine-hydrochloride solution was removed by adding concentrated H_2O_2 and HNO_3. Samples were heated at 120°C for ~2-6 hours and then lids were removed to evaporate. This was repeated a number of times until the solution was clear. 10mls of 3M HNO_3 was added and samples were placed on the hotplate with lids on for ~1 hour to dissolve the samples. ~1g of ^{9}Be solution (375ppm; GFZ carrier) was added to each sample, and then placed on the hotplate with lids off to evaporate liquid. Any trace of silicate residue was then removed by adding 2ml aqua regia, 2ml ΔHNO_3, and 2ml ΔHF, and heating on hotplate for ~1 hour before evaporating. Samples were then covered in ΔHF and heated for ~2 hours before drying down and repeating this step. This ensured all silicate residue was removed before BeF_2 leaching by H_2O and cation exchange chemistry could begin (Norton, 2008).

4.2.3 BeF_2 leaching

BeF_2 is soluble in H_2O while many other cations are less so (Stone, 1998), thus the addition of deionised H_2O enabled BeF_2 to be separated from the fluoride cake for both meteoric and in-situ samples (*figure 4.4*). 5ml of deionised H_2O was added to each sample, swirled, and placed on hotplate for ~5 minutes then sat to cool for ~20 minutes where BeF_2 goes into solution. The supernate was then pipetted into 22ml Teflon beakers. This was repeated an additional 2 times in order to thoroughly leach BeF_2, and samples were finally evaporated. 10ml of 6M HCl was added to each sample to dissolve

so samples could be transferred into 15ml centrifuge tubes and centrifuged at 3000 rpm for 5 minutes in preparation for Fe removal.

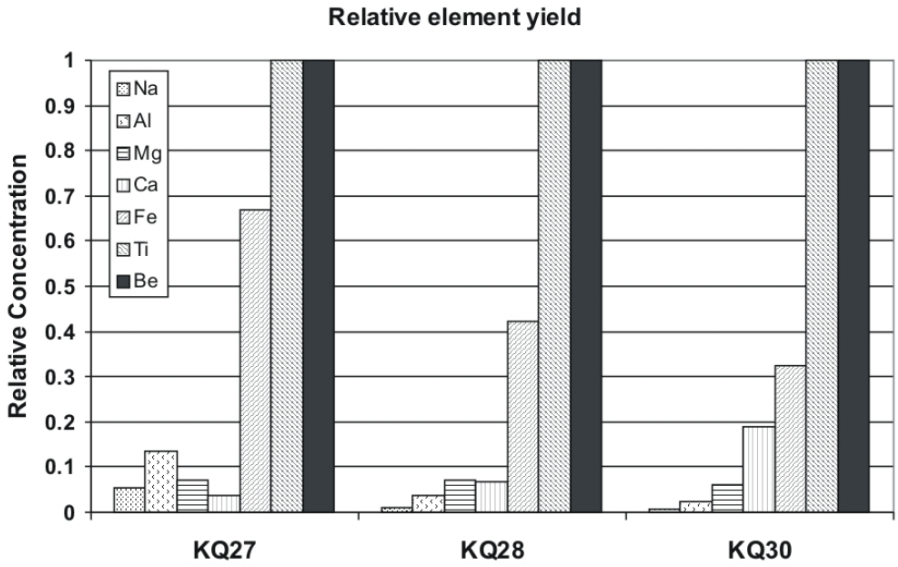

Figure 4.4: Elements present following water leaching and fluoride extraction. Note that all Be is retained in this step. (Source: Norton, 2008)

4.2.4 Cation chemistry – Fe column

7.5ml diameter Eichrom columns were used with 2ml of 1x8 100-200 mesh resin for the removal of Fe. The resin was cleaned with 5ml + 5ml 0.3M HCl and then conditioned with 2ml + 2ml + 2ml 6M HCl. Samples in the 10ml 6M HCl were then added and 2ml + 2ml + 2ml 6M HCl was added to elute the Be which was collected in Teflon beakers and then evaporated on the hotplate. 4ml (20ml for in-situ and depth profile) 0.4M oxalic acid (50.6g oxalic solid in 1000ml deionised H_2O) was added and samples were placed on the hotplate with lids on for ~ 2 hours to redissolve. These were then allowed to cool for ~30 minutes, transferred to 10ml centrifuge tubes and centrifuged at 3000rpm for 5 minutes in preparation for Be elution.

4.2.5 Cation chemistry – Be column

Meteoric Be was eluted using 7.5ml Eichrom columns with 1ml Biorad AG50-X8 200-400 mesh resin (25ml column and 5ml resin for in-situ and depth profile). Column resin is cleaned initially by adding 2ml + 3ml 5M HNO_3, then removing HNO_3 by adding 2ml + 3ml of deionised H_2O. The resin is then conditioned by adding 2ml + 3ml of 0.4M oxalic acid. Samples were then added and washed though with 1ml + 1ml +10ml 0.4M

oxalic acid to elute any remain Fe, and any Al, Ti present (*figure 4.5*). Oxalic acid is then removed by adding 1ml + 2ml deionised H_2O.

Be, Na, K, Ca, and Mg are all non-retentive in 1M HNO_3 or stronger acid; however, only Na and K are non-retentive in 0.5M HNO_3 or weaker acid (von Blanckenburg et al., 1996; von Blanckenburg et al., 2004). Thus Be is retained in the resin with the addition of 2ml + 2ml + 4ml 0.5M HNO_3 where Na and K are removed (*figure 4.5*). The addition of 3ml + 3ml + 5ml 1M HNO_3 then allowed for the elution of only the Be which was collected in 15ml centrifuge tubes.

For in-situ Be and for meteoric depth profile samples, 15ml Eichrom columns were used with 5ml Biorad AG50-X8 200-400 mesh resin. The same procedure was used as with the 7.5ml columns; however, 5x greater quantities of 0.4M oxalic acid, HNO_3, and deionised H_2O were needed to effectively elute the Be.

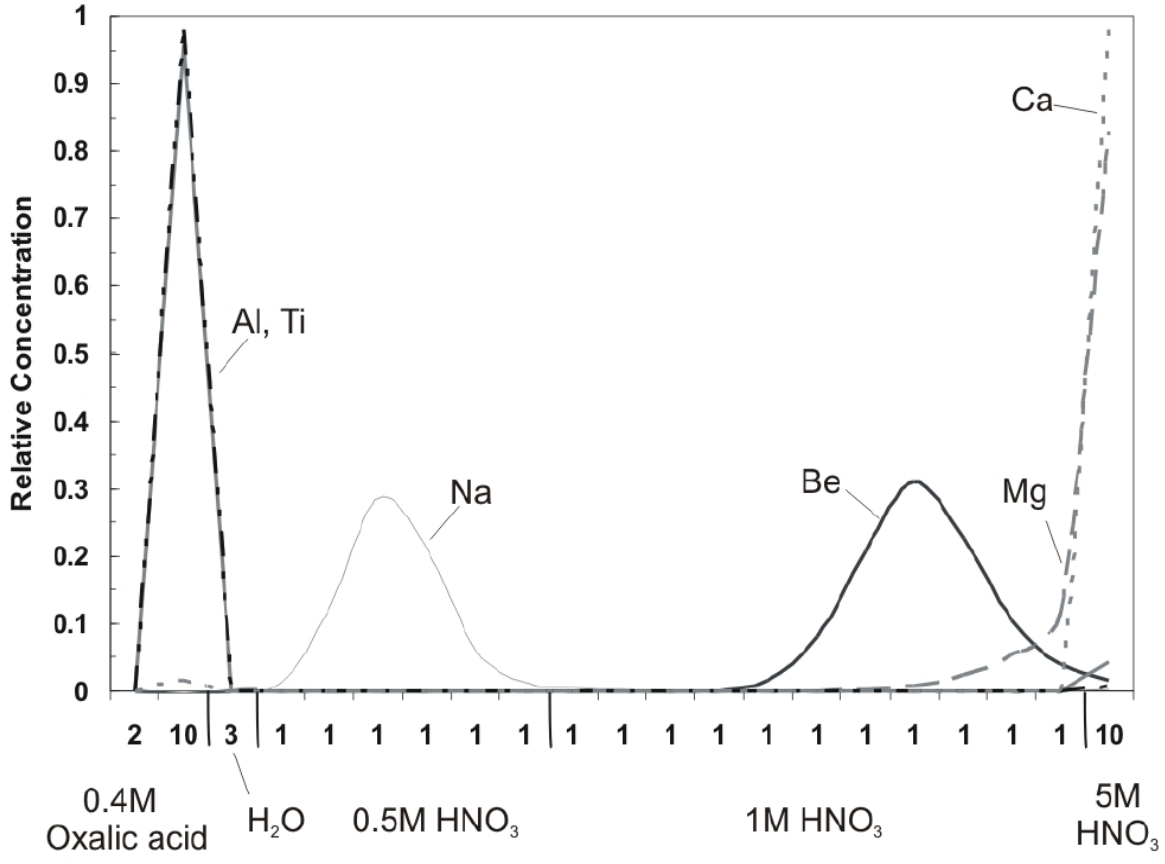

Figure 4.5: The elution of elements with HNO_3 in cation exchange resin. Note that Be is retained in the resin with H_2O and with 0.5M HNO_3 while Al, TI, and Na are eluted. In 1M HNO3, Be is eluted. (Source: Norton, 2008)

4.2.6 Be precipitation

Precipitation cleans the remaining Be. ~1ml ΔNH_4OH (~5ml for in-situ and depth profile) was added to the 11ml 1M HNO_3 elution and samples shaken well until BeOH formed (Ochs & Ivy-Ochs, 1997). This appeared as small white specks in the liquid and samples were centrifuged for 5 minutes at 3000rpm. This segregated a small milky gel at the bottom of the centrifuge tube which allowed for decanting of the supernate.

4.2.7 Accelerator Mass Spectrometer

Samples were sent to the National Isotope Centre (GNS) where they were sintered with H_3PO_4/HF to remove B. They were then oxidised in an oven (convert BeOH to BeO) and pressed into targets with Nb powder. Samples were then measured using the 0.5 MeV XCAMS Accelerator Mass Spectrometer which has the capability of counting individual atoms. Samples were measured against NIST (National Institute of Standards and Technology) 27900 and corrected for laboratory blanks.

4.3 Spatial analysis procedures

4.3.1 Basin delineation

For the purposes of this research, the ArcGIS watershed tool was used to define the contributing basin area upstream of each sample location from a 15m Digital Elevation Model (DEM) *(figure 4.6).* Basins have been labelled 1 – 16, and the rivers which each basin contributes to are labelled accordingly (*figure 4.6*). Basins 1 and 11 are representative of the entire Motueka and Waimea catchments, respectively, as the samples were taken downstream near the mouths of these trunk rivers. Other basins are representative of sub-catchments to the trunk rivers (Motueka and Waimea).

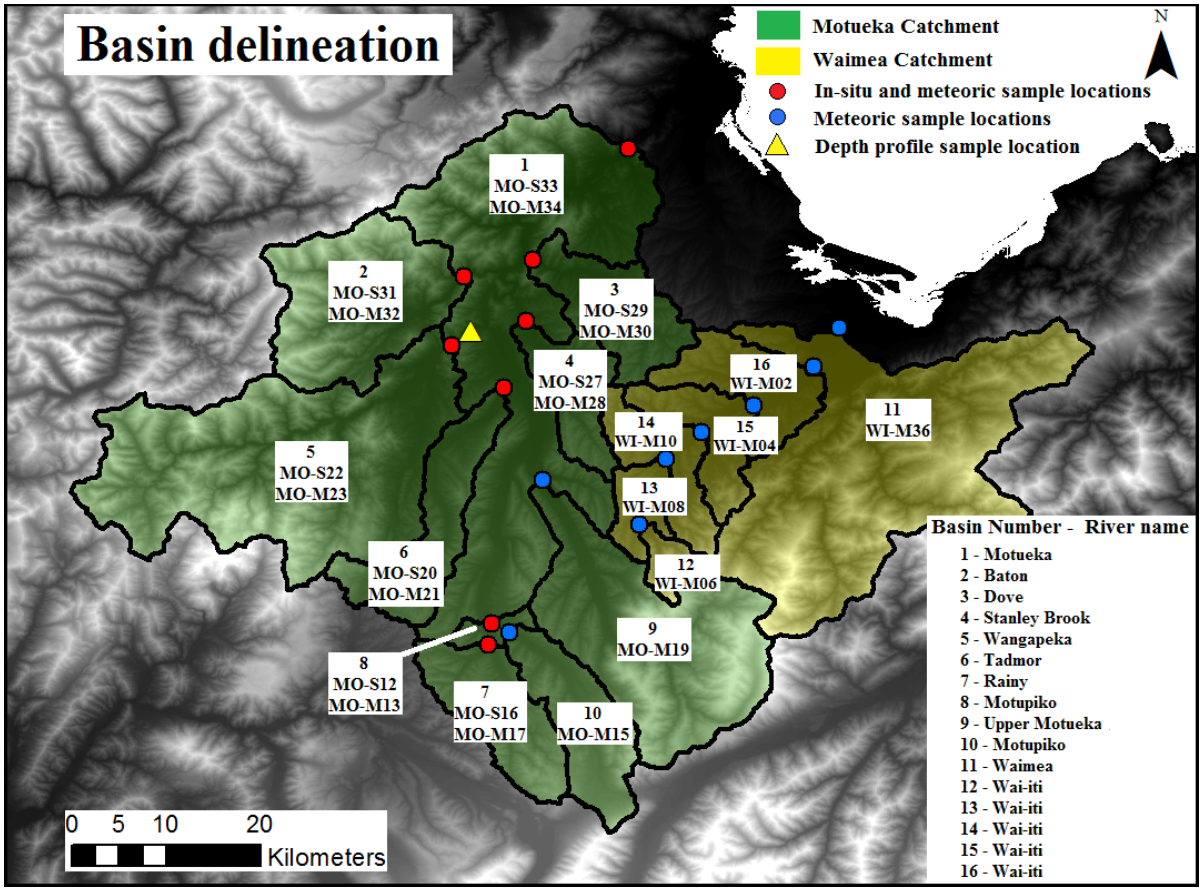

Figure 4.6: The contributing basin areas delineated for each sample location. The following chapters will refer to each basin by its allocated number. Sample names are shown beneath each basin number for reference in tables 5.1 and 5.2. MO indicates the sample was taken from the Motueka catchment, WI indicates the sample was taken from the Waimea catchment, S indicates the sample taken was for in-situ analysis, and M indicates the sample taken was for meteoric analysis.

4.3.2 Shielding calculation

Shielding values were determined by using an ArcMap macro to calculate skyline shielding on a pixel by pixel basis (Guralnik, pers comm). This macro determined the inclination and orientation of each pixel to the horizon. The raster calculator and zonal statistics tools in ArcMap were then used to obtain an average shielding value for each basin.

4.3.3 Denudation rate calculations

When Accelerator Mass Spectrometer concentrations were received, in-situ denudation rates were then obtained using the CRONUS-earth online calculator developed by Balco

et al. (2008b). This calculator derives production rates from latitude, longitude, and elevation of each sample location, the shielding factor, and then applies equation 3 (page 32) to calculate results. Other standard inputs include: density = 2.6 g cm^{-3}, thickness = 0 (surface concentration), Be standardisation = NIST_27900, and the half-life (λ) of ^{10}Be = 1.39 Myr. Meteoric denudation rates were determined by applying equation 5 to the Accelerator Mass Spectrometer concentrations. A production rate of 1.3 x 10^6 atoms cm^{-2} yr^{-1} was used, as determined by Vonmoos et al., (2006).

4.3.4 Basin statistics calculations

Statistics for each derived basin were obtained with the use of various spatial analyst tools in ArcMap. This included basin area (km^2), relief (m), mean slope angle (°), main rock type, mean rainfall (mm/yr), channel steepness (Ksn), fault density (m/km^2), and mean flow (L/S). Ksn values are based on Hack's Law (Hack, 1957) where river profiles can be described by a power–law relationship between local channel gradient and upstream drainage area. Here steepness is normalised to a concavity of 0.45 account for drainage area, and the Ksn value shows channels that are considered oversteepened according to this power-law relationship. All delineated basins were in raster format therefore the raster calculator tool was used to constrain the above variables for each basin. The zonal statistics tool was used to obtain each variable for each delineated basin. The cor function in the statistical package R was then used to perform linear regression analysis to determine the r^2 correlations between all basin variables. R^2 values indicate the strength of the relationship between variables – the closer an r^2 value is to 1 the better the correlation (<0.2 = no correlation, 0.2-0.4 = weak correlation, >0.4 = correlation). The gclus package in R was then used to perform cluster analysis and create a colour-coded graph displaying all r^2 results. These correlations were used to assess any relationships between the denudation rates and basin variables to understand the controlling factors on denudation in this region.

Chapter five: Results

5.1 Cosmogenic ^{10}Be-derived denudation rates

5.1.1 In-Situ

In-situ ^{10}Be concentrations obtained from Accelerator Mass Spectrometer measurement range from 1.09 x 10^4 – 6.00 x 10^4 atoms g^{-1}. Denudation rates were derived from these concentrations with the use of the CRONUS-earth online calculator (Balco et al., 2008b) which applies equation 3 (pg. 32). In-situ denudation rates that range from 112 - 298 t km^{-2} yr^{-1} with the exception of one basin which was eroding exceptionally more rapidly at 626 t km^{-2} yr^{-1} (*figure 5.1; table 5.1*).

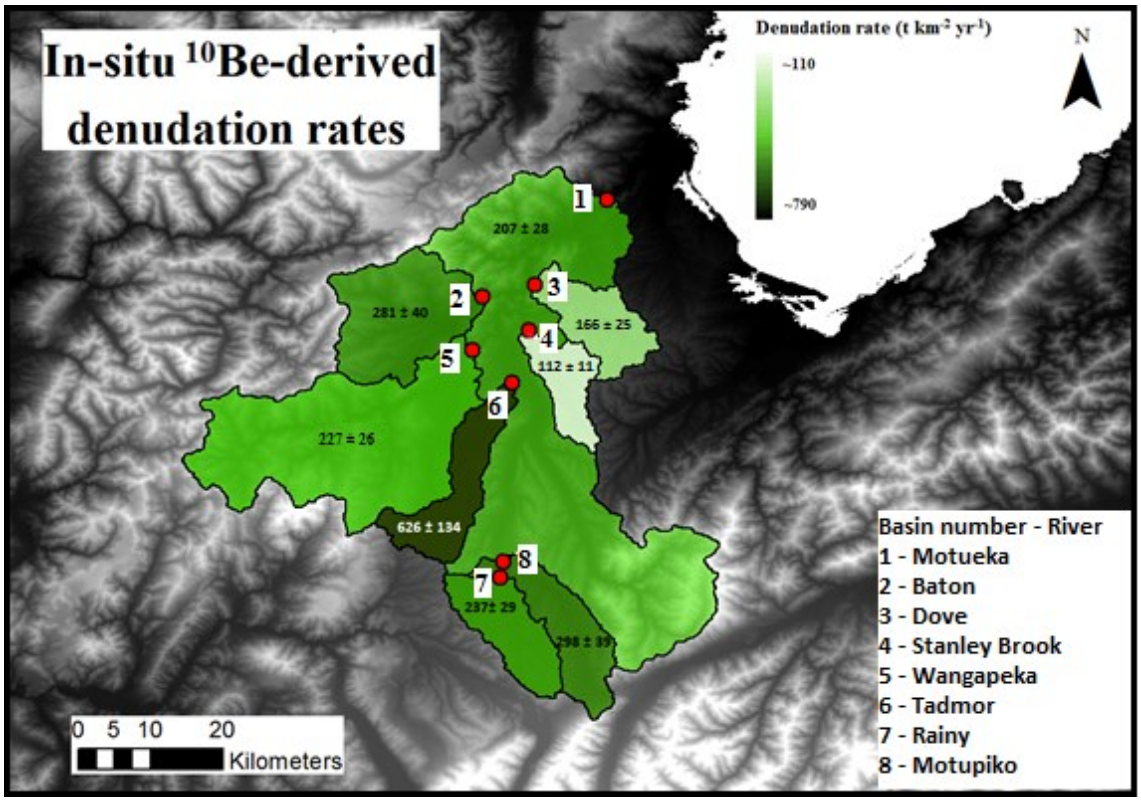

Figure 5.1: In-situ ^{10}Be-derived denudation rates for the Motueka catchment.

Basin	Sample	Location (DD)	Longitude (DD)	Elevation (m)	Production rate (atoms g^{-1} yr^{-1})	Shielding correction	^{10}Be (atoms g^{-1})	+/- (atoms g^{-1})	Erosion (cm/yr)	Erosion (t km^{-2} yr^{-1})	1-sigma error ± (t km^{-2} yr^{-1})	Averaging Timescales (yrs)
1	MO-S33	-41.162	172.922	585	7.09	0.993	3.53×10^4	0.37×10^4	0.017	207	28	2900
2	MO-S31	-41.283	172.766	753	8.12	0.988	2.94×10^4	0.33×10^4	0.023	281	40	2100
3	MO-S29	-41.268	172.831	264	5.41	0.997	3.61×10^4	0.45×10^4	0.014	166	25	3600
4	MO-S27	-41.325	172.824	463	6.44	0.998	6.00×10^4	0.28×10^4	0.009	112	11	5300
5	MO-S22	-41.349	172.754	718	7.9	0.988	3.54×10^4	0.27×10^4	0.019	227	26	2600
6	MO-S20	-41.39	172.803	422	6.22	0.997	1.09×10^4	0.21×10^4	0.052	626	134	960
7	MO-S16	-41.633	172.789	628	7.44	0.998	3.24×10^4	0.28×10^4	0.020	237	29	2500
8	MO-S12	-41.613	172.792	639	7.5	0.997	2.60×10^4	0.25×10^4	0.025	298	39	2000

Table 5.1: Results for in-situ ^{10}Be –derived denudation rates. Results were calculated using the CRONUS-earth online calculator (Balco et al., 2008b). Further values for calculations include: density = 2.6 g cm^{-3}, Elv/Pressure flag value = std, thickness = 0 (surface concentration), Be standardisation = NIST_27900, and the half-life (λ) of ^{10}Be = 1.39 Myr.

5.1.2 Meteoric

Meteoric ^{10}Be concentrations obtained from Accelerator Mass Spectrometer analysis measurement range from 1.65 x 10^{7}– 8.81 x 10^{7} atoms g^{-1}. Denudation rates were then inferred with the use of equation 5 (page 33) concentrations yield denudation rates that range from 148 - 233 t km^{-2} yr^{-1} across the Nelson region, with the exception of one basin which is eroding at 789 t km^{-2} yr^{-1} (*figure 5.2; table 5.2*). Basin-averaged rates for the Waimea catchments (171 t km^{-2} yr^{-1}) were lower than the Motueka (258 t km^{-2} yr^{-1} and 199 t km^{-2} yr^{-1} without the outlier – basin 6).

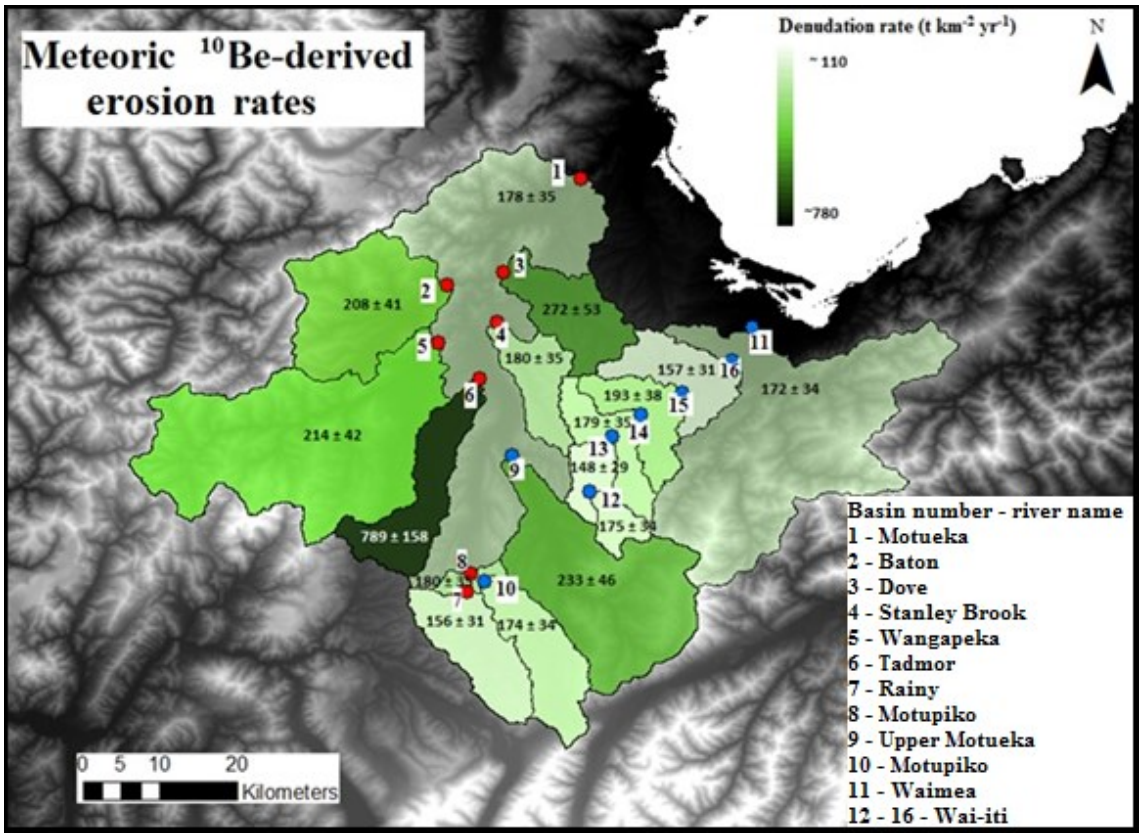

Figure 5.2: Meteoric ^{10}Be derived erosion rates (t km^{-2} yr^{-1}) for the Motueka and Waimea catchments.

Basin	Sample	Latitude (DD)	Longitude (DD)	^{10}Be conc. (atoms/g^{-1})	+/- (atoms/g^{-1})	Erosion (cm/yr)	Erosion (t km^{-2} yr^{-1})	1-sigma error ± (t km^{-2} yr^{-1})	Averaging Timescales(yrs)
1	MO-M34	-41.162	172.922	7.30×10^{7}	0.15×10^{7}	0.015	178	35	5400
2	MO-M32	-41.283	172.766	6.25×10^{7}	0.12×10^{8}	0.017	208	41	4600
3	MO-M30	-41.268	172.831	4.79×10^{7}	0.12×10^{7}	0.023	272	53	3500
4	MO-M28	-41.325	172.824	7.23×10^{7}	0.14×10^{8}	0.015	180	35	5300
5	MO-M23	-41.349	172.754	6.07×10^{7}	0.14×10^{7}	0.018	214	42	4500
6	MO-M21	-41.39	172.803	1.65×10^{7}	0.08×10^{7}	0.066	789	158	1200
7	MO-M17	-41.633	172.789	8.31×10^{7}	0.18×10^{7}	0.013	156	31	6100
8	MO-M13	-41.613	172.792	7.24×10^{7}	0.17×10^{7}	0.015	180	35	5300
9	MO-M19	-41.447	172.841	5.58×10^{7}	0.14×10^{7}	0.019	233	46	4100
10	MO-M15	-41.621	172.809	7.47×10^{7}	0.15×10^{7}	0.015	174	34	5500
11	WI-M36	-41.332	172.122	7.56×10^{7}	0.15×10^{8}	0.014	172	34	5600
12	WI-MO6	-41.519	172.932	7.42×10^{7}	0.16×10^{7}	0.015	175	34	5500
13	WI-MO8	-41.457	172.958	8.81×10^{7}	0.17×10^{7}	0.012	148	29	6500
14	WI-M10	-41.431	172.991	7.26×10^{7}	0.15×10^{7}	0.015	179	35	5400
15	WI-MO4	-41.406	173.041	6.74×10^{7}	0.18×10^{7}	0.016	193	38	5000
16	WI-M02	-41.369	173.098	8.28×10^{7}	0.17×10^{7}	0.013	157	31	6100

Table 5.2: Results for meteoric ^{10}Be-derived rates of denudation. Additional values for calculations include: production rate = 1.3×10^{6} atoms cm^{-2} yr, averaging timescales assume an adsorption depth of 80cm.

5.1.3 In-situ vs meteoric ^{10}Be derived denudation rates

Meteoric and in-situ ^{10}Be derived denudation rates were remarkably consistent between one another (*figure 5.3; table 5.3*). Within 2-sigma, most samples fall within a one to one line (*figure 5.4*). The mean denudation rate derived from meteoric ^{10}Be across all basins where both meteoric and in-situ samples were obtained was 272 (198 t km^{-2} yr^{-1} without the outlying result from basin 6 – Tadmor). This was remarkably similar to values obtained from in-situ ^{10}Be which were 269 (218 t km^{-2} yr^{-1} without the outlying result from basin 6 - Tadmor).

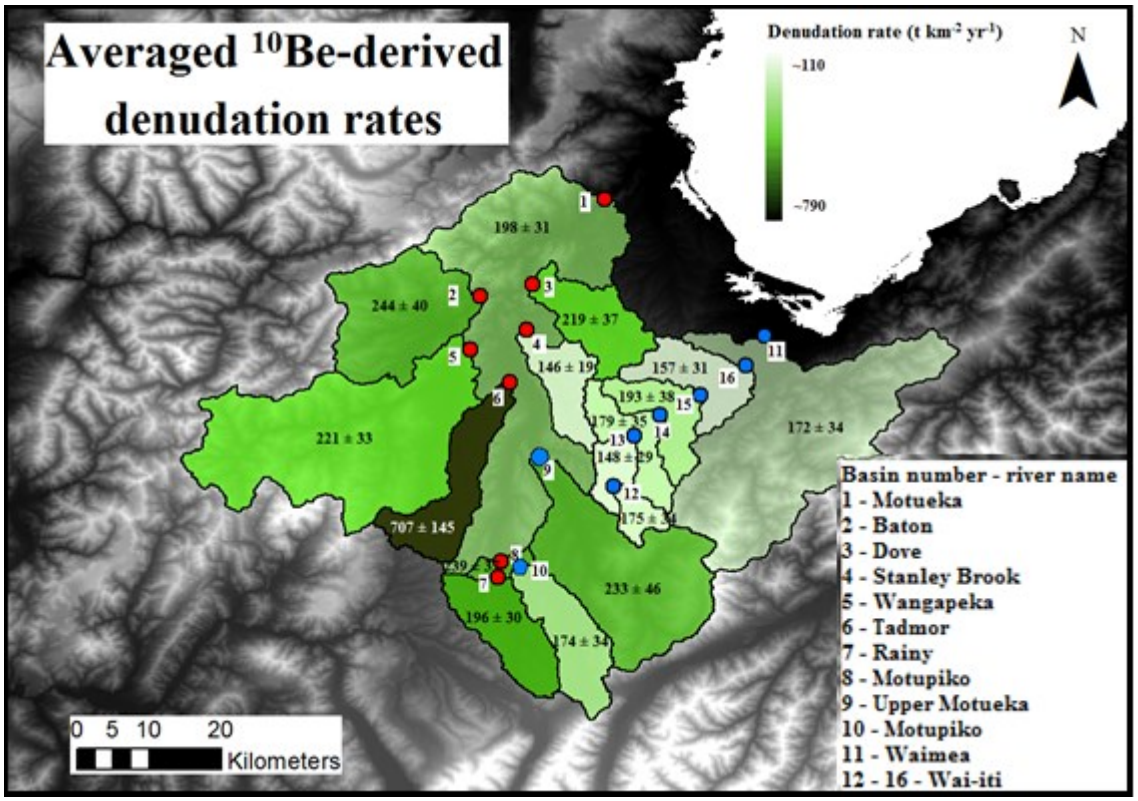

Figure 5.3: Averaged in-situ and meteoric denudation rates (where applicable) for the Motueka and Waimea catchments.

Basin	Sample (In-situ)	Sample (Meteoric)	In-situ erosion (t km^{-2} yr^{-1})	Meteoric erosion (t km^{-2} yr^{-1})	Average Erosion (t km^{-2} yr^{-1})	1-sigma error ± (t km^{-2} yr^{-1})
1	MO-S33	MO-M34	207	178	193	31
2	MO-S31	MO-M32	281	208	244	40
3	MO-S29	MO-M30	166	272	219	37
4	MO-S27	MO-M28	112	180	146	19
5	MO-S22	MO-M23	227	214	221	33
6	MO-S20	MO-M21	626	789	707	145
7	MO-S16	MO-M17	237	156	196	30
8	MO-S12	MO-M13	298	180	239	37

Table 5.3: Averaged in-situ and meteoric denudation rates (where applicable) for the Motueka catchment.

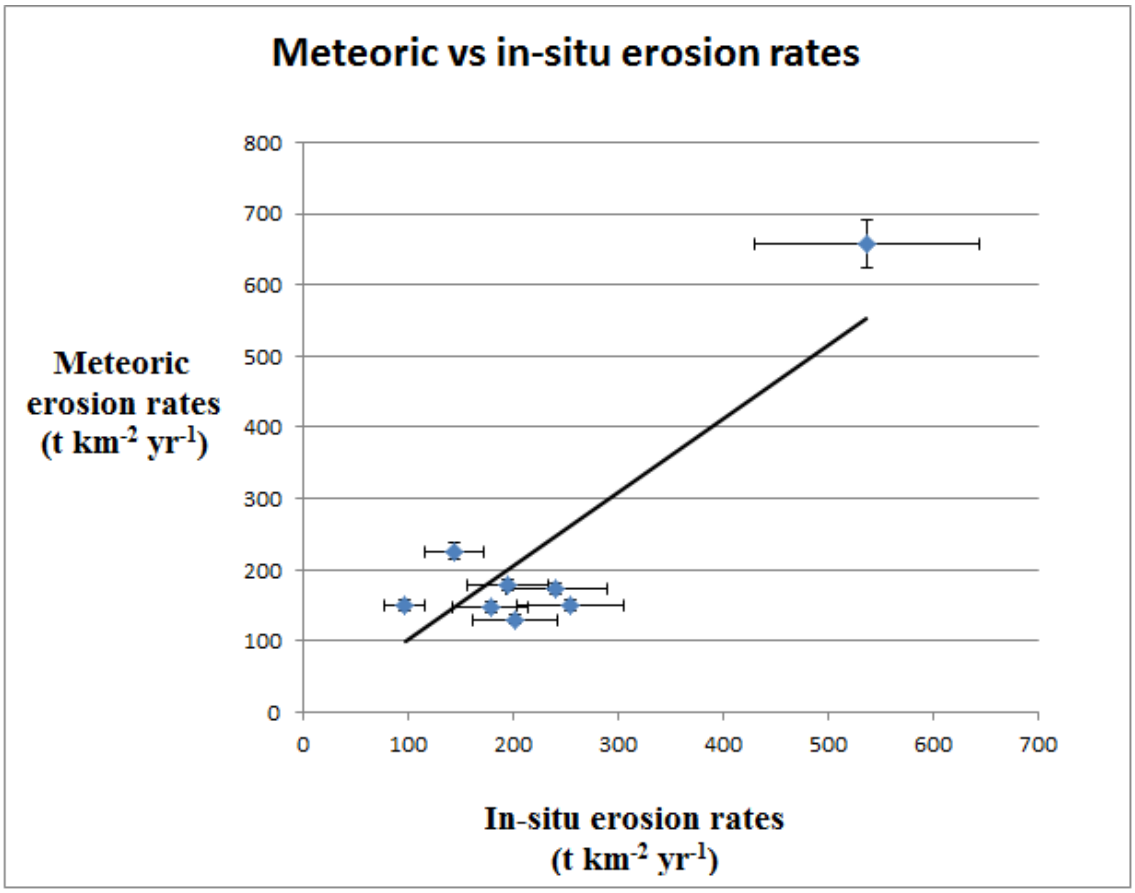

Figure 5.4: Meteoric ^{10}Be derived denudation rates plotted against in-situ ^{10}Be derived denudation rates from the Motueka and Waimea catchments. Note the majority of rates agree within 2-sigma on the one to one line.

5.1.4 Depth profile

The depth profile for meteoric ^{10}Be adsorption analysis was dug from the bedrock interface. In a simple system, ^{10}Be should approach zero before the bedrock surface (Willenbring & von Blanckenburg, 2010). However, the decrease in ^{10}Be concentration with depth is not as distinct as expected. 85 cm below the surface, at the soil/bedrock interface, the concentration had decreased only by ~35% from 2.47 x 10^8 to 1.75 x 10^8 atoms g^{-1} (*figure 5.5; table 5.4*). Because the concentrations do not reach zero before reaching the bedrock, two scenarios provide possible explanations: 1) ^{10}Be is leaching into the bedrock, or 2) the system is open and ^{10}Be is transported on the bedrock interface. These two scenarios are further discussed in section 6.2.2. Note that the samples at 35, 45, and 85cm are considered suspect as minor loss occurred during chemistry. However, their concentrations still fit in the profile.

Furthermore, ^{10}Be increases with depth in the top 10-20cm before decreasing. This is likely explained by the presence of a clay layer in the subsurface leading to efficient adsorption of ^{10}Be where the efficiency of ion exchange capabilities is heightened on the greater surface areas (Brown et al., 1992). Soils of the Moutere Depression commonly exhibit a mid-depth clay later (Basher & Jackson, 2002).

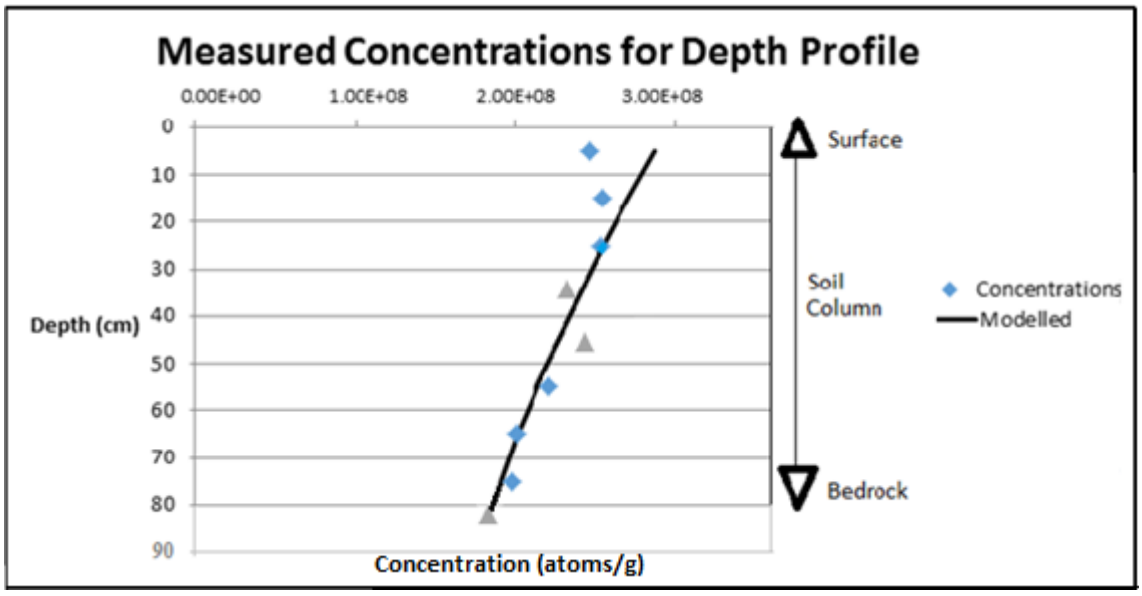

Figure 5.5: ^{10}Be concentrations with depth measured at 10cm intervals to 85cm. Note the increase in concentration at 10–30cm before concentrations decrease. Modelled fit assuming absorption depth of 80cm.

Depth (cm)	Interval depth (cm)	^{10}Be Concentration (atoms/g)	^{10}Be Concentration (atoms/cm^3)
5	10	2.47 x 10^8	2.96 x 10^8
15	10	2.55 x 10^8	3.06 x 10^8
25	10	2.53 x 10^8	3.04 x 10^8
35	10	2.29 x 10^8	2.75 x 10^8
45	10	2.42 x 10^8	2.90 x 10^8
55	10	2.21 x 10^8	2.65 x 10^8
65	10	2.00 x 10^8	2.40 x 10^8
75	10	1.98 x 10^8	2.37 x 10^8
82.5	5	1.75 x 10^8	2.09 x 10^8

Table 5.4: Meteoric ^{10}Be concentrations obtained at 10cm depth intervals to a depth of 85cm.

5.1.5 Averaging timescales

Averaging timescales for in-situ samples were calculated by dividing the denudation rate (mm/ky) by the attenuation depth (0.6m for bedrock) (von Blanckenburg, 2006). Timescales ranged between ~900 – 5000 years with a mean of ~2750 years. Averaging timescales for meteoric samples were calculated by dividing the denudation rate (mm/ky) by the adsorption depth derived from depth profile concentrations. Based on the <1m soil depth and the typical exponential reduction in nuclide concentration with depth, it was expected that the meteoric samples would represent denudational averages of ≤ 1000 years; however, the long adsorption depth resulted in denudational averages of ~5000 years. With this result the in-situ- and meteoric-derived denudation rates integrate over similar timescales with the meteoric rates being slightly longer-term averages. This was fairly represented by the remarkable consistency between meteoric and in-situ derived denudation rates supporting the unexpected but plausible timescale. However, as the ^{10}Be concentration was not 0 at the bedrock, section 6.2.2 will discuss alternative scenarios for meteoric averaging timescales.

5.2 Basin statistics

5.2.1 Basin area

Contributing catchment areas to sample locations (derived in ArcMap with the use of the watershed tool) ranged between 162- 1411 km^2 across the basins (*table 5.5)*. Linear regression analysis (described in section 4.3.4) showed there was no statistically significant relationship between basin size and rates of denudation (*table 5.7*).

5.2.2 Relief

Relief (highest – lowest elevation of catchment) for each basin (derived using the zonal statistics tool in ArcMap) ranged from 464 – 1791 m (*table 5.6*). Linear regression analysis (described in section 4.3.4) showed that there was no statistically significant relationship between relief and the rates of denudation (*figure 5.12; table 5.7*). This lack of relationship is significant because it is common for studies to show a distinct relationship between these two variables (eg. Anhert, 1970; Summerfield & Hulton, 1994)

5.2.3 Rainfall

Mean annual rainfall derived for each catchment ranged from 1200 – 2230 mm yr (*figure 5.6; table 5.6*). Precipitation decreases generally from west/southwest to northeast. Linear regression analysis (described in section 4.3.4) showed that there was no statistically significant correlation between mean rainfall and rates of denudation (*figure 5.11; table 5.7*).

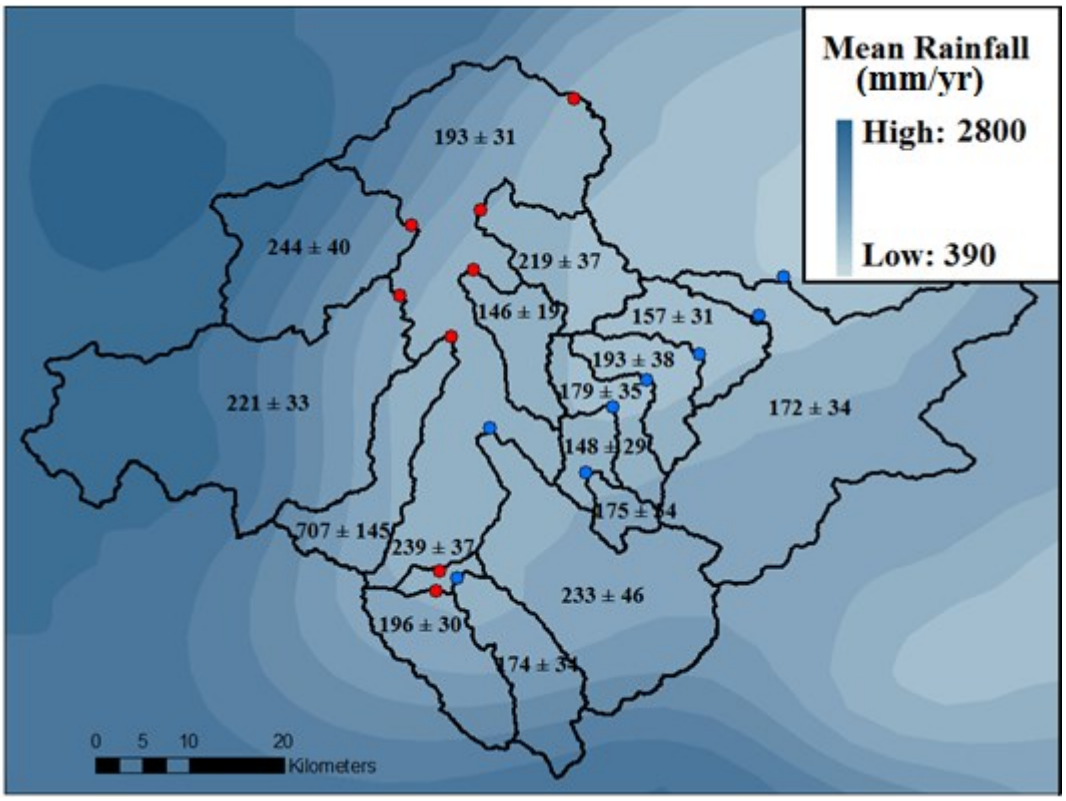

Figure 5.6: Mean annual rainfall across the Nelson/Tasman region. Denudation rates are averages derived from the two methods (meteoric and in-situ). Note the general west/southwest to northeast decrease in rainfall.

5.2.4 Main rock type

Linear regression analysis between major rocktypes and denudation (as discussed in section 4.3.4) found that there was no significant direct correlations between the two variables (*figure 5.7; table 5.5*). Results showed that basins with high percentages of gravel for example did not show significantly different denudation rates to those with high percentages of igneous, sedimentary, or metamorphic rocks.

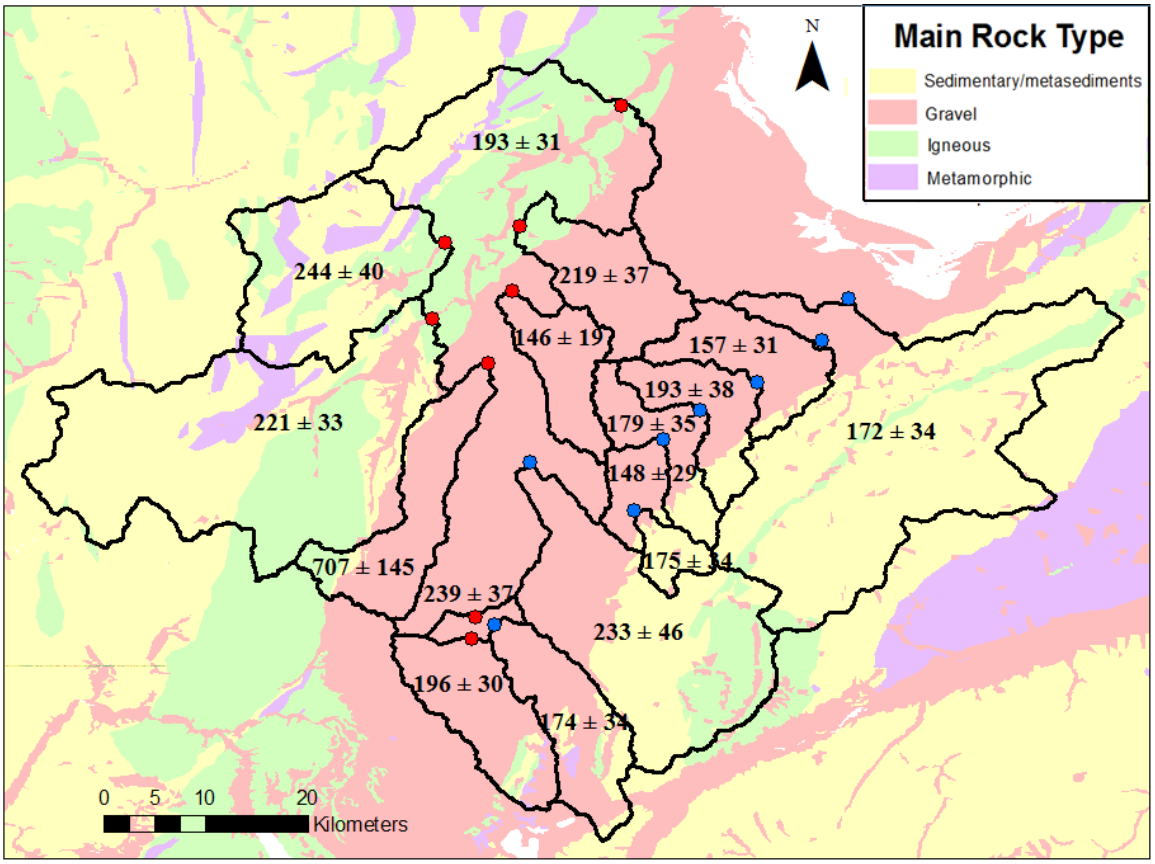

Figure 5.7: Main rock type across the Nelson/Tasman region, broadly grouped into four categories (Sedimentary/metasediments, gravel, igneous, and metamorphic). Note the Moutere Depression comprises entirely gravels while the surrounding ranges are considerably more complex. Denudation rates are averages derived from the two methods. Lithological data were obtained from GNS Q-maps (Rattenbury et al., 1998).

5.2.5 Slope angles

Hillslope angles commonly exceeded 30 degrees in basins of the Motueka and Waimea catchments (*figure 5.8*); however, linear regression analysis showed that there was no significant statistical correlation between percentage of slope > 30 degrees and rates of denudation (*figure 5.12; table 5.7*). Basins with a high percentage of slope above 30 degrees showed no differences in denudation rates than those with low percentage of slope above 30 degrees.

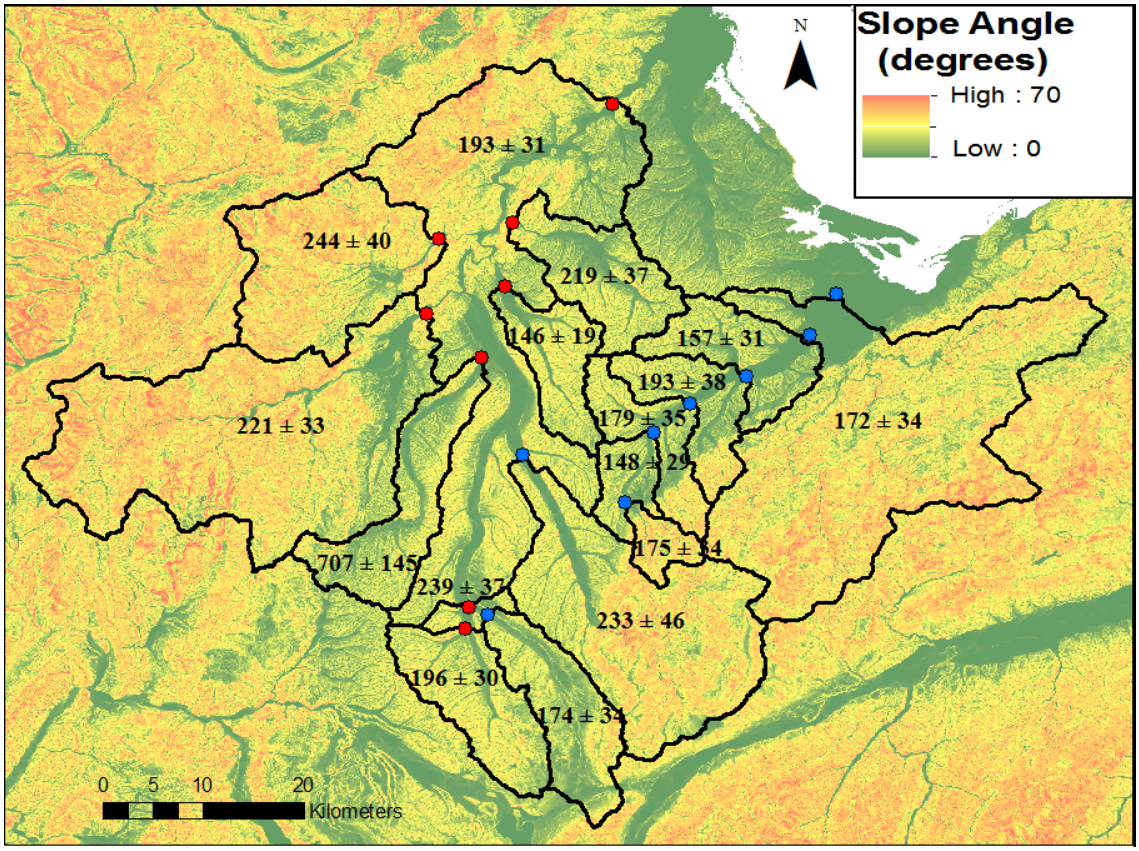

Figure 5.8: Slope angles (˚) across the Nelson/Tasman region. Red areas represent steep slope angles while green represents shallow slope angles. Note that many slope in the ranges surrounding the Moutere Depression are considerably steep, commonly exceeding 30˚. Denudation rates are averages derived from the two methods.

5.2.6 Channel Steepness

Linear regression analysis (described in section 4.3.4) found that there was no statistically significant (>0.4) relationship between channel steepness (Ksn) and the rates of denudation derived for the Motueka and Waimea catchments (*figure 5.11; table 5.7*). There were a number of oversteepened channel segments across both the Motueka and Waimea catchments (*figure 5.9; table 5.6*). These coincided with steeper slopes and areas where there was little Moutere gravel. This is likely the result of stronger lithologies that allow for the maintenance of steep channels while the more erodible Moutere gravel does not.

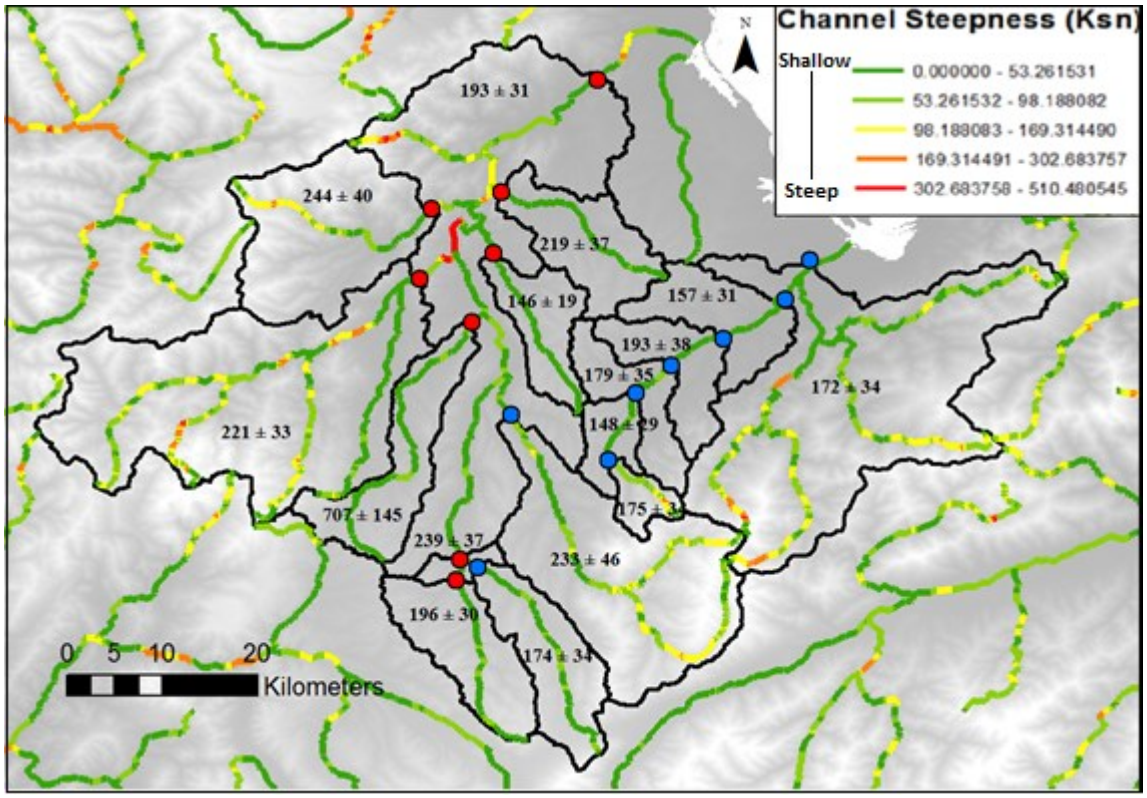

Figure 5.9: Channel steepness across the Nelson/Tasman region. Red segments represent significantly over steepened channels. Note the absence of oversteepened channels in the Moutere Depression. Denudation rates are averages derived from the two methods.

5.2.7 Fault density

Fault density across the Nelson/Tasman region was relatively high (*figure 5.10; table 5.5*), predominantly in steeper slopes and areas where there was little or no Moutere gravel (in the ranges that surround the Moutere Depression). It is uncertain whether this is accurate or whether it is more likely a result of the lack of preservation of fault evidence in the gravels. In either case, linear regression analysis (described in section 4.3.4) showed there was no significant statistical correlation between fault density and denudation rate (*figure 5.12; table 5.7*).

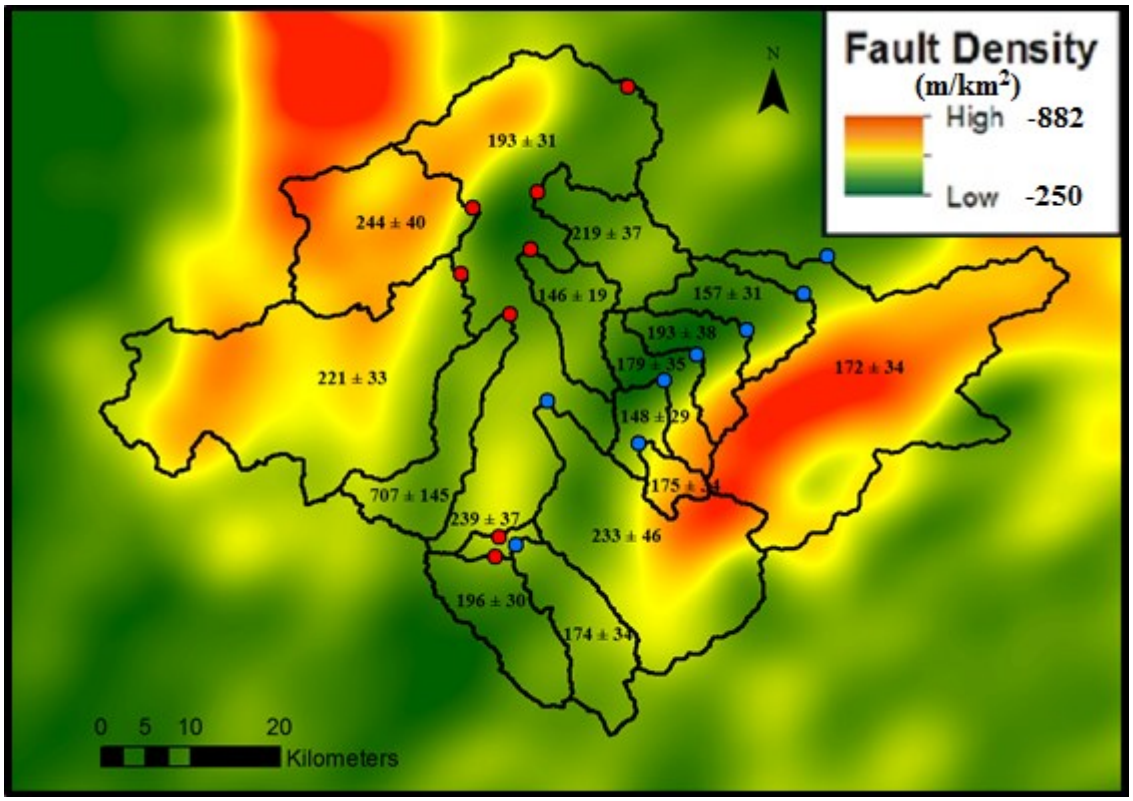

Figure 5.10: The density of faults across the Nelson/Tasman region. Red zones represent high fault densities and green low fault densities. Note the significantly lower fault density in the Moutere Depression which is predominantly underlain by Moutere gravels. Denudation rates are averages derived from the two methods.

Basin	Sample	River	Main rock	Basin area (km^2)	% gravel	% sedimentary/ metasediment	% igneous	% metamorphic	Main rock
1	33_34	Motueka	meta sediments/gravel	1411	45.36	28.38	21.69	4.56	meta sediments/gravel
2	31_32	Baton	meta sediments	449	4.1	52.93	23.53	19.45	meta sediments
3	29_30	Dove	gravel	319	88.5	0	11.5	0	gravel
4	27_28	Stanley Brook	gravel	265	100	0	0	0	gravel
5	22_23	Wangapeka	meta sediments/granite	683	9.37	55.72	28.39	6.52	meta sediments/granite
6	20_21	Tadmor	gravel	342	86.5	4.8	8.7	0	gravel
7	16_17	Rainy River	gravel	326	88.79	4.56	4.49	2.16	gravel
8	12_13	Motupiko	gravel	476	83.25	11.63	3.02	2.1	gravel
9	19	Upper Motueka	gravel/meta sediments	542	47.56	40.41	22.03	0	gravel/meta sediments
10	15	Motupiko	gravel	324	75.16	20.51	1.97	2.36	gravel
11	36	Waimea	meta sediments/gravel	893	35.39	59.46	5.01	0.15	meta sediments/gravel
12	6	Wai-iti	meta sediment	162	11.1	88.5	0	0	meta sediment
13	8	Wai-iti	gravel/meta sediments	253	58.6	41.4	0	0	gravel/meta sediments
14	10	Wai-iti	gravel/meta sediments	362	66.4	33.6	0	0	gravel/meta sediments
15	4	Wai-iti	gravel	450	70.4	29.6	0	0	gravel
16	2	Wai-iti	gravel	536	76	24	0	0	gravel

Table 5.5: Lithological statistics for each of the sampled catchments derived from the zonal statistics tool in ArcMap.

Basin	Sample	River	Mean slope (°)	Relief (m)	% slope above 30°	Mean rainfall (mm/yr)	Mean Ksn	Mean fault density (m/km^2)	Mean flow (L/S)
1	33_34	Motueka	21.43	1790.15	23.4	1733.01	62.1002	537	58560
2	31_32	Baton	28.22	1681.46	45.5	2229.67	76.4327	882	9032
3	29_30	Dove	15.35	557.63	3.7	1228.78	23.0865	278	582
4	27_28	Stanley Brook	18.01	463.29	6.1	1226.8	30.9491	250	1185
5	22_23	Wangapeka	26.01	1679.76	39.8	2203.3	70.3391	650	7854
6	20_21	Tadmor	15.26	1051.57	4.3	1567.7	31.4569	287	2347
7	16_17	Rainy River	18.85	689.45	8.1	1526.13	42.8028	351	1794
8	12_13	Motupiko	16.66	1240.96	6.6	1575.94	44.2094	454	2173
9	19	Upper Motueka	23.51	1570.01	27.1	1457.53	76.7313	683	7067
10	15	Motupiko	14.7	1220.36	5.5	1640	45.4315	555	2176
11	36	Waimea	21.67	1763.4	30.7	1305.86	67.948	675	9520
12	6	Wai-iti	27.08	1262.51	41.7	1420	80.6925	807	ND
13	8	Wai-iti	19.7	1368.72	19.6	1334.5	62.0756	476	890
14	10	Wai-iti	18.61	1413.32	15.4	1270.11	57.0732	410	ND
15	4	Wai-iti	17.72	1456.12	13.3	1240.23	52.892	390	4300
16	2	Wai-iti	16.18	1488.02	10	1199.74	49.5162	347	4300

Table 5.6: Geomorphic and climatic statistics for each of the sampled catchments. Mean flow (L/S) statistics were obtained from Fenemor 1989; 2002; Basher, 2003b; Tasman District Council, 2014.

5.2.8 Cross correlations

Cross correlations were obtained with the use of R (described in section 4.3.4). Denudation rates across the Nelson region showed no significant correlations with any geomorphic, climatic, or lithological variables. However there were very strong cross correlations among lithological and geomorphic indices (*figure 5.11; 5.12; table 5.7*). The strongest correlations exist for percent slope > 30 degrees (0.98), percent gravel and mean fault density (0.92), channel steepness (Ksn) and percent sedimentary/metasediment (0.91), percent slope > 30 degrees and fault density (0.91), and percent slope > 30 degrees and channel steepness (Ksn).

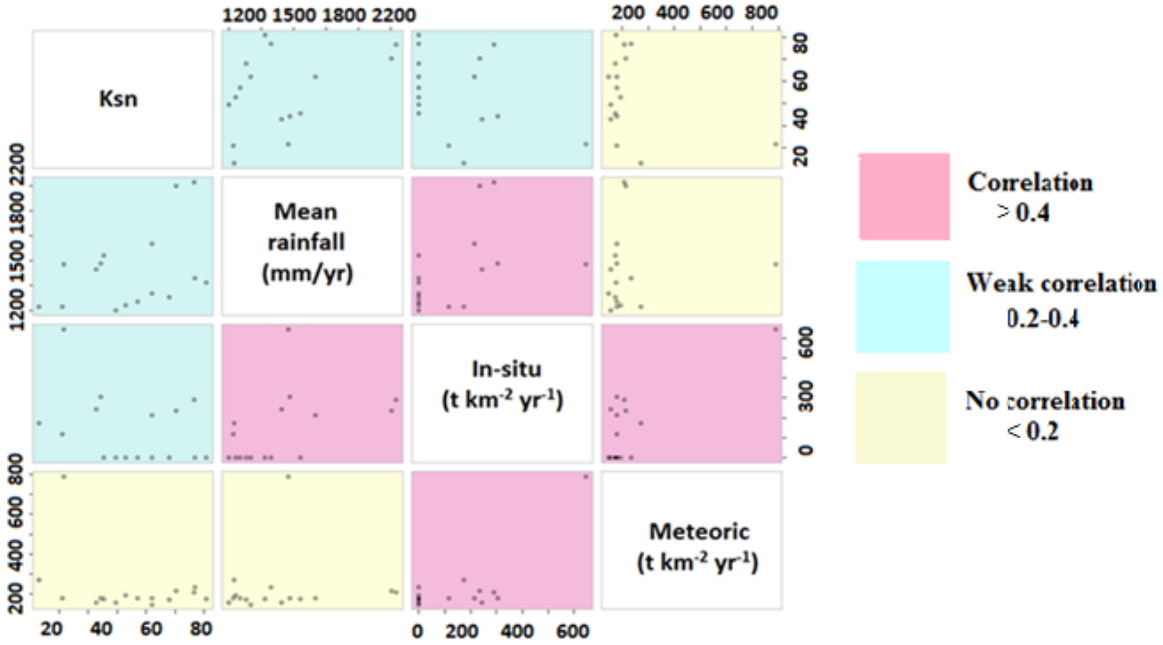

Figure 5.11: Correlations between denudation rates, mean rainfall, and channel steepness derived from the clus package in R (described in section 4.3.4). The denudation rates correlate well with each other (0.76). Mean rainfall has a 0.46 correlation with in-situ denudation rates; however, it is difficult to say whether this is a coincidence due to the limited in-situ data, or whether mean rainfall has somewhat influenced rates of denudation. However, meteoric erosion rates do not correlate significantly with channel steepness or rainfall.

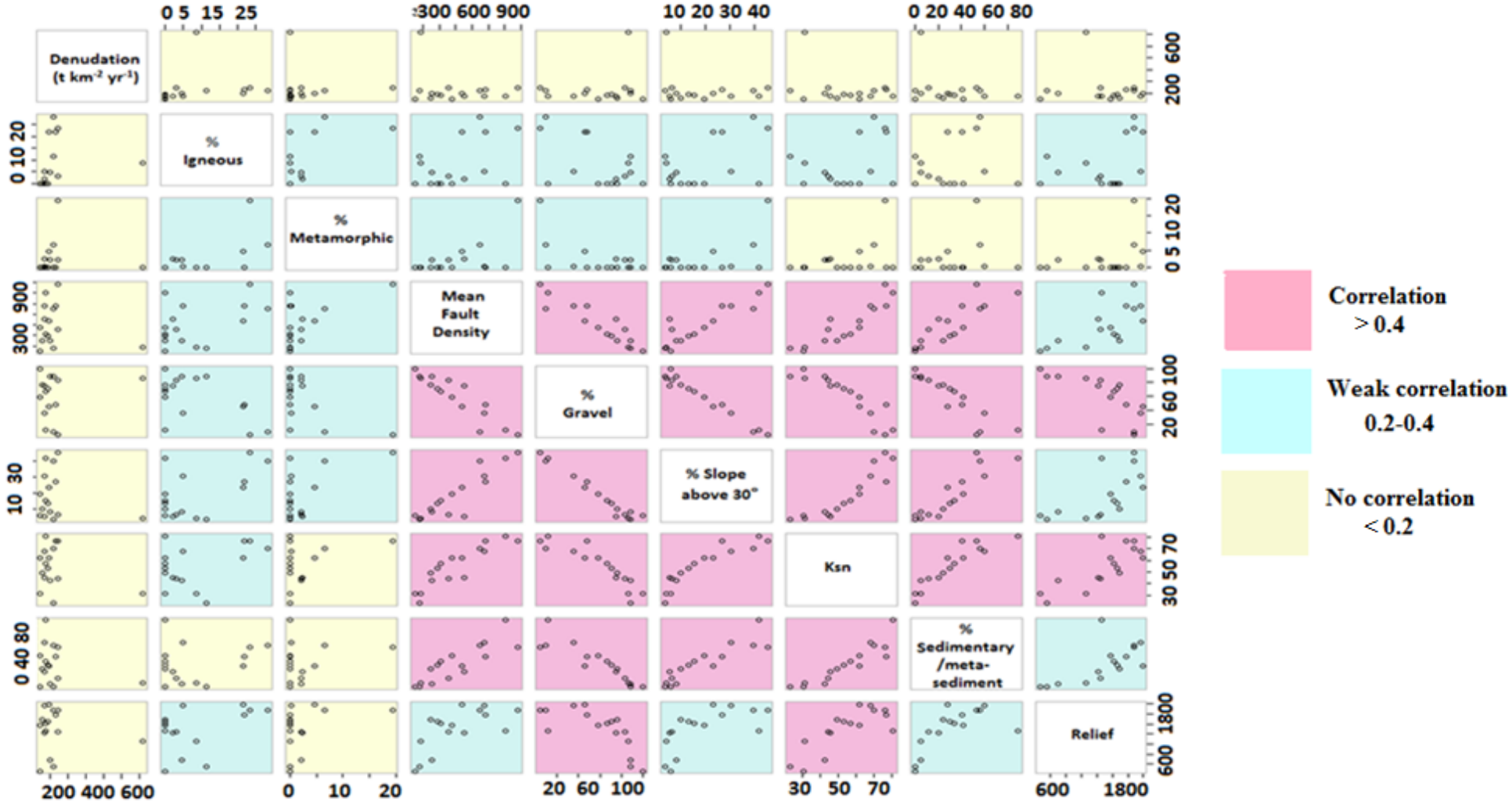

Figure 5.12: Correlations between denudation and geomorphic/lithological indices derived from the gclus package in R (described in section 4.3.4). No significant correlations exist between geomorphic/lithological indices and denudations rates. Denudation rates are averages derived from the two methods.

	Relief	Basin area (m)	% gravel	% Sedimentary/ metasediments	% igneous	% metamorphic	% slope >30°	Mean rainfall (mm/yr)	Max rainfall (mm/yr)	Mean Ksn	Max Ksn	Mean fault density (m/km^2)	Mean flow L/S	In-situ t km^{-2} yr^{-1}	Meteoric t km^{-2} yr^{-1}	Average t km^{-2} r^{-1}
Relief	1.00	0.52	-0.71	0.67	0.41	0.35	0.65	0.40	0.44	0.79	0.79	0.66	0.46	-0.21	-0.18	-0.11
Basin area (m)	0.52	1.00	-0.26	0.11	0.45	0.14	0.23	0.23	0.46	0.25	0.79	0.18	0.97	0.05	-0.12	-0.09
% gravel	-0.71	-0.26	1.00	-0.91	-0.55	-0.57	-0.98	-0.62	-0.43	-0.90	0.69	-0.92	-0.26	0.14	0.21	0.16
% sedimentary/metasediments	0.67	0.11	-0.91	1.00	0.20	0.25	0.90	0.28	0.08	0.91	0.57	0.86	0.07	-0.40	-0.29	-0.27
% igneous	0.41	0.45	-0.55	0.20	1.00	0.61	0.54	0.77	0.74	0.38	0.56	0.47	0.48	0.35	0.13	0.18
% metamorphic	0.35	0.14	-0.57	0.25	0.61	1.00	0.56	0.84	0.71	0.38	0.28	0.57	0.23	0.31	-0.09	0.01
% slope>30°	0.65	0.23	-0.98	0.90	0.54	0.56	1.00	0.57	0.34	0.91	0.66	0.91	0.22	-0.16	-0.25	-0.20
Mean rainfall	0.40	0.23	-0.62	0.28	0.77	0.84	0.57	1.00	0.92	0.41	0.43	0.58	0.29	0.46	0.08	0.19
Max rainfall	0.44	0.46	-0.43	0.08	0.74	0.71	0.34	0.92	1.00	0.26	0.45	0.43	0.52	0.53	0.15	0.27
Mean Ksn	0.79	0.25	-0.90	0.91	0.38	0.38	0.91	0.41	0.26	1.00	0.65	0.90	0.24	-0.37	-0.36	-0.30
Max Ksn	0.79	0.79	-0.69	0.57	0.56	0.28	0.66	0.43	0.45	0.65	1.00	0.51	0.71	-0.14	-0.26	-0.23
Mean fault density	0.66	0.18	-0.92	0.86	0.47	0.57	0.91	0.58	0.43	0.90	0.51	1.00	0.18	-0.20	-0.28	-0.21
In-situ (t km^{-2} yr^{-1})	-0.21	0.05	0.14	-0.40	0.35	0.31	-0.16	0.46	0.53	-0.37	0.14	-0.20	0.11	1.00	0.76	0.83
Meteoric (t km^{-2} yr^{-1})	-0.18	-0.12	0.21	-0.29	0.13	-0.09	-0.25	0.08	0.15	-0.36	0.26	-0.28	-0.10	0.76	1.00	0.98
Average (t km^{-2}yr^{-})	-0.11	-0.09	0.16	-0.27	0.18	0.01	-0.20	0.19	0.27	-0.30	0.23	-0.21	-0.06	0.83	0.98	1.00
Mean flow (L/S)	0.46	0.97	-0.26	0.07	0.48	0.23	0.22	0.29	0.52	0.24	0.71	0.18	1.00	0.11	-0.10	-0.06

Table 5.7: Table of r^2 correlations between all geomorphic, lithological, and climatic variables, and ^{10}Be-derived rates of denudation. As shown on figures 5.11 and 5.12, r^2 correlations of >0.4 indicates a significant correlation, 0.2 – 0.4 indicates a weak correlation, and <0.2 indicates no correlation

Chapter 6: Discussion

6.1 Introduction

Meteoric and in-situ ^{10}Be analysis have both successfully produced spatially-averaged denudation rates for the Nelson region. The use of cosmogenic nuclides to quantify denudation rates in Nelson has provided a useful benchmark for assessment of background erosion rates for comparison with other erosion studies in the area. Competent background rates of erosion have allowed for the assessment of spatial and temporal trends within the northern South Island region including the impact of geomorphology, tectonics, climate, lithology, and anthropogenic clearing on erosion rates among differing sites.

The range of denudation results varied by ~190 t km^{-2} yr^{-1} between 112 – 298 t km^{-2} yr^{-1} across the basins which was somewhat similar to other erosion estimations for the region which varied by ~150 t km^{-2} yr^{-1} between ~50 – 200 t km^{-2} yr^{-1} (NIWA, 2013; Basher). These ^{10}Be results exclude one basin which was eroding exceptionally faster at 789 t km^{-2} yr^{-1} for meteoric and 626 t km^{-2} yr^{-1} for in-situ. The outliers appear to be robust estimates of denudation as they are both taken from the same location in the Tadmor River (basin 6).

The following sections will a) address assumptions made in using cosmogenic ^{10}Be to quantify erosion and where these assumptions could potentially have affected results, b) discuss the temporal and spatial trends of denudation in the Nelson/Tasman region including the rapid denudation of the Tadmor basin, and c) assess the impact of geomorphology, tectonics, climate, lithology, and anthropogenic clearing on rates of denudation.

6.2 Validation of assumptions

A number of assumptions for both meteoric and in-situ ^{10}Be methods were applied to this analysis. This section addresses the validity of some of the assumptions that were discussed in sections 2.4.3 and 2.4.5 and discusses where results could potentially be affected by deviations from the assumptions.

6.2.1 Isotopic steady state and uniform erosion

Isotopic steady state and uniform erosion over the denudational timescale is an assumption that can be difficult to justify for both in-situ and meteoric analysis– it requires isotopic steady state where the amount of ^{10}Be that leaves the catchment in denudation via the river is equal to the production of ^{10}Be in the catchment (von Blanckenburg, 2006). As discussed in section 2.4.3 this can be an issue where deep-seated landslides have occurred exposing and contributing material that was previously isolated from cosmic rays. The Nelson/Tasman region is prone to storm-induced landsliding (*figure 6.1*). While the landslides in the region are usually considered shallow (within the soil column), it is uncertain whether these are contributing to denudation representative of background rates, or whether some are large enough to be contributing deep material extensively and over-representing particular erosion sources. Because in-situ nuclide concentrations are ~equal over the depth of mixing in a soil (Granger and Riebe, 2007), it is unlikely that the shallow landslides in Nelson/Tasman significantly perturb the sediment ^{10}Be concentrations.

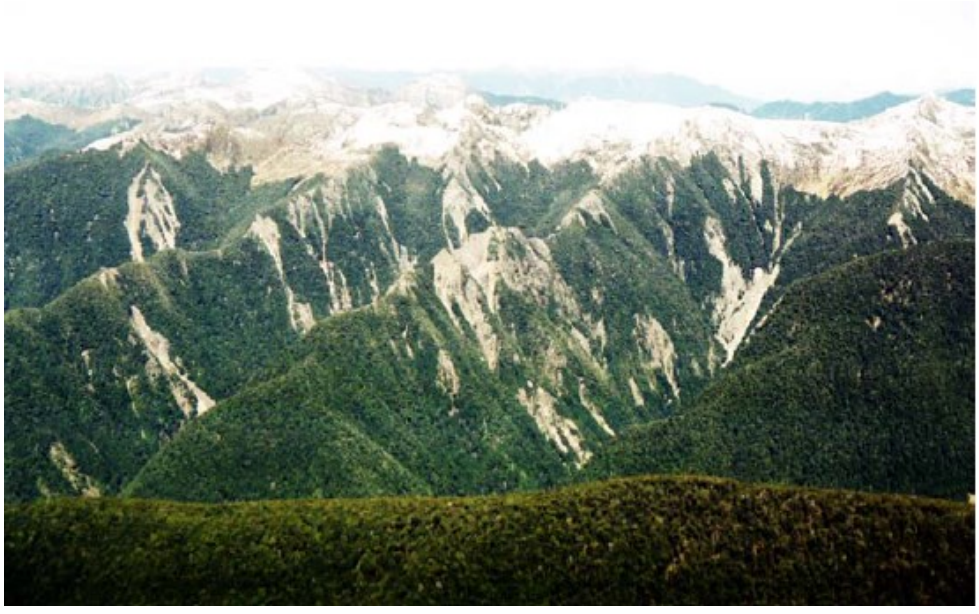

Figure 6.1: Extensive shallow landsliding in the headwaters of the Wangapeka River (*figure 3.2*), a tributary to the Motueka (Basher et al., 2003a)

The time since a major erosive event is also important to consider when sampling. Savi et al. (2014) address the effects of sufficient mixing of sediment where mass wasting has occurred concluding that it is prudent to sample as long as possible after mass

wasting events have occurred. The Nelson/Tasman region experienced a major storm event in December 2011, ~1 year before sampling. It remains uncertain whether the magnitude of this event could have impacted landscape so gravely that nuclide concentrations are affected by insufficient mixing, and it must be considered that this could have impacted the results. However, the distance from the confluence has also been found to affect the mixing of sediment from tributaries; it is suggested that the further downstream the sample was taken the better the mixing of erosion sources (Binnie et al., 2006; Savi et al., 2014). In this study, samples were taken from headwaters, shortly after confluences, and well downstream of confluences. The consistency among results from all of these locations suggests that this has likely not affected the denudation results in the region. The weighted averages of upstream sites are also consistent with the rates obtained near the mouth of each catchment (this will later be discussed), further supporting the likelihood of thorough mixing within the catchments.

There were no obvious large landslides located from satellite images or site analysis aside from the Tadmor Valley slump (this will be further discussed). The denudational timescales are also relatively short, thus it is reasonable to assume that no deep-seated landslides have occurred within these timescales being that there is no obvious evidence for their occurrence. Basins of sufficient size (>100km^2) were chosen minimising the possibility of insufficient mixing of sediment. It is reasonable to assume that no landslides, beyond the Tadmor slump (this will be further discussed in section 6.3.3), could be over-represented in denudation averages, affecting the confidence in the results

6.2.2 Zero concentration of meteoric at the soil/bedrock interface

This assumption does not hold for the Nelson/Tasman region. Where the regolith met bedrock the concentration of meteoric ^{10}Be was still relatively high (*table 5.4*). The meteoric averaging timescales derived from the depth profile produced plausible ~5000 yrs); however, as the ^{10}Be concentration was not 0 at the bedrock, the following two scenarios are considered to explain this occurrence and discuss possibilities of alternative averaging timescales.

6.2.2.1 Permeable bedrock

The bedrock in which meteoric ^{10}Be adsorption would typically discontinue was fractured/weathered significantly and therefore permeable. This is common in a New

Zealand setting due to significant tectonic activity and rapid uplift. The high permeability may allow ^{10}Be to leach into the bedrock with meteoric waters, or be redistributed deeper by diffusion or other means of leaching (*figure 6.2*). Assuming this is the case and the concentrations measured are representative, the meteoric profile would extend to ~800cm (*figure 6.3*) with an adsorption depth of ~130cm. The denudation rate and adsorption depth then produce an averaging timescale of ~8100 yrs. The consistency between the meteoric- and in-situ derived results and the attainment of this meteoric averaging timescale would suggest that erosion has not changed over the past ~8100 years. This is not plausible in a New Zealand setting as the landscape is young and dynamic, meaning geomorphic processes occur over shorter timescales than this. Significant changes in climate also occurred over this longer timescale and this does not appear to show in the meteoric erosion rates.

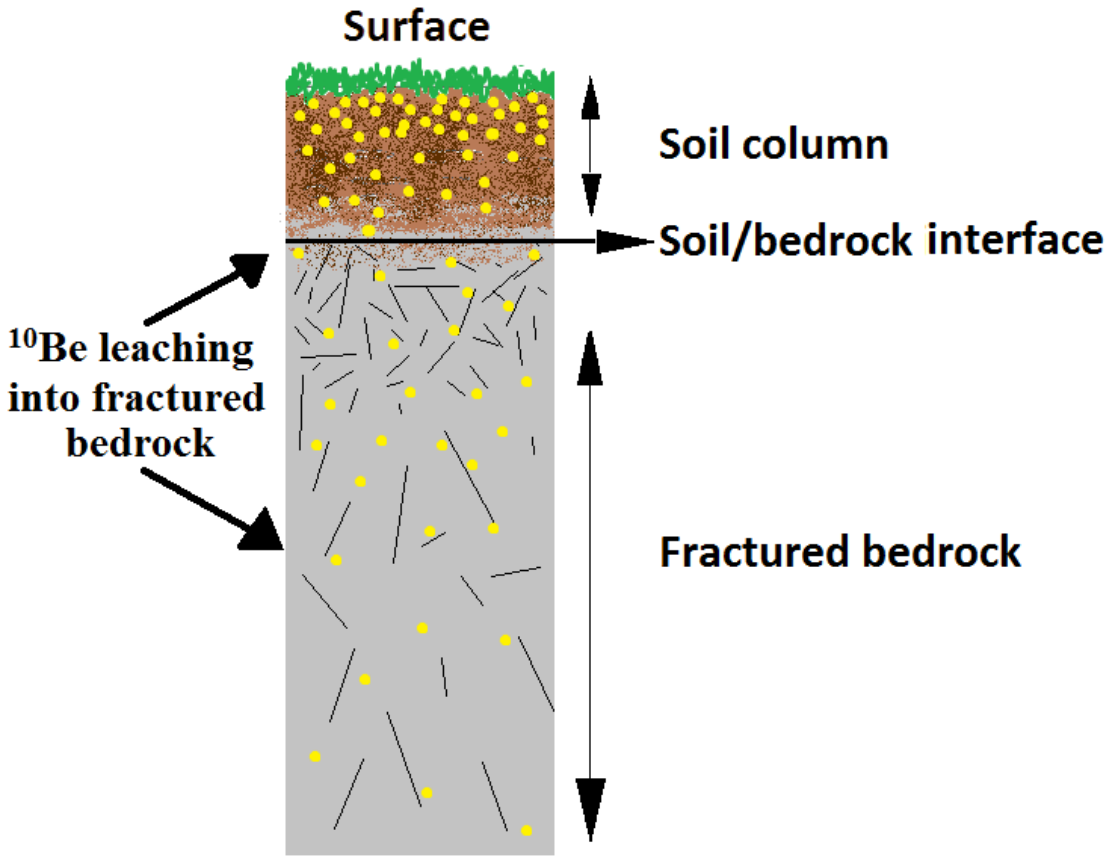

Figure 6.2: Illustration of meteoric ^{10}Be leaching into fractured bedrock. Here meteoric ^{10}Be is not retained within the soil column meaning.

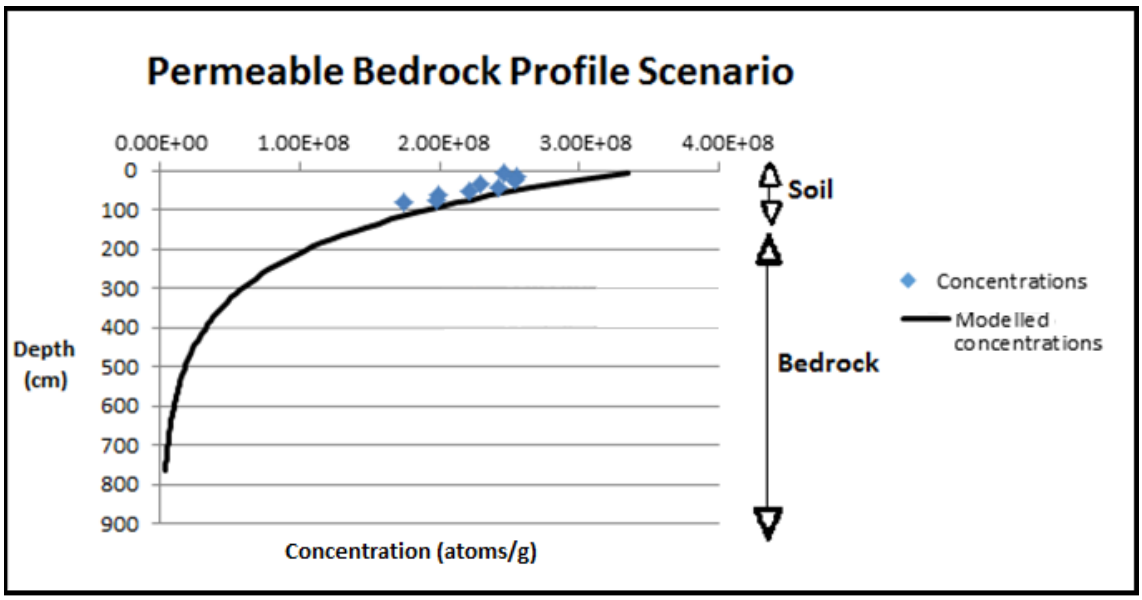

Figure 6.3: ^{10}Be concentrations with depth with the assumption that the bedrock is fractured and therefore ^{10}Be is leaching beneath the soil column. Note, assuming this is the case, ^{10}Be leaches to ~800cm (~700cm into the bedrock) with an absorption depth of 130cm.

6.2.2.2 Impermeable bedrock

An alternative scenario for meteoric ^{10}Be adsorption is that leaching is impeded by impermeable bedrock. Once the ^{10}Be meets bedrock it leaves the system laterally along the bedrock surface as well as from the regolith surface via erosion (*figure 6.4)*. In this case, the base of the soil/bedrock is the lowest concentration in the profile. This can be modelled by setting the concentrations to zero at the bedrock and adjusting the concentrations above accordingly (*figure 6.5*). This maintains the shape of the profile but shorter adsorption depths produce an averaging timescale of ~1200 years. This scenario is plausible as the in-situ derived rates are similar to meteoric derived rates supporting the similarity between the averaging timescales. However, this does imply that the total nuclide inventory may be underestimated. This averaging timescale will be used for the purposes of the following discussions.

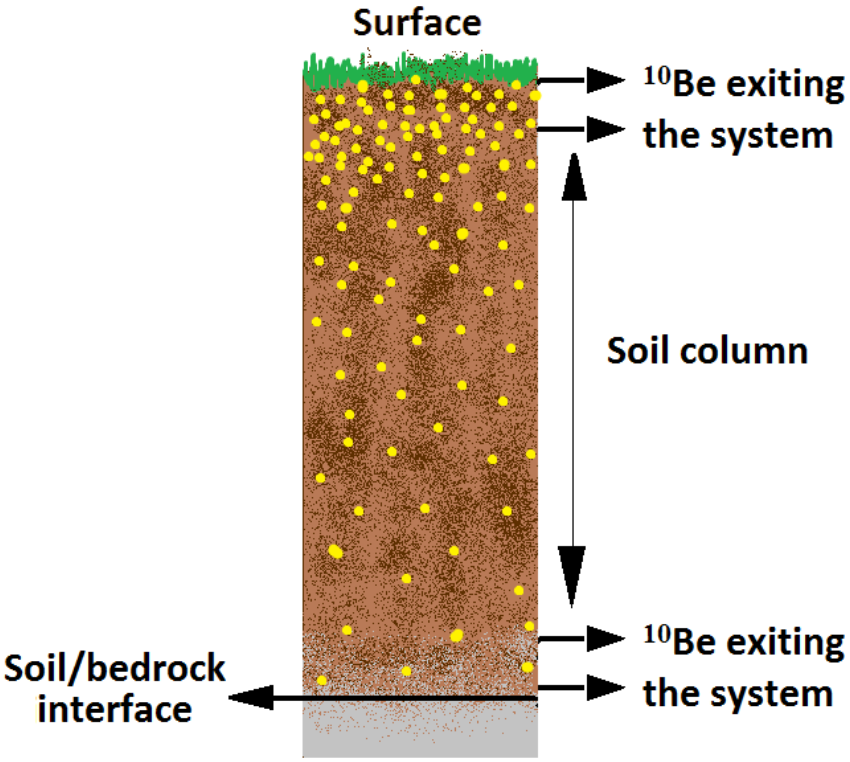

Figure 6.4: Illustration of meteoric ^{10}Be exiting the system along the soil/bedrock interface.

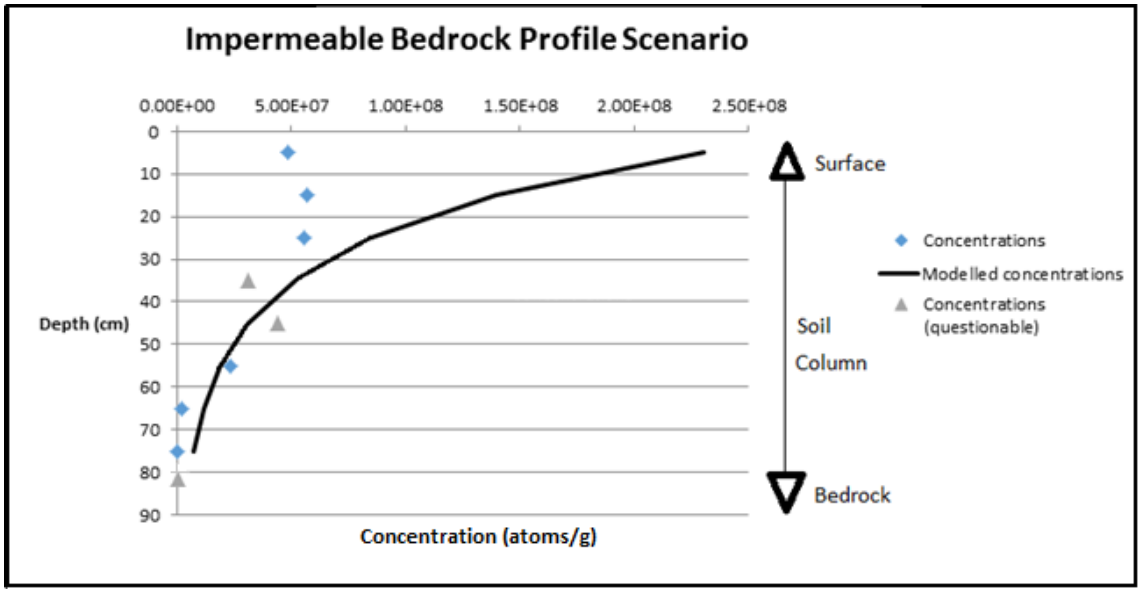

Figure 6.5: ^{10}Be concentrations with depth assuming that the bedrock is impermeable and ^{10}Be exits the system along the soil/bedrock interface as well as at the surface. Absorption depth is 20cm.

The adsorption depth of meteoric ^{10}Be into the soil column is questionable in this location and further research would be needed to convincingly obtain an accurate adsorption depth. However, this affects only the timescales over which the denudation rates average and not the rate at which concentration decreases below the surface or the calculated denudation rates.

6.2.3 Retention of Meteoric ^{10}Be

As discussed in section 2.4.5.2, the retention of meteoric ^{10}Be to sediment particles can be affected by the pH of the sediment where Al^{3+} may compete for ion exchange sites in strongly acidic soils. *Figure 3.6* shows that the Tadmor River (basin 6) and Rainy River (basin 7) basins are the only catchments to be underlain by podzol soils. These soils are considered strongly acidic therefore it must be considered that loss of ^{10}Be through competition with Al^{3+} may have occurred. Bacon et al. (2012) addressed the retentivity of Spodosol soil (the United States equivalent of podzol) in relation to soils residence times in concluding that the assumption of complete ^{10}Be retention is unreasonable for acidic soils such as Spodosols. This could have resulted in a lower concentration of meteoric^{10} Be in the Tadmor sample and explain the Tadmor's elevated erosion rate. However, the equivalence of meteoric and in-situ derived denudation rates in the Tadmor as well as high concentrations for the Rainy River suggest that significant ^{10}Be loss has not occurred.

It must also be considered that Nelson is one of the few places in New Zealand with Ultic soils which are considered strongly acidic. Interestingly, there was some ~106 t km^{-2} yr^{-1} discrepancy between the in-situ and meteoric rates of the Dove River catchment (basin 3) (meteoric being the higher at 272 t km^{-2} yr^{-1}) and this basin also one of the few basins that contains no Ultic soil (*figure 3.6*). The Tadmor catchment also contains no Ultic soil while most other basins in the region do, so perhaps the Tadmor is more representative of meteoric-derived rates than other basins due to the loss of in strongly acidic soils. This cannot, however, explain the elevation of the in-situ result concurrently with the meteoric.

Adsorption of ^{10}Be through the soil column showed a mid-depth maximum which is not an uncommon finding globally and, likely the result of a mid-depth clay layer where ion exchange capabilities are increased (Brown et al., 1992) (*figure 6.6*). Basher & Jackson (2002) suggest that soils of the Moutere Depression commonly exhibit a mid-depth clay

layer. In this case, the mid-depth maximum may be due to recent shallow mixing (i.e. deforestation), or leaching of beryllium from the surface sediments. It was not necessary to apply the normalisation equation described by He and Walling (1996) and Wallbrink & Murray (1996) because analysis was completed using a narrow grainsize range from 45-60 µm. This ensured results could be skewed one way or the other but would remain internally consistent.

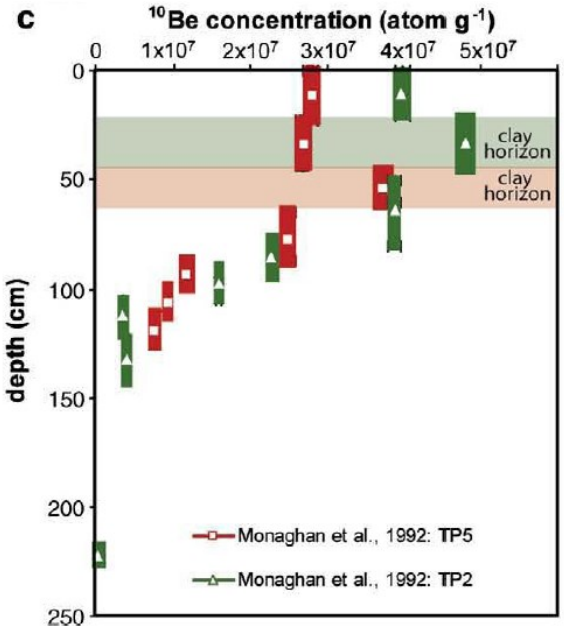

Figure 6.6: Depth profile measurements in Contra Costa Country, California displaying a mid-depth meteoric ^{10}Be maximum (Monaghan et al., 1992).

6.3 Temporal and spatial trends of denudation in the Tasman region

6.3.1 Meteoric vs In-situ

Mean denudation rates across the Motueka where both meteoric and in-situ results were obtained were 272 t km^{-2} yr^{-1} and 269 t km^{-2} yr^{-1}, respectively. With the removal of the outlier, the results change somewhat to 198 t km^{-2} yr^{-1}and 218 t km^{-2} yr^{-1}. Uncertainty exists as to whether this is significant in that perhaps the in-situ results are representative of the slightly longer timescales at ~2750 years than the meteoric at ~1200 years. It is also questionable whether the outlier is representative or should be excluded from calculations due the uncertainty regarding its explanation. The two methods are measuring on different timescales and have different controlling factors in terms of their sensitivity to parameters such as the size and depth of any landslide

events and the different soil characteristics of the catchments. However, what is most interesting in the results is the level of agreement between the methods. In-situ and meteoric ^{10}Be-derived rates for each basin were all equivalent within 2-sigma, and many within 1-sigma (*figure 5.4*). In-situ and meteoric measurement deviated by no more than ~118 t km^{-2} yr^{-1} for basins 3, 6, 7 and 8, and no more than ~81 t km^{-2} yr^{-1} for all other basins. It is clear that more data is needed because eight pairs of measurements of method precision is not enough to draw firm conclusions. However, the agreement between the two methods is much better than one would expect which is very encouraging in that it could be possible to use meteoric ^{10}Be as an alternative to assess catchments where levels of quartz bearing material are low; where the in-situ method is not applicable, the meteoric method may offer a valuable alternative.

6.3.2 Motueka vs Waimea

With analysis of just meteoric ^{10}Be derived rates, the area-weighted mean denudation rate for the Motueka catchment rate is higher (247 t km^{-2} yr^{-1}, and 207 t km^{-2} yr^{-1} without the outlier) than for that of the Waimea catchment (171 t km^{-2} yr^{-1}). The outlying rate of the Tadmor will be excluded for the purposes of this discussion. Uncertainty exists as to whether similar high rates occur in Waimea tributaries because samples were taken only from the trunk of the Wai-iti (one of two tributaries to the Waimea) were obtained. It remains possible, however, that there is an internal or external factor driving the elevated rates of the Motueka catchments. Further study would be needed to draw conclusions. The samples taken from near the mouth of the Motueka and the Waimea however produced very similar results (178 t km^{-2} yr^{-1} and 172 t km^{-2} yr^{-1}, respectively) raising question as to whether all erosion sources are represented accordingly in the Motueka mouth sample. The consistency between the average of all Waimea basins and the sample taken from the mouth of the Waimea River suggests that all erosion sources in this basin are fairly represented (e.g. Granger, et al., 1996; Savi et al., 2014). The difference between the average rate from all Motueka catchments and the rate from the Motueka River mouth is only ~30 t km^{-2} yr^{-1} therefore it is plausible to assume all erosion sources are represented in the sample.

6.3.3 Rapid denudation in the Nelson/Tasman region

The elevated ^{10}Be-derived denudation rates from basin 6 (Tadmor River) (*figure 6.7*) deserve closer inspection. The Tadmor River's Suspended Sediment Yield Estimate of

202 t km^{-2} yr^{-1} (NIWA, 2013) is considerably lower than both the meteoric and in-situ ^{10}Be derived rates of denudation. It remains somewhat inconclusive whether the Tadmor River sample was misrepresentative or whether there was a plausible reason for the exceptionally elevated ^{10}Be-derived denudation rates at this location. The following sections offer a number of possible explanations for this anomaly.

Figure 6.7: The location in the Tadmor River (basin 6) where both meteoric silt samples and in-situ sand samples were taken.

6.3.3.1 Landslide slump

West of Tui, a large slump has intruded in the path of the Tadmor River (*figure 6.8; 6.9*). The river is incising into the toe of the slump which, if the landslide is significant enough, could be exposing material far below the surface that has previously had little or no cosmic ray exposure. This material could potentially be contributing enough material to the basin-averaged samples downstream that explain the significantly lower ^{10}Be concentrations at this site. In a case such as this, it remains uncertain whether the proximity of the land slump and the fluvial incision into its toe could be over representing this particular erosion source for this basin. Here it is prudent to consider the results of both meteoric and in-situ samples and address the erosion mechanisms and therefore transport of each sediment sample. In-situ samples were obtained from fine grained sand and meteoric samples were obtained from suspended silt. It must be considered that the material contributed by incision into the base of the slump is likely coarser grained, introducing consideration of grainsize dependency for in-situ ^{10}Be concentrations. The mechanisms that transport fine suspended sediment (used for

meteoric ^{10}Be rates) unfold on shorter timescales than the transport of sand particles and are delivered via different mechanisms. It could be said that the slump is unlikely to be affecting meteoric ^{10}Be obtained from silt samples as greatly as the in-situ ^{10}Be obtained from sand. This however is not the case; the meteoric-derived denudation rate is elevated above the in-situ-derived result (789 t km^{-2} yr^{-1} and 626 t km^{-2} yr^{-1}, respectively). It is reasonable to assume that the elevated denudation rate is from long term signal; therefore, it is unlikely that the slump is influencing the rates.

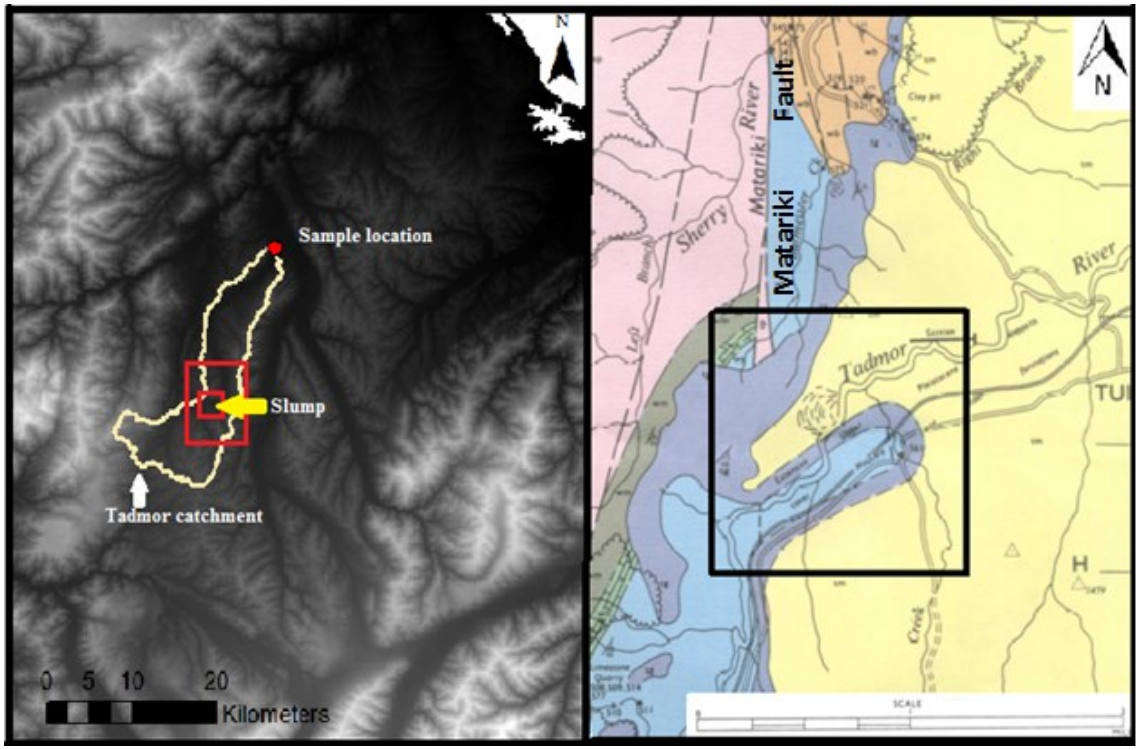

Figure 6.8: Location of the Tadmor landslide slump near Tui (Modified from Johnson, 1971). Note also the location of the Matariki Fault north of the slump.

Figure 6.9: Fluvial incision into the toe of the Tadmor slump (Basher et al., 2003). Note the severe gullying at the base of the slump that could be contributing material that has not long been exposed to cosmic rays (therefore overestimating in the rate of denudation).

6.3.3.2 Tectonic activity

New Zealand has a very tectonically active landscape but research data and complex understanding of tectonic movement and geologic history is relatively limited at a scale relevant to this study. Although current data (Rattenbury et al., 1998) suggests there are no active faults in the vicinity of the Tadmor River it is possible that there is a tectonic influence affecting this basin more so than the other basins. Evidence from channel morphology is shown in *figure 4.1* where it appears an upper section of the Tadmor has deviated from its original flow path to the south to its current flow path to the east. Johnson (1971) highlighted evidence of significant fault downthrow of the Matariki Fault near Sherry River (*figure 6.8*) which is in close proximity the Tadmor. It could be that tectonic activity has deviated this channel section in the past. Johnson, (1971) suggests the lack of research and data in the region, however, means this cannot be supported confidently. Furthermore, the presence of the Moutere gravel likely hinders the preservation of evidence for tectonic activity. Interestingly, the Tadmor River shows no sign of knickpoint propagation, displaying a near linear stream profile (*figure 6.10*) while all other basins have a well-defined knickpoint. This suggests that any disturbance

that occurred on this river happened sufficiently long ago that the knickpoint has propagated up through the entire river, adjusting to its new conditions.

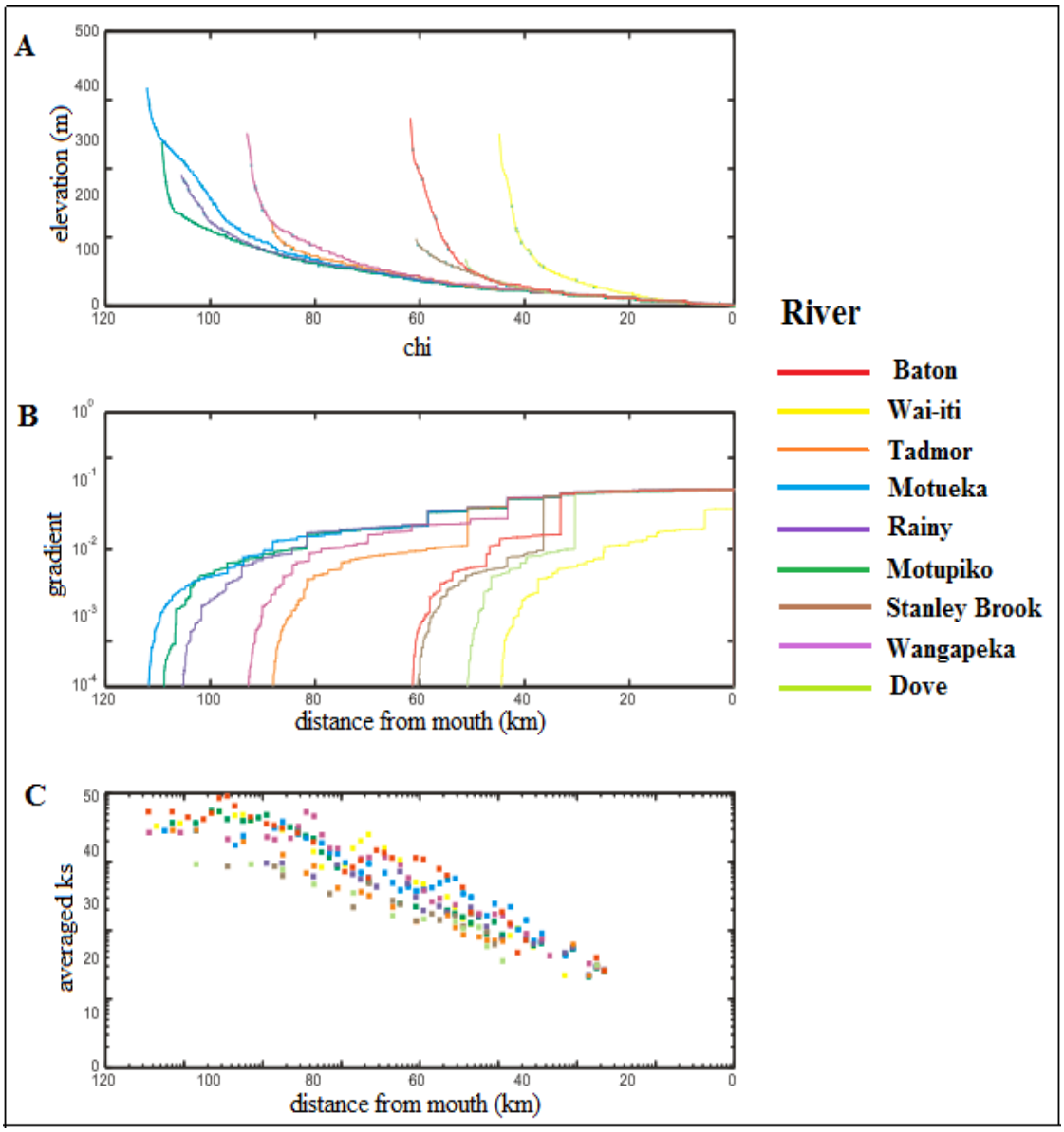

Figure 6.10: Channel profiles of all sampled rivers obtained with the use of Matlab: a) channel elevation (m) plotted against chi. b) channel gradient plotted against distance from river mouth (km) c) averaged channel steepness plotted against distance from river mouth (km).

Because there is no evidence of perturbation in the channel profile, activity in this channel would have to be recent. The Tadmor River may have recently changed to a transient state adjusting to a new base level; the deviation of the river could be resulting in rapid incision of its new path. Alternatively, the lack of a knickpoint could be due to the weak gravel substrate. Here it could be that the river contributing a large amount of

recently incised and therefore recently exposed material via river incision, and that this material is over represented downstream as a result of incomplete mixing (Norton et al., 2008). Channel incision could be occurring more rapidly than hillslope erosion (eg. Abbuhl et al., 2010), due to the deviation of the river to its new path; therefore, the sediment collected from this river could be dominated by the eroded material from channel incision.

6.3.3.3 Interbasin transfer

During the summer months maximum of 0.5m^3 s^{-1} of water is diverted from the Hope River into the Tadmor River. The effects of this are difficult to determine but it is unlikely that this is influencing the elevated denudation rates of the Tadmor for the following reasons. Possible diversion of sediment from the Hope River into the Tadmor could be a factor contributing to the low ^{10}Be concentrations and therefore apparent rapid denudation. The headwaters of the Hope River, where the water is diverted from, are flanked high on the Hope Saddle where slopes and channels are steep. The Hope River is in closer proximity to the epicentres of significant earthquakes such as the Murchison 1929 magnitude 7.8 (*figure 6.11*) that caused extensive landsliding throughout the surrounding region. It must be considered that material from these areas (potentially deep material that was exposed as a result of tectonic events) could be being diverted to the Tadmor River and therefore lowering the ^{10}Be concentration and contributing to the elevated denudation rate.

This theory is unlikely as the diversion transfers only a very small amount of water in relation to the Tadmor River. The size of the interbasin transfer would have to be considerably larger to bring significant material that could affect the Tadmor basin. Diversions are also designed to limit the sediment that is transferred between the basins meaning the total flux of material contributed from the Hope River should be highly insignificant. It has been suggested that the receiving channel can experience change in channel morphology in response to increased flow (Wolman, 1967); however, again the size of the transfer and amount of water diverted is unlikely to be enough to cause such changes. Here it would be more likely that short term yields would be affected as opposed to ^{10}Be denudation rates, which is not the case for the Tadmor River. Unless the construction of the transfer (which occurred in 1989) was so intrusive that it exposed a large amount of deep material that has then been transported down the

Tadmor basin it is unlikely that this would be contributing to the elevated rate of denudation.

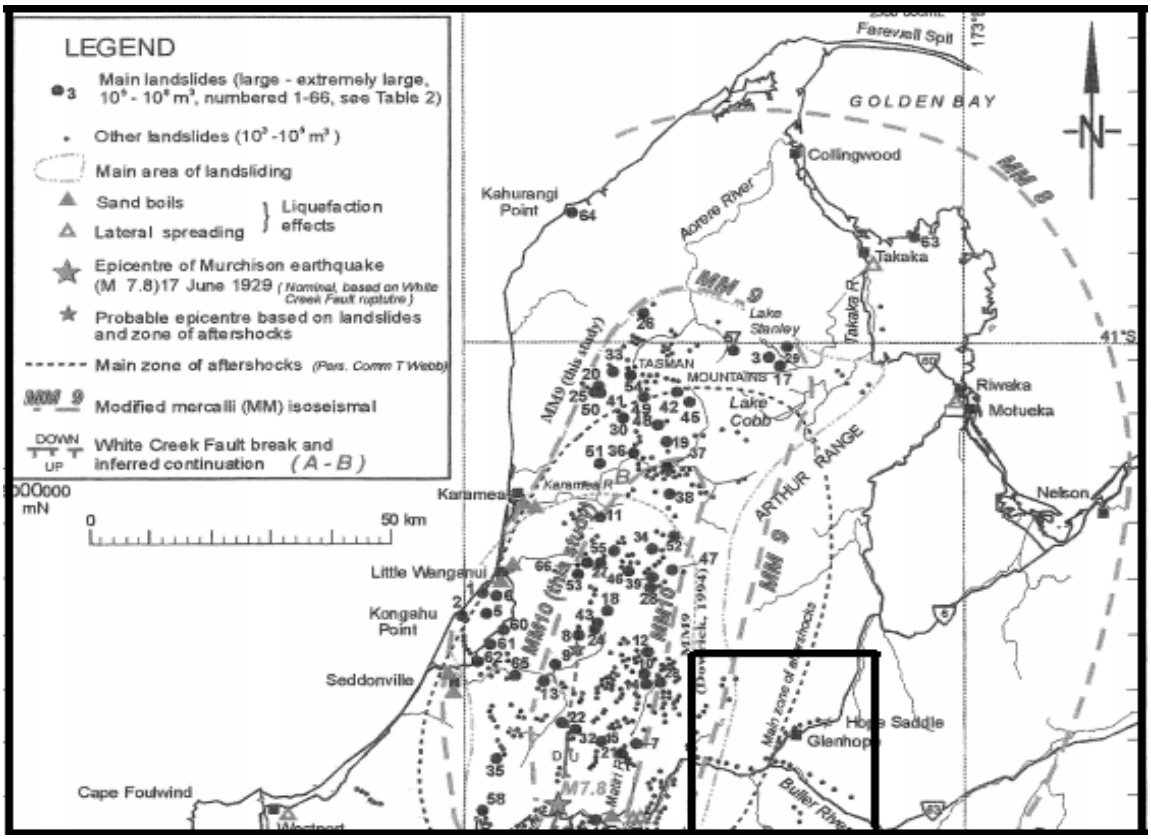

Figure 6.11: Landslide locations following the Murchison earthquake (M 7.8) 17 June 1929 and subsequent aftershocks. The Tadmor River is located to the north-east of Glenhope, on the northern side of the Hope Saddle. The Hope River is located to the south of the Hope Saddle (*figure 3.2*) and the interbasin transfer between the two rivers passes through the saddle (Modified from Hancox et al., 2002).

6.3.3.4 Forest clearing

Intensive deforestation in the region could have affected the Tadmor basin more so than other basins, contributing to the elevated rates of denudation. Forestry is common throughout the study area and this would require that the Tadmor basin has responded differently due to the some external or internal factor. Hippe et al. (2012) found that elevated ^{10}Be-derived denudation rates occurred due to the presence of highly erodible Quaternary sediments that were prone to erosion during flood events (Guyot et al. 1992). It is possible that the combined effects of extensive forest clearing and erodible gravels in the Tadmor Valley have impacted the Tadmor more than other basins in the

area. However, elevated rates from rapid tectonics and deep seated landsliding seem the more plausible factors because a number of the other sampled catchments are similarly located on deforested areas underlain by Moutere gravels.

6.4 Impact of geomorphology on denudation

There were no direct correlations between geomorphic variables and ^{10}Be-derived denudation rates (*figure 5.11; 5.12; table 5.7*); however, the geomorphology parameters correlated exceptionally well among itself and with lithology. *Table 5.7* shows percent gravel is positively correlated with percent slope >30° at 0.98, and mean fault density at 0.92. Channel steepness (Ksn) is positively correlated with percent slope >30° at 0.91. Channel steepness, fault density, lithology, slope angle, and relief correlated between one another exceptionally, but denudation was independent of any of these variables. This is significant in that it suggests that the landscape could be in topographic steady state where there is a balance between erosion and the entire tectonic velocity field (Willett et al., 2001).

6.4.1 Topographic steady state

Matmon et al., (2003b) found that samples taken from the headwaters of their Great Smoky Mountain basins were consistent with samples taken at the outlets, implying spatial homogeneity throughout the catchments. Samples taken from the headwaters and tributaries of the Motueka basin (basins 2-10) had meteoric and in-situ-averaged rates that ranged from 146 – 244 t km^{-2} yr^{-1} (without the outlier) and ~146 – 707 t km^{-2} yr^{-1} (with the outlier) with a mean of ~209 t km^{-2} yr^{-1} (without outlier) and ~271 t km^{-2} yr^{-1} (with the outlier) (basins 2-10). The denudation rate near the outlet was ~193 t km^{-2} yr^{-1} (207 t km^{-2} yr^{-1} for in-situ and 178 t km^{-2} yr^{-1} for meteoric) (basin 1). The Wai-iti had denudation rates that range from ~148 – 193 t km^{-2} yr^{-1} with a mean of ~170 t km^{-2} yr^{-1} while the outlet at the Waimea trunk (basin 11) had a rate of ~172 t km^{-2} yr^{-1}. These results put both the basin's headwaters remarkably similar to the outlets, similar to the findings of Matmon et al., (2003b).

Matmon et al. (2003a; b) found sediment loads, ^{10}Be, and thermochronometry-derived erosion rates were all consistent. Implications for Matmon et al.'s (2003b) finding was the landscape was in equilibrium between erosion and uplift or at topographic steady state. A number of other studies approached the idea of topographic steady state as an

explanation for temporally homogenous denudation rates derived from two or more of the following methods: thermochronological exhumation analysis, ^{10}Be analysis, sediment accumulation volume, and sediment yield data. Studies include the Fort Sage mountains (Granger et al., 1996), Arnhem Land, northern Australia (Nott & Roberts, 1996), the Olympic mountains (Montgomery & Brandon, 2002), a Namibian escarpment, southern Africa (Bierman & Caffee, 2001), and the Himalaya (Vance et al., 2003).

Denudation rates in the Nelson/Tasman region are spatially homogenous and it is possible that they are temporally homogenous also. Broadly derived uplift rates for the Nelson/Tasman region (*figure 6.12*) correspond with^{10}Be-derived denudation rates. Uplift has been estimated at 0 – 1 mm yr for the Nelson/Tasman region while ^{10}Be denudation rates are between 0.1 mm yr and 0.6 mm yr (uplift is estimated to be 1 – 5 mm for the Arthur Range; however, this only represents a portion of basins 1, 2, and 5). However, limited data means uplift rate cannot be assessed accurately for the region. Ferrier et al. (2005) alternatively derived spatial but not temporal homogeneity for denudation rates in Casper Creek, California. They suggested that although denudation was spatially homogenous, this did not necessarily mean the landscape was in topographic steady state. Uplift rates in the their study region, derived from terrace aging, were significantly more rapid than rates of denudation, indicating disequilibrium. Unfortunately the Nelson/Tasman region is limited by consistent data only from sediment yield estimates and modelling. A comparison with short term data (sediment yields and modelling) is not suitable for understanding temporal trends over geological timescales due to the biases associated with short term estimations. However, due to spatial homogeneity of denudation and consistency with broadly derived uplift rates, it seemslikely that the Nelson/Tasman region is approaching or has approached topographic steady state.

6.4.2 Flux steady state

Although denudation rates in Nelson display similar characteristics to the Appalachians, perhaps is it more plausible to suggest that Nelson may be in flux/tectonic steady state as opposed to topographic. Flux steady state requires that the accretionary flux equals the erosional flux but the landscape may still change geomorphically (Brandon et al.,

1998; Willett & Brandon, 2002). In a dynamic and young environment such as New Zealand it is perhaps prudent to assume that the landscape is still changing and in flux/tectonic steady state which is thought to precede topographic steady state (Montgomery, 2001). With the complexity of tectonic movement in New Zealand, the theory that all components of topographic steady state (horizontal and vertical movement, and erosion) have obtained a balance is questionable.

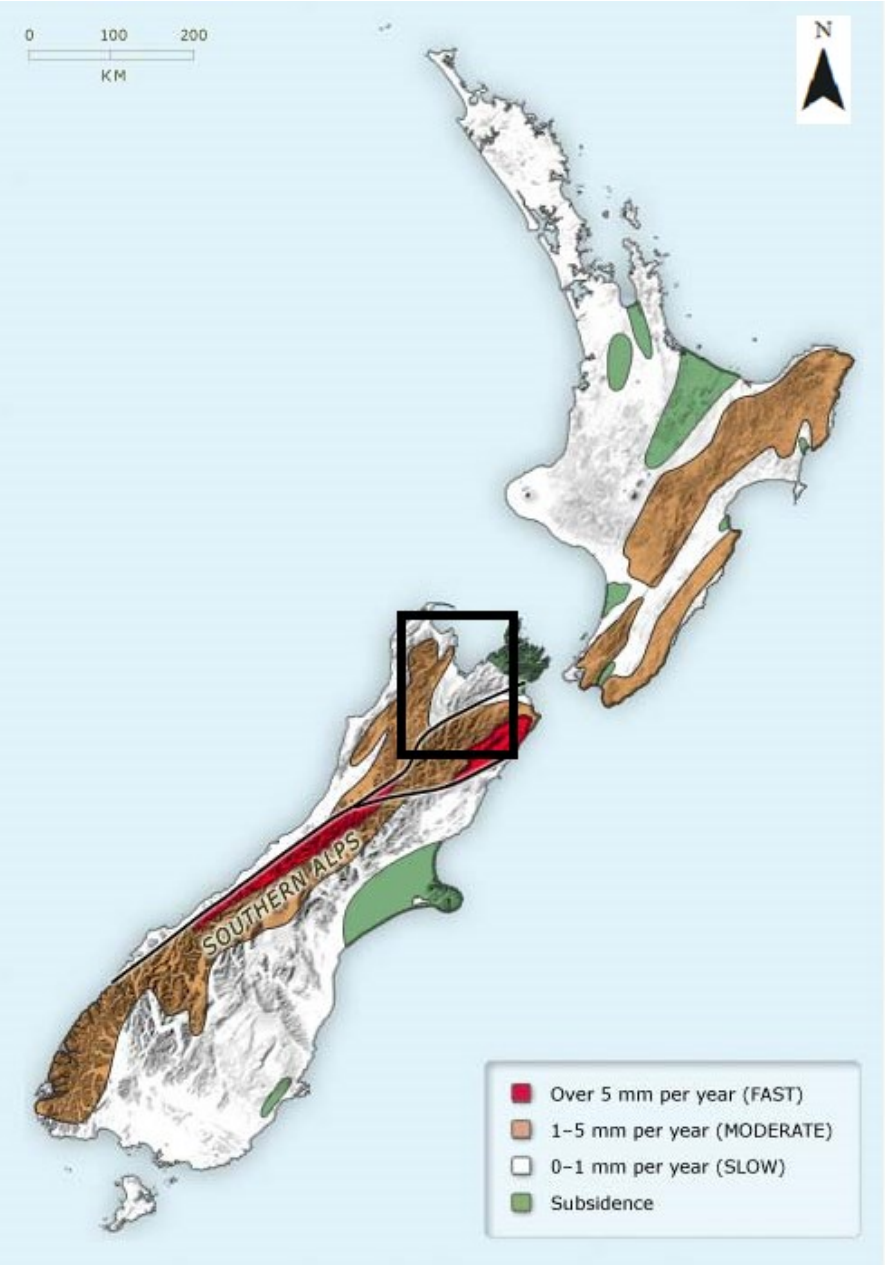

Figure 6.12: Rates of uplift across New Zealand created by Caroline Hume GNS Science, inferred from research by Brad Pillans (North Island) and Harold Wellman (South Island) (Source: McSaveney & Nathan, 2013).

6.4.3 Threshold slope angles

Threshold slope angles are considered the angle at which erosion occurs predominantly as a result of mass wasting as opposed to diffusive hillslope processes (Montgomery, 2001). Denudation is commonly found to increase linearly with increasing slope angle and then increase rapidly where slopes approach and exceed the threshold angle which is often ~30˚ (Roering, 1999; 2001; Montgomery & Brandon, 2002). Here, slopes are categorised based on the percent of each basin steeper than the threshold angle. This shows how much of each basin is likely to be dominated by processes such as landsliding. Many of the catchments in the Nelson/Tasman region have high percentages of area that exceeded threshold slope angles. The areas underlain by Moutere gravels, however, are too weak to maintain steep slopes, but all slopes are at or near threshold. Therefore, the Moutere catchments can have lower mean slope angles than the other lithologies, but remain at threshold conditions. There are no spatial trends between the percentage of slope >30° and the ^{10}Be denudation rates. It has been considered that exceeding threshold slope angle may destroy any relationship between relief and denudation (Binnie et al., 2007; Ouimet et al., 2009); perhaps this theory could be attributed to the Nelson/Tasman region where denudation is spatially homogenous despite significant variation in slope angle and common exceeding of threshold angles.

6.5 Impact of tectonics on denudation

As discussed in section 1.3.2, Quigley et al.(2007) suggest that ^{10}Be can be used to discern landscapes that have recently been affected by tectonics or landscapes that are in 'disequilibrium'. Their study recognised three large surface rupturing earthquakes in the past ~67ka that had had greatly affected rates of erosion in the vicinity of the ruptures. Nelson is thought to experience surface ruptures with recurrence intervals of ~6ky, with at least three recognised in the last ~20ka. Interestingly, all of the basins of the Waimea pass over this active fault system; however, this has not impacted rates of erosion for the Waimea which are lower than for the Motueka. This could be explained by the lack of recent tectonic activity for this region, where the last rupture precedes the timescale in which ^{10}Be averages. The timescale over which the Nelson-derived ^{10}Be rates average (~2ky) is not long enough to capture the recurring major events in the Nelson region; the episodic nature of earthquake-induced erosion increases is not apparent in

these relatively short timescales. Although ~6ka is the last known rupture, there is thought to have been a significant ~6.6 - 6.9 M that occurred in 1893 that did not rupture the surface (Downes, 1995).

Landscape response times to tectonics vary depending on the magnitude of the event and the scale of the landscape. The response of the landscape to earthquakes, or the time it takes for material that is disturbed by large earthquakes to exit the system, was found by Howarth et al., (2012) to be < 100yrs in the South Island, New Zealand. Brocard et al. (2003) examined a 100 km long river for which they conclude that the time to reach re-equilibrium after a significant climatic perturbation (glacial-interglacial transition) is ~20kyrs. Furthermore, Whipple & Meade (2006) used an analytical model to find that response times at the orogeny scale were on the order of millions of years. The landscape appears to recover from short term sediment increases from earthquakes more quickly than the landscape's geomorphic metric adjustments, and perturbations of geologic scale. This supports the idea that sediment yields for the Nelson/Tasman region are no longer responding to earthquake perturbation at ~6kyr and unlikely to the 1883 earthquake. ^{10}Be derived rates regardless of timing are unlikely to have captured earthquake signals unless major landsliding had occurred.

Most river profiles that were sampled, including the Baton, Wangapeka, Rainy, Waimea, and Motueka Rivers, have a relatively well-defined knickpoint at ~60 – 70 km upstream from the Waimea and Motueka mouths (*figure 6.10C*). The Waimea knickpoint is particularly well-defined suggesting that something significant tectonically has occurred in the past (on the order of 10s of kyrs according to Brocard et al.'s, 2003 analyses) and its signature has propagated upstream. There are also a number of oversteepened channels throughout the region (*figure 5.13*) supporting evidence that Nelson is tectonically dynamic, yet rates of denudation are still independent of any direct relationship with these tectonically steepened channels (*figure 5.11; table 5.7*). Although Nelson channel profiles are non-linear and have significant perturbations displaying disequilibrium, it cannot be said that these perturbations are affecting denudation spatially in accordance with the channel disequilibrium. Independence of denudation rates to geomorphology further supports the idea of topographic steady state within the Nelson region.

Geomorphic relationships to fault density further support that tectonics are however influencing the geomorphology of the Nelson/Tasman region. Dense faulting implies rapid uplift and rapid uplift results in steeper slopes and channels (Burbank & Anderson, 2001; Norton et al., 2011a) *Figure 5.12* shows that fault density correlates relatively well with slope angles and channel steepness therefore supporting the idea that the geomorphology of the Nelson/Tasman region is largely controlled by tectonics while denudation is not.

6.6 Impact of climate on denudation

Mean annual rainfall across the sampled catchments ranged from 1200 mm yr to 2230 mm yr. Some basins receive significantly higher rainfall than others allowing for the discernment of climatic influence on rates of denudation. *Figure 5.11* shows no significant correlation between mean annual rainfall and meteoric ^{10}Be denudation rates (0.08) nor between rainfall and the averaged denudation rates (0.19). There was a 0.46 correlation between mean annual rainfall and in-situ ^{10}Be denudation rates (*table 5.7*); however, whether this is significant is questionable and further samples would be needed to convincingly argue that long term, spatial climatic variation is having an impact on the in-situ ^{10}Be rates of denudation. Without further sampling this remains inconclusive.

Comparison of ^{10}Be-derived denudation rates and sediment yield and modelling estimates for the region is useful for the assessment of the effects of anthropogenic change on the landscape and of short term climatic variation (precipitation events). ^{10}Be-derived erosion rates were higher than those derived from other erosion quantification methods in the Nelson/Tasman region. Annual sediment yields and erosion modelling suggest that the landscape is eroding at ~50 – 362 t km^{-2} yr^{-1}, while ^{10}Be rates suggest denudation rates of ~112 – 788 t km^{-2} yr^{-1}. This has been a finding in other erosion studies (Kirchner et al., 2001; Schaller et al., 2001; Schaller et al., 2002; Ferrier et al. 2005; Lupker et al., 2012). Sediment yields have also been found to be higher than ^{10}Be rates, with the implication that elevated denudation rates are due to recent anthropogenic change (Brown et al., 1995; Clapp et al., 2000; 2001; Hewawasam et al., 2003; Vanacker et al., 2007). Most of the results in Nelson, however, can be explained by the significant contribution of low frequency, high magnitude events to erosion (Schaller et al., 2001; Kirchner et al., 2001; Ferrier et al., 2005). Basher et al.

(2011) recorded sediment yields following storm events in the region and found that many of the rates had become considerably elevated, one sample location in the Upper Motueka reaching ~2535 t km^{-2} yr^{-1}. Coker & Fahey (1993) similarly found sediment yields that were reaching ~2800 near road cuttings in the region, following major storm events.^{10}Be-derived denudation rates incorporate but smooth (*figure 6.13*) these major storm-driven erosive events where sediment yields and erosion modelling may not, providing natural background rates.

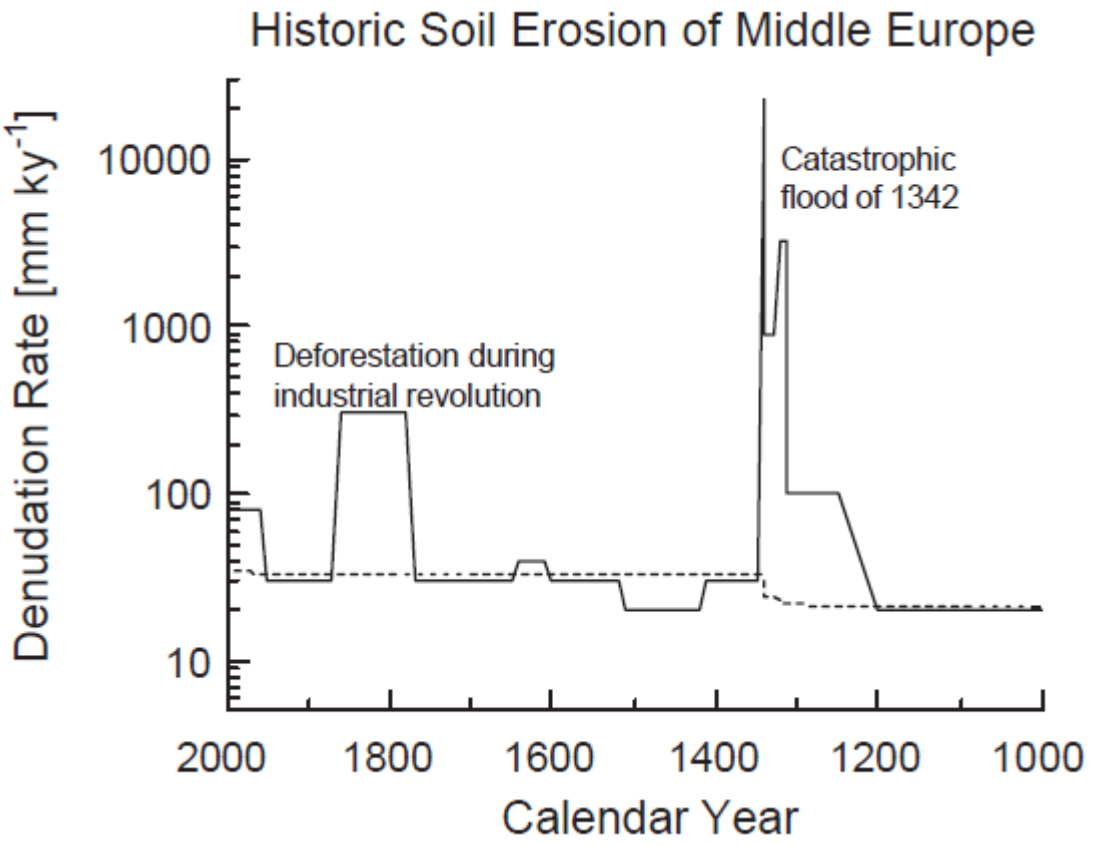

Figure 6.13: Numerical model indicating the minimal effects of the catastrophic flood in 1342 and deforestation in the 1800s on ^{10}Be-derived denudation rates (dashed line). The effects are negligible – they are not large enough to perturb ^{10}Be-derived rates of erosion. The black line indicates changes in the erosion flux over time but ^{10}Be captures the impact of the short term effects of the flood by raising natural background rates according to how they would have impacted long term rates of denudation. (Source: von Blanckenburg, 2006).

Meyer et al. (2010) attributed high ^{10}Be-derived denudation rates in the Rhenish Massif, Germany to changes in factors such as vegetation coverage, evapotranspiration, and soil exposure as a result of climate change. This can be confidently excluded from a Nelson explanation due to the short averaging timescales during which climate changed very

little. Riebe et al. (2001b) suggest that for climate-driven environmental changes to impact ^{10}Be-derived denudation rates, change must be extensive and prolonged such as that of the transitions between glacial-interglacial periods. The averaging timescales derived for Nelson cover only the Late Holocene where, even the 'Little Ice Age' and the Medieval Warm Period' were not significant enough to have dramatically changed climatic-driven variation.

The major storm-driven erosive event that caused the sediment yield of the Upper Motueka to reach ~2535 t km^{-2} yr^{-1} occurred within the basin that produced a ^{10}Be rate of 233 t km^{-2} yr^{-1} (basin 9). The annual sediment yield covering the period of 1965-2009 suggested this basin has been eroding at 507 t km^{-2} yr^{-1} (Basher et al., 2011), exceptionally higher than the ^{10}Be-derived rates. Other sediment yield estimates for the region (where there were sufficient data) were all lower than the ^{10}Be-derived rates. The SSYE (NIWA, 2013) which uses geology and rainfall to model erosion, also produces rates that are all lower than the ^{10}Be-derived rates with the exception again of the Upper Motueka and also the Motupiko. The SSYE estimate for the Upper Motueka is 362 t km^{-2} yr^{-1} while the ^{10}Be-derived estimate is 233 t km^{-2} yr^{-1} (basin 9). The SSYE for the Motupiko is 290 t km^{-2} yr^{-1} while the ^{10}Be-derived estimates are 239 t km^{-2} yr^{-1} (basin 8) and 174 t km^{-2} yr^{-1} (basin 10).

Interestingly, basin 8 (for which both meteoric and in-situ results were obtained) produced the largest discrepancy between the in-situ and meteoric Be methods (with the exception of the outlier). It is possible that these particular basins have been affected by anthropogenic clearing more significantly than others in the region. Hippe et al. (2012) similarly found that most of their study locations in Bolivia had higher ^{10}Be rates of denudation than sediment yield estimates, with the exception of one location. It was considered that it could be the result of the presence of highly erodible Quaternary sediments that were prone to erosion during flood events (Guyot et al., 1992); however, they concluded that it was more likely a result of short term increase in sediment flux across the gauging period. The gauging period for the Upper Motueka basin with the high sediment yield (basin 9) was relatively long (1965-2009), however, it could be that this basin (and the others with high sediment yields) are is still responding to deforestation where the other's may not be. This remains unclear and a point that future could explore.

The implication of the above findings is that although long term average climate variation does not appear to be affecting denudation variation in the Nelson/Tasman region, it is likely that short term extreme climatic events are having an impact on the elevated denudation rates for the region. The landscape's reaction to these storm events is likely a result of its adjustment to topographic steady state; the landscape has adjusted to be able to react to these extreme climatic events. Here it seems that the impact of major storm events incorporated into ^{10}Be analysis is greater than the anthropogenic signature of landscape clearing for most basins. It is probable that the extensive clearing of forest in the Nelson region elevated erosion rates for a period of time, exacerbating the impact of storm events and raising short term sediment yields; however, it is unlikely that these recent short-lived erosive events have been so grave as to contribute deep material that misrepresents natural erosion as they are largely limited to the mobile regolith. It is more likely that low frequency, high magnitude events have been incorporated into the ^{10}Be signature where they have not necessarily been in sediment yield estimates.

6.7 Impact of lithology on denudation

Various studies have identified lithology as an important factor in the variation of denudation rates (eg. Schaller et al., 2001; Palumbo et al., 2009). There was no direct correlation between rates of denudation and variation in lithology in the Nelson region; however, geomorphic variation has impacted the way in which lithology could affect denudation. It is likely that had all catchments had uniform mean slope angles the varying erodibility of the likes of granite and gravel would have been widely apparent. However, catchments with a high percentage of granite did not appear to erode differently to catchments with a high percentage of gravel because the sturdiness of the rock was counteracted by the significant steepness of slopes. Accordingly, gravel-ridden catchments were characteristically shallower meaning their erodibility was counteracted by lack of gravitational force from slopes. Here it is apparent that although lithology cannot directly account for the variation in denudation across the Nelson region, it indirectly influences it through determination of slope angles and topography. This further supports the idea of topographic steady state; rocks must create slopes that yield appropriate erosion rates.

6.8 Impact of anthropogenic clearing

Studies in New Zealand have recognised forest clearing as a primary contributor to increased landslide activity (e.g. Page et al., 1994; Hicks et al., 2000). Various parts of the Nelson/Tasman region have been heavily deforested (*figure 6.14*). It is difficult to quantify the amount of surface material has been removed anthropogenically, therefore exposing fresh material. However, it must be considered that this could be contributing to the elevated denudation rates across the Nelson/Tasman region and could contribute to why short term erosion rates are lower than the millennial term ^{10}Be-derived rates. Although it is uncommon for recent anthropogenic changes to affect at least in-situ ^{10}Be-derived denudation rates, it can be found that the anthropogenic changes are so intense that a significant amount of deep material that hasn't previously been exposed to cosmic rays has become exposed and eroded (eg. Vanacker et al., 2007)**.** In this case although the short term sediment transport has now declined, the material that is present in ^{10}Be sampling contains a significant amount of material that has not long been exposed causing the ^{10}Be-derived rates to appear elevated. However, it is more likely that the significant contribution to erosion comes from low frequency, high magnitude events, irrespective of anthropogenic change. Forest clearing, although not likely contributing to elevated ^{10}Be denudation now, could be influencing the extent to which major storm events are having an effect by exaggerating the impact of extreme climatic events. This is something that could be seen in ^{10}Be analysis in the future.

Figure 6.14: Modern clear cutting of exotic forest plantation to the east of the Waimea River. Initial deforestation occurred ~100 years ago in this region.

6.9 Future work

An important result of this research was the remarkable consistency between in-situ and meteoric derived results. This offers an important opportunity for further research; where in-situ ^{10}Be analysis is not applicable such as where the landscape is quartz poor (common in New Zealand), meteoric could be used as an alternate method for denudation quantification. This method is dependent on the denudational timescales derived for meteoric analysis which can be highly variable; however, with further research and a better understanding of the adsorption of meteoric ^{10}Be through the soil column, this could become a valuable tool for understanding the dynamics of erosion in New Zealand. With some additional sampling (particularly for in-situ) perhaps in the Waimea catchment, stronger conclusions could be drawn, particularly in regards to the climatic influence on the in-situ samples discussed in section 6.6. Both meteoric and in-situ ^{10}Be has the potential to provide competent millenial term estimates of natural background rates of erosion for the assessment of the impacts that topography, tectonics, climate, and lithology have on rates of denudation for the country. A better understanding of the interactions of these controlling influences on erosion will allow for the development of better erosion modelling for the future and more competent predictions of how erosion may respond to changes in these controlling factors; to better understand how the landscape may respond to the likes of climate change in the future.

Conclusions

Meteoric and in-situ ^{10}Be analysis has successfully determined basin-averaged rates of denudation for the Tasman region, South Island, New Zealand. Both meteoric and in-situ denudation rates ranged between ~112 – 298 t km^{-2} yr^{-1}, with the exception of one basin which was denuding at 789 t km^{-2} yr^{-1}and 626 t km^{-2} yr^{-1}for meteoric and in-situ, respectively. Results between the two methods were remarkably consistent between each other and produced denudation rates that are spatially homogenous across the region.

The lack of correlation between geomorphic, tectonic, and lithological variables, and homogeneity of rates of denudation in the region supports the idea that this landscape may be approaching or has approached flux and/or topographic steady state. The landscape has likely adjusted to the ~6ky rupture in the Waimea-Flaxmore Fault system as its signature is not captured in the ^{10}Be-derived rates of denudation. The lack of response to the rupture appears to be a result of the relatively short denudational timescales (~2750 for in-situ, and ~1200 for meteoric).

Millennial term (^{10}Be-derived) denudation rates are more rapid than those inferred from other conventional methods in the same region. This is likely the result of the significant contribution of low frequency, high magnitude erosive events to overall erosion of the region. Sediment yields following major storm events are shown to be severely elevated above normal sediment yield data and contribute high proportions of the annual sediment yield in single events. These extreme climatic events are incorporated into the ^{10}Be signature due to its long integration time where they are not always in other conventional short term methods such as sediment gauging. The episodic nature of erosion is smoothed within the ^{10}Be derived denudation rates presenting a viable background rate against which to gauge conventional methods of erosion quantification.

The most significant result of this research was the remarkable consistency between in-situ and meteoric derived results. Where in-situ ^{10}Be analysis is not applicable such as where the landscape is quartz poor (common in New Zealand), meteoric^{10}Be has the potential to be used as an alternate method for denudation quantification. With further research and a better understanding of the adsorption of meteoric ^{10}Be through the soil column, this could become a valuable tool for understanding the dynamics of erosion in

New Zealand. It has the potential to provide competent long term estimates of natural background rates of erosion for the assessment of the impacts that topography, tectonics, climate, and lithology have on rates of denudation for the country. A better understanding of the interactions of these controlling influences on erosion will allow for the development of better erosion modelling for the future and more competent predictions of how erosion may respond to changes in these controlling factors; to better understand how the landscape may respond to the likes of climate change in the future.

References

Abbuhl, L., Norton, K., Jansen, J., Schlunegger, F., Aldahan, A., & Possnert, G. (2011). Erosion rates and mechanims of knickzone tetreat inferred from ^{10}BE measured across strong climate gradients on the Northern and Central Andes Western Escarpment. *Earth Surface Processes and Landform, Vol. 36, No., 11* , 1464-1473.

Abbuhl, L., Norton, K., Schlunegger, F., Kracht, O., Aldahan, A., & Possnert, G. (2010). El Niño forcing on ^{10}Be-based surface denudation rates in the northwestern Peruvian Andes? *Geomorphology, Vol. 123* , 257-268.

Adams, J. (1980). Contemporary uplift and erosion of the Southern Alps, New Zealand. *Bulletin of Geological Society of America, Vol. 91* , 1-114.

Adams, J. (1979). Sediment loads of North Island rivers, New Zealand - a reconnaissance. *Journal of Hydrology (NZ), Vol. 18* , 36-48.

Allen, P., Armitage, J., Carter, A., Duller, R., Michael, N., Sinclair, H., et al. (2013). The Qs problem: Sediment volumetric balance of proximal foreland basin basins. *Sedimentology, Vol 60, Issue 1* , 102-130.

Anhert, F. (1970). Functional relationship between denudation, relief, and uplift in large mid-latitude drainage basins. *American Journal of Science, Nol. 268* , 243-263.

Armitage, J., Jones, P., Whittacker, A., & Phillip, P. (2013). Temporal buffering of climate-driven sediment flux cycles by transient catchment response. *Earth and Planetary Science Letters, Vol. 369-370* , 200-210.

Askin, R., & Davidson-Arnott, R. (1981). Micro-erosion meter modified for use under water. *Marine Geology, Vol. 40* , M45-M48.

Bacon, A., Richter, D., Bierman, P., & Rood, D. (2012). Coupling meteoric ^{10}Be with pedogenic losses of ^{9}Be to improve soil residence time estimates on an ancient North American interfluve. *Geology, Vol. 40* , 1-4.

Badding, M., Brinner, J., & Kaufman, D. (2013). ^{10}Be ages of late Pleistocene deglaciation and Neoglaciation in the north-central Brooks Range, Arctic Alaska. *Journal of Quaternary Science, Vol. 28, No. 1* , 95-102.

Balco, G., & Rovey, C. (2008a). An ischron method for cosmogenic nuclide dating of buried soils and sediments. *American Journal of Science, Vol. 308* , 1083-1114.

Balco, G., & Schuster, D. (2009). Production rate of cosmogenic ^{21}Ne in quartz estimated from ^{10}Be, ^{26}Al, and ^{21}Ne concentrations in slowly eroding Antarctic bedrock surfaces. *Earth and Planetary Science Letters, No. 281* , 48-58.

Balco, G., Stone, J., Lifton, N., & Dunai, T. (2008b). A complete and easily accessible means of calculating surface exposure ages or erosion rates from ^{10}Be and ^{26}Al measurements. *Quaternary Geochronology, Vol. 3* , 174-195.

Barnes, P., Cheung, K., Smiths, A., Almagor, G., Read, S., Barker, P., et al. (1991). Geotechnical analysis of the Kidnappers slide, upper Continental Slope, New Zealand. *Marine Geotechology, Vol. 10* , 159-188.

Basher, L., & Jackson, R. (2002). *Soil properties and hydrological processes on Moutere gravels, Nelson.* Landcare Research - Integrated Catchment Management for the Motueka River.

Basher, L., Botha, N., Dodd, M., Douglas, G., Lynn, I., Marden, M., et al. (2008). *Hill country erosion: a review of knowledge on erosion processes, mitigation options, social learning and their long term effectiveness in the management of hill country erosion.* Landcare Research Contract Report: LC0708/081, 201p.

Basher, L., Hicks, D., Clapp, B., & Hewitt, T. (2011). Sediment yield response to large storm events and forest harvesting, Motueka River, New Zealand. *New Zealand Journal ofMarine and Freshwater Research, Vol. 45, No. 3* , 333-356.

Basher, L., Marden, M., & Barringer, J. (2003a). *Identification of major sediment sources in the Motueka River.* Lincoln: Landcare Research ICM Report No. 2003-03/01.

Basher, L;. (2003b). *The Motueka and Riwaka catchments.* Canterbury: Landcare Research.

Bellin, N., Vanacker, V., & Kubik, P. (2014). Denudation rates and tectonic geomorphology of the Spanish Betic Cordillera. *Earth and Planetary Science Letters, Vol. 390* , 19-30.

Belmont, P., Pazzaglia, F., & Gosse, J. (2007). Cosmogenic ^{10}Be as a tracer for hillslope and channel sediment dynamics in the Clearwater River, western Washington State. *Earth and Planetary Science Letters, No. 264* , 123-135.

Berggren, D., & Mulder, J. (1995). The role of organic matter in controlling aluminum solubility in acidic mineral horizons. *Geochimica et Cosmochimica Acta, Vol. 50* , 4167-4180.

Bierman, P., & Caffee, M. (2001). Steady state rates of rock surface erosion and sediment production across the hyperarid Namib desert and the Namibian escarpment, southern Africa. *American Journal of Science, Vol. 301* , 321-358.

Binnie, S., Phillips, W., Summerfield, M., & Fifield, K. (2006). Sediment mixing and basin-wide cosmogenic nuclide analysis in rapidly-eroding mountainous environments. *Quaternary Geochronology, Vol. 1* , 4-14.

Binnie, S., Phillips, W., Summerfield, M., & Fifield, L. (2007). Tectonic uplift, threshold hillslopes and denudation rates in a developing mountain range. *Geology, Vol. 35* , 743-746.

Brandon, M., Roden-Tice, M., & Garver, J. (1998). Late Cenozoic exhumation of the Cascadia accretionary wedge in the Olympic Mountains NW Washington State. *Geological Society of America Bulletin, Vol. 110* , 986-1009.

Brocard, G., van der Beek, P., Bourles, D., Siame, L., & Mugnier, J. (2003). Long-term fuvial incision rates and postglacial river relaxation time in the French Western Alps from ^{10}Be dating of alluvial terraces with assessment of inheritance, soil development and wind ablation effects. *Earth and Planetary Science Letters, Vol. 209* , 194-214.

Brown, E., Edmond, J., Raisbeck, G., Bourles, D., Yiou, F., & Measures, C. (1992). Beryllium isotope geochemistry in tropical river basins. *Geochimica et Cosmochimica Acta, Vol. 56* , 1607–1624.

Brown, E., Stallard, R., Larsen, M., Bourles, D., Raisbeck, G., & Yiou, F. (1998). Determination of predevelopment denudation rates of an agricultural watershed (Cayaguas River, Puerto Rico) using in-situ-produced 10Be in river-borne quartz. *Earth and Planetary Science Letters, Col. 160* , 723-728.

Brown, E., Stallard, R., Larsen, M., Raisbeck, G., & Yiou, F. (1995). Denudation rates determined from the accumulation of in situ-produced ^{l0}Be in the Luquillo Experimental Forest, Puerto Rico. *Earth and Planetary Science Letters, No. 129* , 193-202.

Burbank, D. (2002). Rates of erosion and their implications for exhumation. *Mineralogical Magazine, Vol. 66, No. 1* , 25-52.

Burbank, D., & Anderson, B. (2001). *Tectonic Geomorphology.* Oxford: Blackwell Scientific.

Burbank, D., Blythe, A., Putkonen, J., Pratt-Situala, B., Gabet, E., Oskin, M., et al. (2003). Decoupling of erosion and precipitation in the Himalaya. *Nature, Vol. 426* , 652-656.

Carter, L., Manighetti, B., Elliot, M., Trustrum, N., & Gomez, B. (2002). Source, sea Level and circulation effects on the sediment flux to the deep ocean over the past 15ka off eastern New Zealand. *Global and Planetary Change, Vol. 33* , 339-355.

Cerling, T., & Craig, H. (1994a). Cosmogenic ^{3}He production rates from 39 to 46 N latitude, western USA and France. *Geochemica et Cosmochemica Acta, Vol. 58* , 249-255.

Chmeleff, J., von Blanckenburg, F., Kossert, K., & Jacob, D. (2009). Determination of the ^{10}Be half-life by multicollector ICP-MS and liquid scintillation counting. *Nuclear Instruments and Methods B* , doi:10.1016/j.nimb.2009.09.012.

Clapp, E., Bierman, P., Nichols, K., Pavivh, M., & Caffee, M. (2001). Rates of sediment supply to arroyos from upland erosion determined using in situ produced cosmogenic ^{10}Be and ^{26}A. *Quaternary Research, Vol. 55* , 235-245.

Clapp, E., Bierman, P., Schick, A., Lekach, J., Enzel, Y., & Caffee, M. (2000). Sediment yield exceeds sediment production in arid region drainage basins. *Geology, Vol. 28* , 995– 998.

Codilean, A. (2006). Calculation of the cosmogenic nuclide production topographic shielding scaling factor for large areas using DEMs. *Earth Surface Processes and Landforms, Vol. 31* , 785-794.

Coker, R., & Fahey, D. (1993). Road-related mass movement in weathered granite, Golden Downs and Motueka forests, New Zealand: A note. *Journal of Hydrology (NZ), Vol. 34, No. 1* , 65-69.

Cording, A., Hetzel, R., Kober, M., & Kley, J. (2014). ^{10}Be exposure dating of river terraces at the southern mountain front of the Dzungarian Alatau (SE Kazakhstan) reveals rate of thrust faulting over the past ~ 400 ka. *Quaternary Research, Vol. 81, Issue. 1* , 168-178.

Crozier, M. (2005). Multiple-occurrence regional landslide events in New Zealand: hazard management issues. *Landslides, Vol. 2* , 247-256.

Cyr, A., & Granger, D. (2008). Dynamic equilibrium among erosion, river incision, and coastal uplift in the northern and central Apennines, Italy. *Geology, Vol. 36* , 103-106.

de Vente, J., & Poesen, J. (2005). Predicting soil erosion and sediment yield at the basin scale: scale issues and semi-quantitative models. *Earth Science Reviews, Vol. 71* , 95-125.

Dehnert, A., & Schluchter, C. (2008). Sediment burial dating using terrestrial cosmogenic nuclides. *Quaternary Science Journal, Vol. 57* , 210-225.

DiBiase, R., Whipple, K., Heimsath, A., & Ouimet, R. (2010). Landscape form and millennial erosion rates in the San Gabriel Mountains, CA. *Earth and Planetary Science Letters, Vol. 289* , 134-144.

Diehl, R., Halloin, H., Kretschmer, K., Lichti, G., Schonfelder, V., Strong, A., et al. (2006). Radioactive Al-26 from massive stars in the Galaxy. *Nature, Vol. 439* , 45-47.

Downes, G. (1995). *Atlas of isoseismal maps of New Zealand earthquakes.* Lower Hutt: Institute of Geological and Nuclear Sciences.

Dunai, T. (2010). *Cosmogenic puclides: principles, concepts and applications in the earth surface sciences.* Cambridge: Cambridge University Press.

Dunne, J., Elmore, D., & Muzikar, P. (1999). Scaling factors for the rates of production of cosmogenic nuclides for geometric shielding and attenuation at depth on sloped surfaces. *Geomorphology, Vol. 27* , 3-11.

Dymond, J. (2010b). Soil erosion in New Zealand is a net sink of CO2. *Earth Surface Processes and Landforms, Vol. 35* , 1763-1772.

Dymond, J., Betts, H., & Schierlitz, C. (2010a). An erosion model for evaluating regional landuse scenarios. *Environmental Modelling and Software, Vol. 25* , 289-298.

Dymond, J., Jessen, M., & Sheperd, J. (1999). Computer simulation of shallow landsliding in New Zealand hill country. *International Journal of Applied Earth Observation and Geoinformation, Vol. 1* , 122-131.

Elhers, T., & Farley, K. (2003). Apatite (U–Th)/He thermochronometry: methods and applications to problems in tectonics and surface processes. *Earth and Planetary Science Letters Frontiers, Vol. 206* , 1-14.

Elhers, T., & Poulsen, C. (2009). Influence of Andean uplift on climate and paleoaltimetry estimates. *Earth and Planetary Science letters, Vol. 281* , 238-248.

Fahey, B., Marden, M., & Phillips, C. (2003). Sediment yields from plantation forestry and pastoral farming, coastal Hawkes Bay. *New Zealand Journal of Hydrology, Vol. 42,* 27-38.

Feely, H., Larsen, R., & Sanderson, C. (1989). Factors that cause seasonal variations in beryllium-7 concentrations in surface air. *Journal of Environmental Radioactivity, Vol. 9* , 223-249.

Fenemor, A. (2002). Affidavit evidence on behalf of the Tasman District Council for the application for a National Water Conservation Order for the Tasman District. *Richmond: Tasman District Council.*

Fenemor, A. (1989). Motueka and Riwaka catchments water management plan. *Nelson: Nelson Regional Water Board.*

Ferrier, K., Kirchner, J., & Finkel, R. (2005). Erosion rates over millennial and decadal timescales at Caspar Creek and Redwood Creek, Northern California Coast Ranges. *Earth Surface Processes and Landforms, Vol. 30* , 1025-1038.

Field, C., Schmidt, G., Koch, D., & Salyk, C. (2006). Modeling production and climate-related impacts on $_{10}$Be concentration in ice cores. *Journal of Geophysical Research, Vol. 111* , D15107, doi:10.1029/2005JD006410.

Fraser, J. (2005). Paleoearthquake Investigation of the Waimea-Flaxmore Fault System, Nelson, New Zealand. *Master's Thesis* . Canterbury: University of Canterbury.

Glade, T. (2003). Landslide occurrence as a response to land use change: a review of evidence from New Zealand. *Catena, Vol. 53* , 297-314.

Gosse, J., & Phillips, F. (2001). Terrestrial in situ cosmogenic nuclides: theory and application. *Quaternary Science Reviews, Vol. 20* , 1475–1560.

Graham, I., Ditchburn, R., & Barry, B. (2003). Atmospheric deposition of ^{7}Be and ^{10}Be in New Zealand rain (1996-98). *Geochimica et Cosmochimica Acta, Vol. 67, No. 3* , 361-373.

Granger, D. (2006). A review of burial dating methods using ^{26}Al and ^{10}Be . *Geological Society of America Special Papers, Vol. 418* , 1-16.

Granger, D., & Riebe, C. (2007). Cosmogenic nuclides in weathering and erosion. In J. Drever, *Treatise on Geochemistry: Surface and Ground Water, Weathering and Soils, Vol. 5* (pp. 1-43). London: Elsevier.

Granger, D., & Smith, A. (2000). Dating burial sediments using radioactive decay and muogenic production of ^{26}Al and ^{10}Be. *Nuclear Instruments and Methods in Physics Research B Vol. 172* , 822-826.

Granger, D., Kirchner, J., & Finkel, R. (1996). Spatially-averaged long-term erosion rates measured from in-situ-produced cosmogenic nuclides in alluvial sediment. *The Journal of Geology, Vol. 104,* , 249-257.

Grant, P. (1981). *Major Periods of Erosion and Sedimentation in the North Island, New Zealand, Since the 13th Century.* Christhurch: IAHS Publication No. 132.

Gregory, K., & Walling, D. (1973). *Drainage Basin Form and Process.* New York: Wiley and Sons.

Griffiths, G. (1979). High sediment yields from major rivers of the western Southern Alps, New Zealand. *Nature, Vol. 282* , 61-63.

Griffiths, G. (1981). Some suspended sediment yields from South Island catchments, New Zealand. *Water Resources Bulletin, No. 17* , 662-671.

Griffiths, G. (1982). Spatial and temporal variability in suspended sediment yields of North Island basins, New Zealand. *Water Resources Bulletin, Vol. 18* , 575-584.

Griffiths, G., & Glasby, G. (1985). Input of river-derived sediment to the New Zealand Continental Shelf: I. Mass. *Estuarine, Coastal and Shelf Science, Vol. 21* , 773-787.

Griffiths, G., & McSaveney, M. (1986). Sedimention and river containment on Waitangitaona alluvial fan—South Westland, New Zealand . *Zeitschrift für Geomorphologie, Vol. 30* , 215-230.

Grujic, D., Coutand, I., Bookhagen, B., Bonnet, S., Blythe, A., & Duncan, G. (2006). Climatic forcing of erosion, landscape, and tectonics in the Bhutan Himalayas. *Geology, Vol. 34* , 801-804.

Guralnik, B. pers, com

Guyot, J., Wasson, J., Quintanilla, J., & Calle, H. (1992). Dissolved matter in sediment loads in some inflow rivers and in the Rio Desaguadero. In C. Dejoux, & A. Iltis, *Lake Titicaca: A Synthesis of Limnological Knowledge* (pp. 113-119). Dordrecht: Kluwer Academic Publishers.

Hack, J.T. (1957). Studies of longitudinal stream profiles in Virginia and Maryland. *U.S. Geological Survey Professional Paper 294-B, 97*

Hallet, B., Hunter, L., & Bogen, J. (1996). Rates of erosion and sediment evacuation by glaciers: a review of field data and their implications. *Global and Planetary Change, Vol. 12* , 213-235.

Hancox, G., Perrin, N., & Dellow, G. (2002). Recent studies of earthquake-induces landsliding, ground damage, and MM intensity in New Zealand. *Bulletin for the New Zealand Society for Earthquake Engineering, Vol. 35, No. 2* , 59-95.

He, Q., & Walling, D. (1996). Use of fallout Pb-210 measurements to investigate longerterm rates and patterns of overbank sediment deposition on the floodplains of lowland rivers. *Earth Surface Processes and Landforms, Vol. 21* , 141-154.

Heikkila, U. (2007). Modeling of the atmospheric transport of the cosmogenic radionuclides ^{10}Be and ^{7}Be using the ECHAM5-HAM General Circulation Model. *PhD Thesis* . ETH-Zurich.

Heikkila, U., Beer, J., & Alfimov, V. (2008). Beryllium-10 and Beryllium-7 in precipitation in Dübendorf (440 m) and at Jungfraujoch (3580 m), Switzerland (1998–2005). *Journal of Geophysical Research, Vol. 113* , D11104. doi:10.1029/2007JD009160.

Herman, F., Cox, S., & Kamp, P. (2009). Low-temperature thermochronology and thermokinematic modeling of deformation, exhumation, and development of topography in the central Southern Alps, New Zealand. *Tectonics, Vol. 28* , 1-21.

Herman, F., Rhodes, E., Braun, J., & Heiniger, L. (2010). Uniform erosion rates and relief amplitude during glacial cycles in the Southern Alps of New Zealand, as revealed from OSL-Thermochronology. *Earth and Planetary Science Letter, Vol. 297* , 183-189.

Herzig, A., Dymond, J., & Marden, M. (2011). A gully complex model for assessing gully stabilisation strategies. *Geomprphology, Vol. 133, 23-33* .

Hewawasam, T., von Blanckenburg, F., Schaller, M., & Kubik, P. (2003). Increase of human over natural erosion rates in tropical highlands constrained by cosmogenic nuclides. *Geology, Vol. 31* , 597–600.

Hicks, D., Hill, J., & Shankar, U. (1996). Variation of suspended sediment yields around New Zealand: the relative importance of rainfall and geology. In D. Walling, & B. Webb, *Erosion and Sediment Yield: Global and Regional Perspectives* (pp. 149-156). IAHS Publication, Vol. 236.

Hicks, M., Gomez, B., & Trustrum, N. (2000). Erosion thresholds and suspended sediment yields, Waipaoa River Basin, New Zealand. *Water Resources Research, Vol. 36, No. 4* , 1129-1142.

High, C., & Hanna, F. (1970). A method for the direct measurement of erosion on rock surfaces. *Britain Geomorphological Group Technical Bulletin, No. 5* , 1-25.

Hinderer, M. (2001). Late quaternary denudation of the Alps, valley and lake fillings and modern river loads. *Geodinamica Acta, Vol. 14* , 231-263.

Hippe, K., Kober, F., Zeilinger, J., Ivy-Ochs, S., Maden, C., Wacker, L., et al. (2012). Quantifying denudation rates and sediment storage on the eastern Altiplano, Bolivia using cosmogenic ^{10}Be, ^{26}Al, and in situ ^{14}C. *Geomorphology, Vol. 179* , 58-70.

Hippolyte, J., Brocard, G., Tardy, M., Nicoud, G., Bourles, D., Braucher, R., et al. (2006). The recent fault scarps of the Western Alps (France): Tectonic surface ruptures or gravitational sackung scarps? A combined mapping, geomorphic, levelling, and ^{10}Be dating approach. *Tectonophysica, Vol. 418* , 255-276.

Hovius, N., Stark, C., & Allen, P. (1997). Sediment flux from a mountain belt derived by landslide mapping. *Geology, Vol. 25, No. 3* , 231-234.

Howarth, J., Fitzsimons, S., Norris, R., & Jacobsen, G. (2012). Lake sediments record cycles of sediment flux driven by large earthquakes on the Alpine fault, New Zealand. *Geology, Vol. 40* , 1091-1094.

Inkpen, R. (2007). Interpretation of Erosion Rates on Rock Surfaces. *Area, Vol. 39, No 1* , 31-42.

Inkpen, R., Stephenson, W., Kirk, R., & Hemmingsen, M. (2010). Analysis of relationships between micro-topography and short- and long- term erosion rates on shore platforms at Kaikoura Peninsula, South Island, New Zealand. *Geomorphology, Vol. 121* , 266-273.

Ivy-Ochs, S., Schluchter, C., Kubik, P., Dietrich-Hannen, B., & Beer, J. (1995). Minimum ^{10}Be exposure ages of early Pliocene for the Table Mountain plateau and the Sirius Group at Mount Fleming, dry valleys, Antarctica. *Geology, Vol. 23* , 1007-1010.

Johnson, M. (1971). Pre-hawera geology of the Kaka District, northwest Nelson. *New Zealand Journal of Geology and Geophysics, Vol. 14, No. 1* , 82-102.

Jones, I., & Howie, W. (1970). The measurement and control of erosion and sedimentation. *NZ Water Conference Proceedings, Part 2* (pp. 46.1-46.25). Christchurch: Lincoln College Press.

Kamp, P. (2000). Thermochronology of the Torlesse accretionary complex, Wellington region, New Zealand. *Journal of Geophysical Research: Solid Earth, Vol. 105, Issue. B8* , 19253–19272.

Kelly, M., Kubik, P., von Blanckenburg, F., & Schulchter, C. (2004). Surface exposure dating of the Great Aletsch Glacier Egesen moraine system, western Swiss Alps, using the cosmogenic nuclide ^{10}Be. *Journal of Quaternary Science, Vol. 19, Issue 5* , 431-441.

Kirchner, J., Finkel, R., Riebe, C., Granger, D., Clayton, J., King, J., et al. (2001). Mountain Erosion over 10 yr, 10 k.y, and 10 m.y Time Scales. *Geology, Vol. 29, No. 7* , 591-594.

Kirk, R. (1977). Rates and forms of erosion on intertidal platforms at Kaikoura Peninsula, South Island, New Zealand. *NZ Journal of Geology and Geophysics, Vol. 20,* 571-613.

Kober, F., Ivy-Ochs, S., Schlunegger, F., Baur, H., Kubik, P., & Wieler, R. (2007). Denudation rates and a topography-driven rainfall threshold in northern Chile: Multiple cosmogenic nuclide data and sediment yield budgets. *Geomorphology, Vol. 83* , 97-120.

Korschinek, Bergmaier, A., Faestermann, T., Gerstmann, U., Knie, K., Rugel, G., et al. (2009). A new value for the half-life of ^{10}Be by heavy ion elastic recoil detection and liquid scintillation counting. *Nuclear Instruments and Methods, B* , doi:10.1016/j.nimb.2009.09.020.

Korup, O., & Schlunegger, F. (2009). Rock-type control on erosion-induced uplift, eastern Swiss Alps. *Earth and Planetary Science Letters, Vol. 278* , 278-285.

Korup, O., McSaveney, M., & Davies, T. (2004). Sediment generation and delivery from large historic landslides in the Southern Alps, New Zealand. *Geomorphology, Vol. 61* , 189-207.

Lal, D. (1991). Cosmic ray labelling of erosion surfaces: in situ production rates and erosion models. *Earth and Planetary Science Letters, Vol. 104* , 424-439.

Lal, D., & Peters, B. (1967). Cosmic rays produced radioactivity on the Earth. In K. Site, *Handbuch der Physik* (pp. 551-612). New York: Springer-Verlag.

Landcare Research. (2014). *New Zealand Soil Portal*. Retrieved February 12, 2014, from Landcare Research: New Zealand Soils: https://soils.landcareresearch.co.nz/contents/index.aspx?menuItem=index

Larsen, I., Almond, P., Eger, A., Stone, J., Montgomery, D., & Malcolm, B. (2013). Rapid soil production and weathering in the Southern Alps, New Zealand. *Science, Vol. 343* , 637-640.

Lewis, K., & Barnes, P. (1999). Kaikoura, New Zealand: Active conduit from near shore sediment zones to trench-axis channel. *Marine Geology, Vol. 162* , 39-69.

Licciardi, J., Kurz, M., Clark, P., & Brook, E. (1999). Calibration of cosmogenic ^{3}He production rates from Holocene lava flows in Oregon, USA, and effects of the Earth's magnetic field. *Earth adn Planetary Science Letters, Vol. 172* , 261-271.

Lihou, J. (1992). Reinterpretation of seismic reflection data from the Moutere Depression, Nelson region, South Island, New Zealand. *New Zealand Journal of Geology and Geophysics, Vol. 35* , 477-590.

Litchfield, N. (2008). Using fluvial terraces to determine Holocene coastal erosion and Late Pleistocene uplift rates: an example from Northwestern Hawke Bay New Zealand. *Geomorphology, Vol. 99* , 369-386.

Loso, M., Anderson, R., & Anderson, S. (2004). Post–Little Ice Age record of coarse and fine clastic sedimentation in an Alaskan proglacial lake. *Geology, Vol. 32, No. 12* , 1065-1068.

Lupker, M., Blard. P., Lave. J., France-Lanord. C., Leanni. L., Puchol. N., Charreau. J.,&Bourles. D. (2012).10Be-derived Himalayan denudation rates and sediment budgets in the Ganga basin.*Earth and Planetary Science Letters, No. 333-334, 146-156*

Malusa, M., & Vezolli, G. (2006). Interplay between erosion and tectonics in the Western Alps. *Terra Nova, No 18* , 104-108.

Mancktelow, N., & Graesemann, T. (1997). Time-dependent effects of heat advection and topography on cooling histories during erosion. *Tectonophysics, Vol. 270* , 167-195.

Marden, M. (2012). Effectiveness of reforestation in erosion mitigation and implications for future sediment yields, East Coast catchments, New Zealand: a review. *New Zealand Geographer, Vol. 68* , 24-35.

Marden, M., Betts, H., Arnold, G., & Hambling, R. (2008). Gully erosion and sediment load: Waipaoa, Waiapu and Uawa rivers, eastern North Island, New Zealand. *Sediment Dynamics in Changing Environments* (pp. 339-350). Christchurch: Preceedings Christchurch Imposium. IAHS Publication No. 325.

Martin, Y., Rood, K., Schwab, J., & Church, M. (2002). Sediment transfer by shallow landsliding in the Queen Charlotte Islands, British Columbia. *Canadian Journal of Earth Science, Vol. 39* , 189-205.

Masarik, J., & Beer, J. (1999). Simulation of particle fluxes and cosmogenic nuclide production in the Earth's atmosphere. *Journal of Geophysical Research, Vol. 104 D* , 12099–12111.

Masarik, J., & Reedy, R. (1995). Terrestrial cosmogenic-nuclide production systematics calculated from numerical simulations. *Earth and Planetary Science Letters, Vol. 136* , 381-396.

NMatmon, A., Bierman, P., Larsen, J., Southworth, S., Pavich, M., & Caffee, M. (2003a). Temporally and spatially uniform rates of erosion in the Appalachian Great Smoky Mountains. *Geology, Vol. 31, No. 2* , 155-158.

Matmon, A., Bierman, P., Larsen, J., Southworth, S., Pavich, M., Finkel, R., et al. (2003b). Erosion of an ancient mountain range, the Great Smoky Mountains, North Carolina and Tennessee. *American Journal of Science, Vol. 303* , 817-855.

McHargue, L., & Damon, P. (1991). The global beryllium-10 cycle. *Reviews of Geophysics, Vol. 29* , 141-158.

McSaveney, E., & Nathan, S. (2013, Septempber 4). *Geology – overview - Holocene – the last 10,000 years*. Retrieved from Te Ara - the Encyclopedia of New Zealand: http://www.TeAra.govt.nz/en/map/8406/uplift-of-new-zealand

Megahan, W. (1976). Sediment storage in channels draining small forested watersheds in the mountains of central Idaho. *Proceedings of Third Federal Inter-Agecy Sedimentation Conference*, (pp. 4.115-4.126). Denver.

Meyer, H., Hetzel, R., & Strauss, H. (2010). Erosion rates on different timescales derived from cosmogenic ^{10}Be and river loads: implications for landscape evolution in the Rhenish Massif, Germany. *International Journal of Earth Science (Geol Rundsch) Vol. 99* , 395-412.

MfE. (2008). *Meeting the Challenges of Future Flooding in New Zealand.* Wellington: Ministry for the Environment.

Michel, R., Leya, I., & Borges, L. (1996). Production of cosmogenice nuclides in meteoroids: accelorator experiments and model calculations to decipher the cosmic ray record in extraterrestrial matter. *Nuclear Instruments and Methods in Physics Research, Vol. B, No 113* , 434-444.

Milliman, J., Qin, Y., Ren, M., & Saito, Y. (1987). Man's influence on the erosion and transport of sediment by Asian Rivers. *Journal of Geology, Vol. 95* , 751-762.

Molnar, P., Anderson, R., & Anderson, S. (2007). Tectonics, fracturing of rock, and erosion. *Journal of Geophysical Research, Vol. 112* , F03014, doi:10.1029/2005JF000433.

Monaghan, M., McKean, J., Dietrich, W., & Klein, J. (1992). ^{10}Be chronometry of bedrock-to- soil conversion rates. *Earth and Planetary Science Letters, Vol. 111* , 483-492.

Montgomery, D. (2001). Slope distributions, hillslope thresholds, and steady-state topography. *American Journal of Science, Vol. 301* , 432-454.

Montgomery, D., & Brandon, M. (2002). Topographic controls on erosion rates in tectonically active mountain ranges. *Earth and Planetary Science Letters. No. 201* , 491-489.

Morrison, M., Lowe, M., Parsons, D., Usmar, N., & McLeod, I. (2009). *A Review of Land-Based Effects on Coastal Fisheries and Supporting Biodiversity in New Zealand.* Wellington: Ministry of Fisheries.

Mullan, D., Favis-Mortlock, D., & Fealy, R. (2012). Addressing key limitations associated with modelling soil erosion under the impacts of future climate change. *Agricultural and Forest Meteorology, Vol. 156* , 18-30.

Niemi, N., Oskin, M., Burbank, D., Heimsath, A., & Gabet, E. (2005). Effects of bedrock landslides on cosmogenically determined erosion rates. *Earth and Planetary Science Letters, Vol. 267* , 480-497.

Nishiizumi, K., Imamura, M., Caffee, M., Southon, J., Finkel, R., & McAninch, J. (2007). Absolute calibration of Be-10 AMS standards. *Nuclear Instruments and Methods in Physics Research, Vol. B, No. 258* , 403-413.

NIWA. (2013, February). *Suspended Sediment Yield Estimator.* Retrieved February 8, 2-14, from The National Institute of Water and Atmospheric Research: http://www.niwa.co.nz/our-science/freshwater/tools/suspended-sediment-yield-estimator

NIWA. (2012). *Tasman: Climate*. Retrieved from National Institute of Water and Atmospheric Research: https://www.niwa.co.nz/climate/national-and-regional-climate-maps/tasman

Norton, K. (2008). Response of the landscape in the Swiss Alps to the late glacial to Holocene climate transition. *P.h.D Thesis* . Hannover: University of Hannover.

Norton, K., & Vanacker, V. (2009). Effects of terrain smoothing on topographic shielding correction factors for cosmogenic nuclide-derived estimates of basin-averaged denudation rates. *Earth Surface Processes and Landforms, Vol. 34* , 145-154.

Norton, K., Abbhul, L., & Schlunegger, F. (2010). Glacial conditioning as erosional driving force in the Central Alps. *Geology, Vol. 38* , 655-658.

Norton, K., von Blanckenburg, F., DiBiase, R., Schlunegger, F., & Kubik, P. (2011a). Cosmogenic ^{10}Be-derived denudation rates of the Eastern and Southern European Alps. *International Journal of Earth Science (Geol Rundsch), Vol. 100* , 1163–1179.

Norton, K., von Blanckenburg, F., Schlunegger, F., Schwab, M., & Kubik, P. (2008). Cosmogenic nuclide-based investigation of spatial erosion and hillslope channel coupling in the transient foreland of the Swiss Alps. *Geology, Vol. 95, No. 34* , 474-486.

Nott, J., & Roberts, R. (1996). Time and process rates over the past 100 m.y.; a case fordramatically increased landscape denudation rates during the late Quaternary in northern Australia. *Geology, Vol. 24* , 883-888.

Ochs, M., & Ivy-Ochs, S. (1997). The chemical behavior of Be, Al, Fe, Ca and Mg during AMS target preparation from terrestrial silicates modeled with chemical speciation. *Nuclear Instruments and Methods in Physics Research B, Vol. 123* , 235-240.

O'Loughlin, C., Rowe, L., & Pearce, A. (1978). Sediment yields from small Forested catchments North Westland-Nelson, New Zealand. *Journal of Hydrology, Vol. 17, No. 1,* 1-15.

Orpin, A., Carter, L., Page, M., Cochran, U., Trustrum, M., Gomez, B., et al. (2010). Holocene sedimentary record from Lake Tutira: A template for upland watershed erosion proximal to the Waipaoa Sedimentary System, Northeastern New Zealand. *Marine Geology, Vol. 270* , 11-29.

Ouimet, W., Whipple, K., & Granger, D. (2009). Beyond threshold hillslopes: channel adjustment to base-level fall in tectonically active mountain ranges. *Geology, Vol. 37* , 579-582.

Page, M., Trustrum, N., & Dymond, J. (1994). Sediment budget to assess the geomorphic effect of a cyclonic storm, New Zealand. *Geomorphology, Vol. 9* , 169-188.

Page, M., Trustrum, N., & Gomez, B. (2000). Implications of a century of anthropogenic erosion for future land use in the Gisborne-East Coast region of New Zealand. *New Zealand Geographer, Vol. 56, No. 2* , 13-24.

Palumbo, L., Hetzel, R., Tao, M., & Li, X. (2009). Topographic and lithologic control on catchment-wide denudation rates derived from cosmogenic 10Be in two mountain ranges at the margin of NE Tibet. *Geomorphology, Vol. 117* , 130-142.

Pavich, M., Brown, L., Harden, J., Klein, J., & Middleton, R. (1986). ^{10}Be distribution in soils from Merced River terraces, California. *Geochimica et Cosmochimica Acta, Vol. 50* , 1727–1735.

Pavich, M., Brown, L., Klein, J., & Middleton, R. (1984). ^{10}Be accumulation in a soil chronosequence. *Earth and Planetary Science Letters, Vol. 68* , 98-204.

Pazzaglia, F., & Brandon, M. (2001). A fluvial record of long-term steady-state uplift and erosion across the Cascadia forearc high, western Washington State. *American Journal of Science, Vol. 301* , 385-431.

Pickrill, R. (1993). Sediment yields in Fiordland. *NZ Journal of Hydrology, Vol. 31* , 39-55.

Porcelli, D., Ballentine, C., & Wieler, R. (2002). An overview of noble gas geochemistry and cosmochemistry. *Reviews in Mineral Chemistry, Vol. 47* , 1-20.

Putnam, A., Schaefer, J., Barrell, D., Vandergos, M., Denton, G., Kaplan, M., et al. (2010). In situ cosmogenic ^{10}Be production-rate calibration from the Southern Alps. *Quaternary Geology, Volume 5, No. 4* , 392-409.

Quigley, M., Sandiford, M., Fifield, K., & Alimanovic, A. (2007). Landscape responses to intraplate tectonism: Quantitative constraints from ^{10}Be nuclide abundances. *Earth and Planetary Science Letters, No. 261* , 120-133.

Rahl, J., Elhers, T., & van der Pluikm, B. (2007). Quantifying transient erosion of orogens with detrital thermochronology from syntectonic basin deposits. *Earth and Planetary Science Letters, Vol. 267* , 147-169.

Rattenbury, M., Cooper, R., & Johnston, M. (1998). *Geology of the Nelson area: 1:250 000 geological map 9.* Lower Hutt: Institute of Geological and Nuclear Sciences.

Reusser, L., & Bierman, P. (2010). Using meteoric ^{10}Be to track fluvial sand through the Waipaoa River basin, New Zealand. *Geology, Vol. 38, No. 1* , 47-50.

Riebe, C., Kirchner, J., & Granger, D. (2001a). Quantifying quartz enrichment and its consequences forcosmogenic measurements of erosion rates from alluvial sediment and regolith. *Geomorphology, Vol. 40* , 15-19.

Riebe, C., Kirchner, J., Granger, D., & Finkel, R. (2001b). Minimal climatic control on erosion rates, Sierra Nevada, California. *Geology, Vol. 29, No. 5* , 447-450.

Riebe, C., Kirchner, K., Granger, D., & Finkel, R. (2000). Erosional equilibrium and disequilibrium in the Sierra Nevada, inferred from cosmogenic ^{26}Al and ^{10}Be in alluvial sediment. *Geology, Vol. 28* , 803-806.

Robinson, B., Brooks, R., Kirkman, J., Gregg, P., & Gremigmi, P. (1996). Plant-available elements in soil and their influence on the vegetation over ultramafic ("serpintine") rocks in New Zealand. *Jounral of the Royal Society of New Zealand, Vol. 26* , 457-468.

Roe, G., Montgomery, D., & Hallet, B. (2003). Orographic precipitation and the relief of mountain ranges. *Journal of Geophyical Research, Vol. 108, Issue. B6* , DOI: 10.1029/2001JB001521.

Roering, J., Kirchner, J., & Dietrich, W. (1999). Evidence for nonlinear, diffusive sediment transport on hillslopes and implications for landscape morphology. *Water Resources Research, Vol. 35, No 3* , 853-870.

Roering, J., Kirchner, J., & Dietrich, W. (2001). Hillslope evolution by non-linear, slope dependent transport: steady state morphology and equilibrium adjustment timescales. *Journal of Geophysical Research, Vol. 105, No. B8* , 16499-16513.

Safran, E., Bierman, P., Aalto, R., Dunne, T., Whipple, K., & Caffee, M. (2005). Erosion rates driven by channel network incision in the Bolivia Andes. *Earth Surface Processes and Landforms, Vol. 30* , 1007-1024.

Savi, S., Norton, K., Picotti, V., Brardinoni, F., Akcar, N., Kubik, P., et al. (2014). Effects of sediment mixing on ^{10}Be concentrations in the Zielbach catchment, central-eastern Italian Alps. *Quaternary Geology, Vol. 19* , 148-162.

Schaller, M., von Blackenburg, F., Veldkamp, A., Tebbens, L., Hovius, N., & Kubik, P. (2002). 30,000 yr record of erosion rates from cosmogenic ^{10}Be in middle European river terraces. *Earth and Planetary Science Letters, Vol. 204* , 307-320.

Schaller, M., von Blanckenburg, F., Hovius, N., & Kubik, P. (2001). Large-scale erosion rates from in-situ produced cosmogenic nuclides in European river sediments. *Earth and Planetary Science Letters, Vol. 188* , 441-458.

Schlunegger, F., Norton, K., & Zeilinger, G. (2011). Climatic forcing on channel profiles in the Eastern Cordillera of the Coroico Region, Bolivia. *Journal of Geology, Vol. 119, No. 1* , 97-107.

Selby, M. (1974). Rates of denudation. *New Zealand Journal of Geography, No. 56* , 1-13.

Seward, D., & Kohn, B. (1997). New zircon fission-track ages from New Zealand Quaternary tephra: an interlaboratory experiment and recommendations for the determination of young ages. *Chemical Geology, Vo. 141* , 127-140.

Shepard, M., Arvidson, R., Caffee, M., Finkel, R., & Harris, L. (1995). Cosmogenic exposure ages of basalt flows: Lunar Crater volcanic field, Nevada . *Geology, Vol. 23, Vol. 1* , 21-24.

Staiger, J., Gosse, J., Toracinta, R., Oglesby, B., Fastook, J., & Johnson, J. (2007). Atmospheric scaling of cosmogenic nuclide production: climate effect. *Journal of Geophysical Research - Solid Earth, Vol. 112* , B02205. doi:10.1029/2005JB003811.

Stephensen, W. (1997). Improving the traversing micro-erosion meter. *Journal of Coatal Research, Vol. 13* , 226-241.

Stephensen, W., & Finlayson, B. (2009). Measuring erosion with the Micro-Erosion Meter - contributions to understanding landform evolution. *Earth Science Reviews, Vol. 95* , 53-62.

Stephensen, W., & Kirk, R. (1996). Measuring erosion rates using the micro- erosion meter: 20 years of data from shore platforms, Kaikoura Peninsula, South Island New Zealand. *Marine Geology, Vol. 131* , 209-218.

Stephensen, W., & Kirk, R. (1998). Rates and patterns of erosion on inter-tidal shore platforms, Kaikoura Peninsula, South Island, New Zealand. *Earth Surface Processes and Landforms, Vol. 23* , 1071-1085.

Stone, J. (1998). A rapid fusion method for the extraction of ^{10}Be from soils and silica. *Geochimica and Cosmochimica Acta, Vol. 62* , 555-561.

Stone, J. (2000). Air pressure and cosmogenic isotope production. *Journal of Geophysical Research, Vol. 105* , 23753–23759.

Summerfield, M., & Hulton, N. (1994). Natural controls of fluvial denudation rates in major world drainage basins. *Journal of Geophysical Research, Vol. 99, No. B7* , 13871-13873.

Tasman District Council. (2014, January 14). *Rivers.* Retrieved from Tasman District Council: http://www.tasman.govt.nz/environment/water/rivers/

Trauerstein, M., Norton, K., Preusser, F., & Schlunegger, F. (2013). Climatic imprint on landscape morphology in the western escarpment of the Andes. *Geomorphology, Vol. 174* , 76-83.

Trudgill, S., High, C., & Hanna, F. (1981). Improvements to the Micro-erosion meter. *British Geomorphological Research Group Technical Bulletin, Vol. 29* , 3-17.

Ursic, S., & Dendy, F. (1963). Sediment yields from small watersheds under various land used and forest publication. *USDA Miscellaneous Publication, No 970* , 47-51.

Valla, P., van der Beek, P., & Lague, D. (2010). Fluvial incision into bedrock insights from morphometric analysis and numerical modeling of gorges incising glacial hanging valleys (Western Alps, France) . *Journal of Geophysical Research, Vol. 115* .

van der Post, K., Oldfield, F., Haworth, E., Crooks, P., & Appleby, P. (1997). A record of accelerated erosion in the recent sediments of Blelham Tarn in the English Lake District. *Journal of Paleolimnology, Vol. 18* , 103-120.

Vanacker, V., von Blanckenburg, F., Govers, G., Molina, A., Poesen, J., Deckers, J., et al. (2007). Restoring dense vegetation can slow mountain erosion to near natural benchmark levels. *Geology, Vol. 35, No. 4* , 303-306.

Vance, D., Bickle, M., Ivy-Ochs, S., & Kubik, P. (2003). Erosion and exhumation in the Himalaya from cosmogenic isotope inventories from river sediments. *Earth and Planetary Science Letter, Vol. 206* , 273-288.

von Blanckenburg, F. (2006). The control mechanisms of erosion and weathering at basin scale from cosmogenic nuclides in river sediment. *Earth and Planetary Science Letters, Vol. 242* , 224-239.

von Blanckenburg, F., Belshaw, N., & O'nions, R. (1996). Separation of Be-9 and cosmogenic Be-10 from environmental materials and SIMS isotope dilution analysis. *Chemical Geology, Vol. 129* , 93-99.

von Blanckenburg, F., Bouchez, J., & Wittmann, H. (2012). Earth Surface Erosion and Weathering from the 10Be (meteoric)/9Be Ratio. *Earth and Planetary Sciences, in press* , 1-21.

von Blanckenburg, F., Hewawasam, T., & Kubik, P. (2004). Cosmogenic nuclide evidence for low weathering and denudation in the wet tropical Highlands of Sri Lanka. *Journal of Geophysical Research, Vol. 109*, FO3008 doi10.1029/2003JF000049.

Vonmoos, M., Beer, J., &Muscheler, R. (2006). Large variation in Holocene solar activity: constraintsfrom 10Be intheGreenlandIceCoreProjecticecore. *Journal of Geophysical Research, Vol. 111,* http://dx.doi.org/10.1029/2005JA011500.

Walcott, R. (1969). Geology of the Red Hill complex, Nelson, New Zealand. *Tranactions of the Royal Society of New Zealand (earth science), Vol. 7* , 57-88.

Wallbrink, P., & Murray, A. (1996). Distribution and variability of ^{7}Be in soils under different surface cover conditions and its potential for describing soil redistribution processes. *Water Resources Research, Vol. 32* , 467-476.

Walling, D. (1983). The sediment delivery problem. *Journal of Hydrology, Vol. 65* , 209-237.

Walrond, C. (2012, November 15). *Nelson region - Geology and landforms updated 15-Nov-12* . Retrieved February 6, 2014, from Te Ara - the Encyclopedia of New Zealand: http://www.TeAra.govt.nz/en/photograph/28805/moutere-depression

Whipple, K., & Meade, B. (2006). Orogen response to changes in climatic and tectonic forcing. *Earth and Planetary Sciences, Vol. 243* , 218-228.

Whitehouse, I. (1983). Distribution of large rock avalanche deposits in the central Southern Alps, New Zealand. *New Zealand Journal of Geology and Geophysics, Vol. 26, No. 3* , 271-279.

Willenbring, J., & Von Blanckenburg, F. (2010). Meteoric Cosmogenic Beryllium-10 Absorbed to River Sediment and Soil: Applications for Earth-Surface Process Dynamics. *Earth-Science Reviews, Vol. 98* , 105-122.

Willett, S., & Brandon, M. (2002). On steady states in mountain belts. *Geology, Vol. 30, No. 2* , 175-178.

Willett, S., Slingerland, R., & Hovius, N. (2001). Uplift, shortening, and steady state topography in active mountain belts. *American Journal of Science, Vol. 301* , 455-485.

Wilmhurst, J., Eden, D., & Froggatt, P. (1999). A Late Holocene terrestrial and marine record of forestry disturbance by volcanism, fire, and settlement, Gisborne, New Zealand. *New Zealand Journal of Botany, Vol. 37* , 523-540.

Wilson, P., Schnabel, C., Wilcken, K., & Vincent, P. (2013). Surface exposure dating (^{36}Cl and ^{10}Be) of post-Last Glacial Maximum valley moraines, Lake District, northwest England: some issues and implications. *Journal of Quaternary Science, Vol. 28, Issue 4,* 379-390.

Wittmann, H., & von Blanckenburg, F. (2009). Cosmogenic nuclide budgeting of floodplain sediment transfer. *Geomorphology, Vol. 109* , 246-256.

Wittmann, H., Von Blanckenburg, F., Kruesmann, T., Norton, K., & Peter, K. (2007). Relation between uplift and dendudation from cosmogenic nuclides in river sediments inthe Central Alps of Switzerland. *Journal of Geophysical Research, Vol. 112* , F04010, doi:10.1029/2006JF000729.

Wolman, G. (1967). A cycle of sedimentation and erosion in urban river channels. *Physical Geography, Vol. 49* , 385-395.

Wratt, D., Mullan, B., Ramsay, D., & Baldi, M. (2008). *Climate Change and Variability – Tasman District.* Wellington: NIWA Client Report: WLG2008-51for the Tasman District Council.

Yanites, B., Tucker, G., & Anderson, R. (2009). Numerical and analytical models of of cosmogenic radionuclide dynamics in landslide-dominate drainage basins. *Journal of Geophysical Research: Earth Surface, Vol. 114, Issue 1* , DOI: 10.1029/2008JF001088.

Yount, J., & Niemi, G. (1990). Recovery of lotic communities and ecosystems from disturbance—A narrative review of case studies. *Environmental Management, Vol. 14* , 547-569.

Zachariasen, J., Berryman, K., Prentice, C., Langridge, R., Stirling, M., Villamor, P., et al. (2001). *Size and timing of large prehistoric earthquakes on the Wairau Fault, South Island.* Lower Hutt: Institute of Geological and Nuclear Sciences.

Zaprowski, B., Pazzaglia, F., & Evenson, E. (2005). Influences on profile concavity and river incision. *Journal of Geophysical Research, Vol. 110* , doi:10.1029/2004JF000138.